

**MODELLING AND CONTROL OF A 3-RRS
PARALLEL MANIPULATOR**

**A Thesis Submitted to
the Graduate School of Engineering and Sciences of
İzmir Institute of Technology
in Partial Fulfillment of the Requirements for the Degree of
MASTER OF SCIENCE
in Mechanical Engineering**

**by
Halil TETİK**

**July 2016
İZMİR**

We approve the thesis of **Halil TETİK**

Asst. Prof. Dr. Gökhan KİPER

Department of Mechanical Engineering, İzmir Institute of Technology

Asst. Prof. Dr. Fatih Cemal CAN

Department of Mechatronics Engineering, İzmir Katip Çelebi University

Asst. Prof. Dr. M. İ. Can DEDE

Department of Mechanical Engineering, İzmir Institute of Technology

14 July 2016

Prof. Dr. Metin TANOĞLU

Head of the Department of
Mechanical Engineering

Prof. Dr. Bilge KARAÇALI

Dean of the Graduate School of
Engineering and Sciences

ACKNOWLEDGMENTS

I would love to express my sincere gratitude to Republic of Turkey and Turkish Military Forces for giving me the highest possible motivation to proceed with my graduate education.

I also would like to thank all of my professors from whom I attained the knowledge that made this thesis possible. Especially my supervisor Dr. Gökhan KİPER, my co-advisor Dr. F. Cemal CAN, and my honored professor Dr. M.İ. Can DEDE for providing support and guidance throughout my graduate studies.

Even though I cannot find correct words to express my appreciation, I also would love to thank my dearest colleagues and lab mates Mr. Jovichikj, Mr. Demirel, Mr. Uzunoğlu, Miss. Ateş, Miss. Özkahya, Mr. Şahin, Mr. Eraz and Mr. Karagöz. Without their companionship, long study hours wouldn't be bearable and productive.

In the end, I would love to thank my family for being such supportive with my studies and my life.

ABSTRACT

MODELLING AND CONTROL OF A 3-RRS PARALLEL MANIPULATOR

The focus of this thesis study is to model and control a parallel robot manipulator located in Rasim Alizade Mechatronics Laboratory (Izmir Institute of Technology Mechanical Engineering Department). The purpose of this robot is to manipulate heavy payloads. It is considered as the base part of a hybrid manipulator.

This thesis study deals with a 3-RRS parallel manipulator with 3 identical limbs. Each limb comprises two parallel revolute joint axes. The manipulator has a base and a moving platform which are in the shape of equilateral triangles. The mobile platform of this manipulator has 3-degrees-of-freedom: it can rotate around x - and y -axes and translate along the z -axis.

To obtain the mathematical model of the parallel manipulator, firstly the mobility analysis is performed. Then, a constraint analysis is performed to obtain the dependent pose parameters of the moving platform in terms of the independent parameters. Following that kinematic, singularity, workspace and inverse dynamic analyses are performed. To validate the mathematical model of the PM, several simulations are run in MATLAB/Simulink[®] environment. Once the mathematical model is validated, the control studies are carried out.

The motion of the 3-RRS PM is controlled by activating stepper motors with two different controllers (a CNC controller and a PCI card). To obtain a desired motion of the moving platform, firstly the desired task space coordinates of the moving platform are transformed into joint space coordinates using inverse kinematics. With the CNC controller a trapezoidal velocity, with the PCI card a trapezoidal jerk profile is generated. To test the control over the PM, 3 magnetic encoders are attached to the shafts of input links at each limb. Furthermore, a 3-axis gyroscope is attached to the center of the moving platform to track its rotational trajectory.

ÖZET

3-RRS PARALEL MANİPÜLATÖRÜN MODELLENMESİ VE DENETİMİ

Bu tez çalışmasının amacı Rasim Alizade Mekatronik Laboratuvarı'nda (İzmir Yüksek Teknoloji Enstitüsü - Makine Mühendisliği Bölümü) mekanik yapısı hazır bulunan paralel manipülatörün modellenmesi ve denetimidir. Üzerinde çalışılan manipülatör ağır yüklerin taşınması için tasarlanmış olan bir hibrit manipülatörün taban kısmıdır.

Tezin konusu 3 adet aynı kinematik yapıya sahip bacadan oluşmuş, 3-RRS kinematik zincir yapısına sahip bir paralel manipülatördür. Her bacakta bulunan döner mafsalların eksenleri birbirine paraleldir. Eşkenar üçgen şeklindeki taban ve hareketli platformlar bacakları birleştirir. Hareketli platform 3 serbestlik derecesine sahiptir: x ve y eksenleri etrafında dönebilir ve z ekseni boyunca öteleme hareketi yapabilir.

Manipülatörü modellemek için öncelikle mobilite analizi yapılmıştır. Ardından, kısıt denklemleri kullanılarak bağımlı uç eleman parametreleri bağımsız parametreler cinsinden ifade edilmiştir. Daha sonra, kinematik, tekillik ve çalışma uzay analizleri yapılmıştır. Geliştirilmiş formülasyonları doğrulamak için MATLAB/Simulink® ortamında hazırlanmış simülasyonlar koşturulmuştur. Formülasyonların doğrulanmasını müteakiben denetim çalışmalarına başlanmıştır.

Manipülatörün hareketi stepper motorların aktive edilmesiyle denetlenmiştir. Bunun için iki farklı denetleyici (bir CNC kontrolcü ve PCI kart) kullanılmıştır. İstenen hareketi elde edebilmek için, ters kinematik formülasyonlar kullanılarak, gereken motor hareketi hesaplanmıştır. CNC kontrolcü ile trapezoidal hız, PCI kart ile trapezoidal sarsım profilleri oluşturulmuştur. Uygulanan denetimin testi için 3 adet manyetik döner sensör aktif mafsallara, 1 adet jiroskop hareketli platforma bağlanmıştır.

TABLE OF CONTENTS

LIST OF FIGURES	viii
LIST OF TABLES	x
LIST OF SYMBOLS	xi
LIST OF ABBREVIATIONS	xii
CHAPTER 1. INTRODUCTION	1
1.1. The Aim of the Thesis and Objectives	5
1.2. Organization of the Thesis	6
CHAPTER 2. LITERATURE REVIEW	8
2.1. Kinematic Analysis	8
2.2. Singularity Analysis	9
2.3. Workspace Analysis	10
2.4. Dynamic Analysis	11
CHAPTER 3. MODELLING OF THE 3-RRS PARALLEL MANIPULATOR	14
3.1. Manipulator Geometry	14
3.2. Mobility Analysis	15
3.3. Constraint Analysis	16
3.3.1. Manipulator Constraints	16
3.3.2. Rotation Matrix Constraints	18
3.4. Inverse Kinematics	18
3.5. Forward Kinematics	20
3.6. Velocity and Acceleration Analysis	26
3.7. Singularity Analysis	28
3.8. Workspace Analysis	31
3.9. Dynamic Analysis	34
3.9.1. Mass Center Positions, Velocities and Accelerations	34
3.9.2. Inertial, Gravitational and External Forces and Moments	36

3.9.3. Virtual Work Method.....	38
3.9.4. Lagrange’s Approach	38
CHAPTER 4. DYNAMIC SIMULATIONS	43
4.1. Mechanical Structure of the PM.....	43
4.2. Inverse Dynamic Model.....	45
4.3. SimMechanics Model	50
CHAPTER 5. CONTROL OF THE PM	55
5.1. Control Setup	55
5.2. Cabling of the Control Setup	56
5.3. Control Algorithm.....	59
5.4. Control Test.....	60
CHAPTER 6. DISCUSSIONS AND CONCLUSION	67
REFERENCES	69
APPENDIX A. TIME DERIVATIVES OF JACOBIAN MATRICES	74

LIST OF FIGURES

<u>Figure</u>	<u>Page</u>
Figure 1.1. Schematic Representation of a)Serial, b)Parallel, c)Hybrid Manipulators	1
Figure 1.2. Amusement Device	2
Figure 1.3. Positioning Device	3
Figure 1.4. Tire Testing Machine	3
Figure 1.5. Klaus Cappel's Simulator Design	4
Figure 1.6. Stewart's Flight Simulator	4
Figure 1.7. Deficient PM Designs	5
Figure 1.8. Physical Model of the 3-RRS PM	6
Figure 3.1. Kinematic Diagram of the 3-RRS PM	15
Figure 3.2. Inverse Kinematics Results	20
Figure 3.3. Forward Kinematics Results for 8 Real Solutions	24
Figure 3.4. Forward Kinematics Results for 16 Real Solutions	25
Figure 3.5. The 1 st Type Singularity Surface of the 1 st Limb	30
Figure 3.6. 1 st Type Singular Configurations of the 3-RRS PM	31
Figure 3.7. 2 nd Type Singular Configurations of the 3-RRS PM	31
Figure 3.8. Link Interference Condition for Spherical Joints	32
Figure 3.9. a) Reachable Workspace and b)Safe Working Zone	33
Figure 3.10. Reachable Workspace and Safe Working Zone for: a-b) $O_{7,z} = 750$ mm, c-d) $O_{7,z} = 1000$ mm	33
Figure 3.11. Mass Centers	34
Figure 4.1. Manipulator's Base and Its Components	43
Figure 4.2. a) Lower Limb, b) Upper Limb and c) Spherical Joint	44
Figure 4.3. Moving Platform	45
Figure 4.4. Trajectory of the Task Space	46
Figure 4.5. Active R Joint Displacements	47
Figure 4.6. Active R Joint Velocity	47
Figure 4.7. Active R Joint Acceleration	48
Figure 4.8. Passive R Joint Displacement	48
Figure 4.9. Passive R Joint Velocity	49
Figure 4.10. Passive R Joint Acceleration	49

Figure 4.11. Required Input Torques	50
Figure 4.12. Body Block of the Bottom Link at Limb 1	51
Figure 4.13. SimMechanics Blocks for 3-RRS PM	52
Figure 4.14. Virtual Model of the 3-RRS PM	53
Figure 4.15. Input Torque Errors	54
Figure 5.1. Control Setup	55
Figure 5.2. Control Setup Components	55
Figure 5.3. Wiring Configurations of the Stepper Motors	57
Figure 5.4. Motor Driver's Connection Diagram	58
Figure 5.5. a) Driver Connection Port of Controller, b) Signal Inputs of Driver	58
Figure 5.6. Point-to-point Control Algorithm	61
Figure 5.7. Desired Active Joint Trajectories	62
Figure 5.8. Desired Moving Platform Trajectory	62
Figure 5.9. Displacement and Errors of Active Joints	64
Figure 5.10. Orientation Errors of the Moving Platform	64
Figure 5.11. Simulink [®] Model for Humusoft [®] MF624 PCI Card	65
Figure 5.12. Displacement and Errors of Active Joints with Humusoft [®] MF624 PCI Card	66

LIST OF TABLES

<u>Table</u>	<u>Page</u>
Table 5.1. Desired Task Space Positions and Corresponding Input Values	60

LIST OF SYMBOLS

O_{0i}	Active R Joint on i^{th} Limb
O_{ij}	Passive R Joint on i^{th} Limb
O_{7j}	S Joint on i^{th} Limb ($j = i + 3$)
$O_0 - xyz$	Fixed Coordinate Frame
O_0	Center of Base Platform
b	Radius of the Base Circle
α_{1i}	Angle between \vec{b}_1 and \vec{b}_i
$O_7 - uvw$	Moving Coordinate Frame
p	Radius of the Moving Platform's Circle
O_7	Center of Moving Platform
α_{4j}	Angle between \vec{p}_4 and \vec{p}_j
$O_{7,z}$	Height of the Platform Center
ψ_x	Rotation of the Platform about x Axis
ψ_y	Rotation of the Platform about y Axis

LIST OF ABBREVIATIONS

SM	Serial Manipulator
PM	Parallel Manipulator
HM	Hybrid Manipulator
-dof	-Degree of Freedom
R	Revolute Joint
U	Universal Joint
S	Spherical Joint
P	Prismatic Joint
PWM	Pulse Width Modulation

CHAPTER 1

INTRODUCTION

According to Robotics Institute of America, a robot is a reprogrammable multifunctional manipulator that can move materials, parts, tools, or specialized devices through variable programmed motions for the performance of a variety of tasks. Mechanical manipulators, numerical controlled machines, walking machines, and humanoids are in the scope of this definition. However, a mechanical manipulator is usually recognized as a robot which resembles the human arm in the industry (Taghirad, 2013).

Manipulators can be divided into three different types with respect to their kinematic structures as presented in Figure 1.1. The first type, serial manipulators (SM) are composed of open loop kinematic chain structures. On the other hand, parallel manipulators (PM) have closed loop kinematic chain structures and all links comprise at least two joints. The third type, hybrid manipulators (HM) consist of both open loop and closed loop chains (Tsai, 1999).

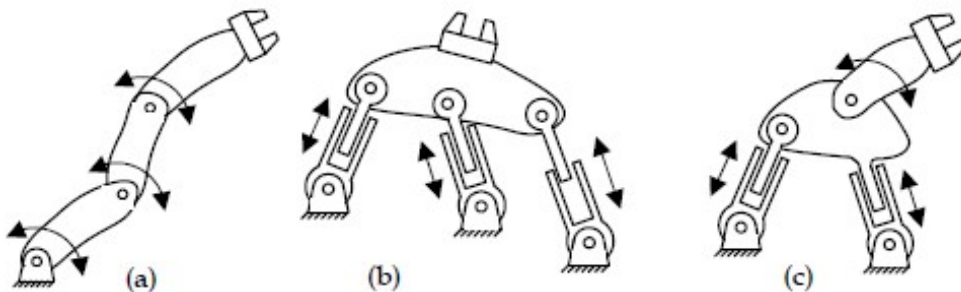


Figure 1.1. Schematic Representation of a)Serial, b)Parallel, c)Hybrid Manipulators
(Source: Harib et al. 2012)

For designers to decide on whether to use SM or PM depends on different characteristics. These characteristics can be listed as workspace, singularity, payload capability, accuracy and speed. In general, PMs have much smaller workspace to footprint ratio than their serial counterparts (Lee and Shah, 1988; Siciliano, 1999; Li et al., 2007; Elkady et al., 2008; Zhang, 2009; Vallés et al., 2012). One other drawback of PMs is their

singularities. PMs may have singularities within the workspace while SMs have at the boundaries (Elkady et al., 2008). On the other hand, payload capacity of PMs is greater than SMs since there are several limbs sharing the weight of the payload. Moreover, PMs can handle more accurate positioning than their equivalent serial counterpart. PMs have better stiffness characteristics than SMs. Also PMs generally can achieve relatively higher velocity and accelerations in contrast to their serial counterparts, especially in pick and place applications (Lee and Shah, 1988; Siciliano, 1999; Dasgupta and Mruthyunjaya, 2000; Tsai et al., 2003; Briot and Bonev, 2007; Li et al., 2007; Li and Xu, 2007; Elkady et al., 2008; Zhang, 2009; Bi and Jin, 2011; Vallés et al., 2012; Patel et al., 2012; Zhang and Ting, 2013; Chen et al., 2014).

The known studies on parallel manipulators go back to 17th century. It is known that Sir Christopher Wren mentioned parallel structured mechanisms in his studies. After him, Cauchy, Lebesgue and Bricard have worked on parallel mechanisms (Merlet, 2001).

The first known and practical design came out in 1931, by Gwinnett (1931). The patent is about a rotatable platform to be used in entertainment industry. The aim is to simulate the physical effects for the audience. As can be seen in Figure 1.2, multiple arms are attached to the platform and actuation systems are at the base joints.

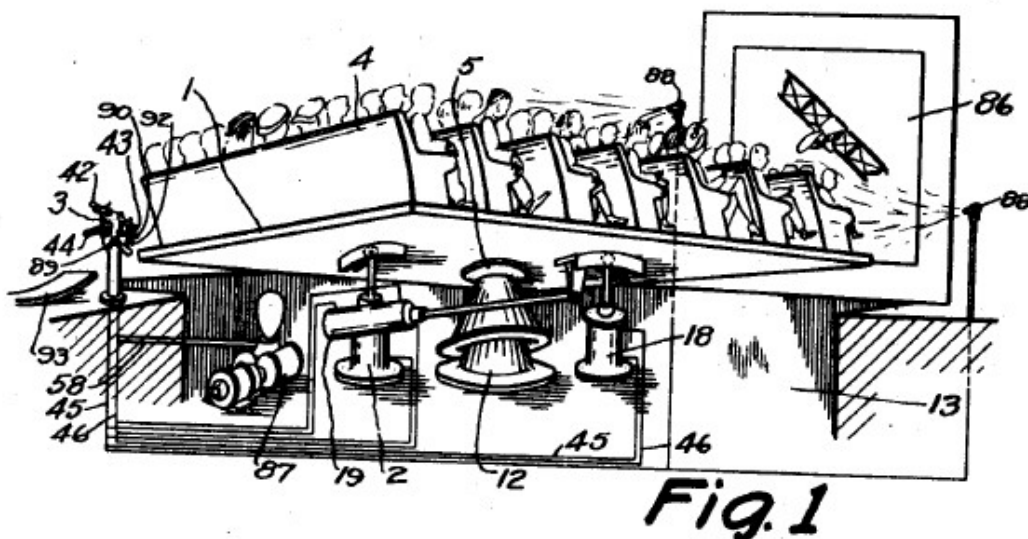


Figure 1.2. Amusement Device
(Source: Gwinnett, 1931)

In 1942, a position control device for spray guns is invented by Pollard (1942) (see Figure 1.3). The device has some advantages in energy usage and has a relatively large workspace. The mechanism has 5 degrees-of-freedom (dof) and each limb consists of one active revolute (R) joint and passive universal (U) and spherical (S) joints.

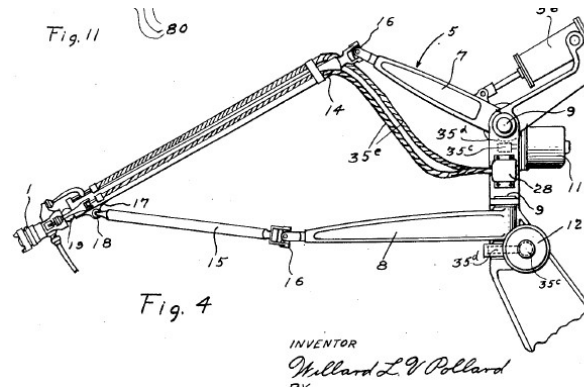


Figure 1.3. Positioning Device
(Source: Pollard, 1942)

Another useful PM design is done by Gough for testing airplane tires in 1947 (Zhang, 2009). It was the first octahedral hexapod design and a revolution in the robotics industry. The robot has 6-dof with 6 legs composed of a U joint at the base, an active prismatic (P) joint and an S joint at the moving platform. This robot is used until 2000 (see Figure 1.4).

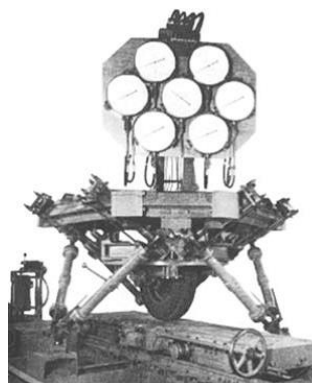


Figure 1.4. Tire Testing Machine
(Source: Zhang, 2009)

In 1962, an engineer from Franklin Institute Research Laboratories, proposed the same octahedral hexapod as presented in Figure 1.5, to use as motion simulator (Zhang, 2009). Klaus Cappel, the inventor, had the patent of his 6-dof robot in 1967.

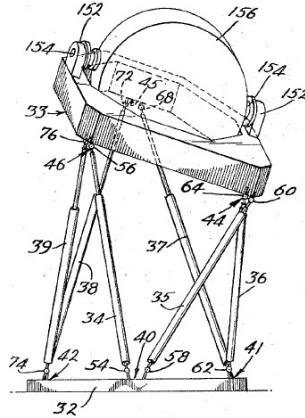


Figure 1.5. Klaus Cappel's Simulator Design
(Source: Cappel, 1967)

In 1965, a famous paper was published by Stewart (1965). The paper proposes a 6-dof flight simulation robot that can be used for training pilots. The proposed robot has 6-dof and is also based on the octahedral hexapod (Zhang, 2009). In figure 1.6 the schematic representation of Stewart's simulator is given.

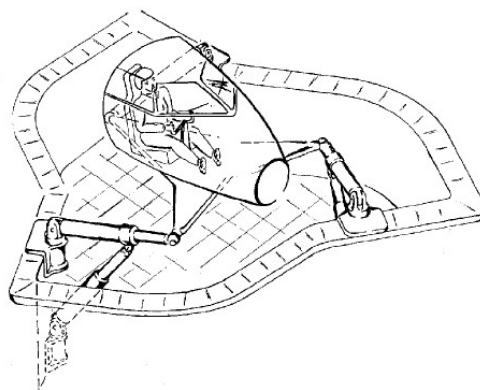


Figure 1.6. Stewart's Flight Simulator
(Source: Stewart, 1965)

PMs with less than 6-dof are deficient manipulators and have attracted a lot of attention in the past few decades since they are simpler in architecture, cheaper in design and production and easier to control (Fan et al., 2009). The most successful designs of PMs that are used in the industry are deficient (Chen et al., 2014). These manipulators are used for pick and place (Clavel, 1988; Pierrot et al., 2001), machining (Bi and Jin, 2011; Siciliano, 1999; Wahl, 2002), pointing (Gosselin et al., 1996; Dunlop and Jones, 1999), motion simulating (Pouliot et al., 1998) and telescope applications (Carretero et al., 1998)). Some of them are presented in Figure 1.7.

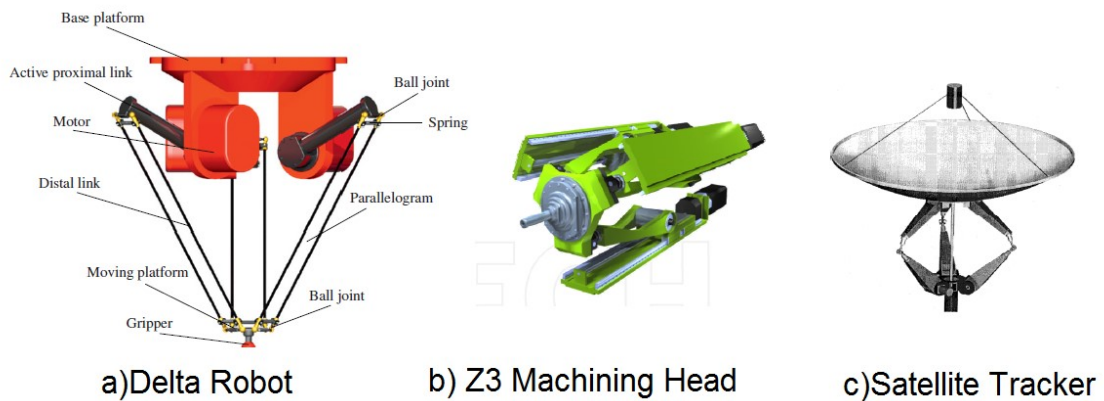


Figure 1.7. Deficient PM Designs
 (Sources: a)Zhao, 2013, b)Chen et al., 2014, c)Patel et al., 2012)

A 3-RRS PM is investigated in this thesis study. Each limb has the same kinematic structure (RRS) and these limbs are attached to the base and moving platform symmetrically. The moving platform has 1-dof translating motion along the vertical axis (z) and 2-dof rotational motion about the horizontal axes (x and y). This type of motion characteristics is called 1T2R motion in the literature (Fan et al., 2009; Li and Hervé, 2010). 1T2R PMs are generally used in machining devices and positioning of telescopes, simulating motions and coordinate measuring machines etc. (Fan et al., 2009; Li and Hervé, 2010).

1.1. The Aim of the Thesis and Objectives

The aim of this thesis study is to obtain a mathematical model of the 3-RRS PM and then perform a position control over the physical model of the PM located in Rasim Alizade Mechatronics Laboratory in İzmir Institute of Technology. The physical model of the 3-RRS PM presented in Figure 1.8 is produced by Dr. Fatih Cemal Can, during his PhD studies in Izmir Institute of Technology. Structural details of the model are presented in (Can, 2008).



Figure 1.8. Physical Model of the 3-RRS PM

1.2. Organization of the Thesis

Chapter 2 consists of the literature review performed for this thesis study. Firstly the available methodologies for kinematic analysis of 1T2R type PMs are presented. Then, techniques that are used to perform workspace, singularity and dynamic analyses are given.

In Chapter 3, modelling studies, which consist of position, velocity and acceleration level of kinematics, workspace, singularity and inverse dynamic analyses, are presented in the given order. The simulations for confirmation of the mathematical model given in Chapter 3 are presented in Chapter 4. Conducted control studies are given in Chapter 5. The discussion on the results and the conclusion are presented in Chapter 6.

CHAPTER 2

LITERATURE REVIEW

In the literature, there are several kinematic structures available to obtain a 1T2R type of motion from a PM. These manipulators can be listed as 3-RPS, 3-PRS, 3-RRS and some other kinematic structures. The literature review study presented in this chapter consists of modelling and control of 1T2R type of PMs available in the literature. This chapter includes available methods for kinematic, workspace, singularity and dynamic analyses to obtain the mathematical model of the 3-RRS PM.

2.1. Kinematic Analysis

For the position level kinematic analysis, there are two distinct types of analyses. The first type, inverse kinematics, is defined as to obtain actuated joint coordinates for a given pose of the end-effector (Merlet, 2001). There are many studies on the inverse kinematics of 1T2R PMs available in the literature.

Since this study is dealing with deficient manipulators, the first step of the inverse kinematics is to obtain the dependent pose parameters of the moving platform in terms of independent pose parameters by making use of constraint equations. For the 1T2R PMs there are 2 different types of constraints: the first type is due to the planar motion of each limb and the second type is due to the rotation matrix. Investigated studies on 1T2R PMs use the condition that all the limbs are constrained to move on planes as presented in (Tsai, 1999; Zhang et al., 2006; Li and Xu, 2007; Verdes et al., 2009; Vallés et al., 2012; Rao and Rao, 2013; Chen et al., 2013). After obtaining these constraint equations, the relationship in between the elements of the rotation matrix is obtained. It is observed that in some applications it is preferred to use the orthogonality conditions of the rotation matrix for transformation between the moving platform and base coordinate systems, as in (Tsai, 1999; Verdes et al., 2009) or making use of rotation sequences as in (Zhang et al., 2006; Li and Xu, 2007; Vallés et al., 2012; Chen et al., 2013; Rao and Rao, 2013). After obtaining all of the pose parameters of the moving platform, active joint variables are solved from the loop closure equations in terms of the defined pose parameters for the moving platform.

The forward position level kinematic analysis problem of PMs is more complex than the inverse kinematics task as it is stated in (Patel et al., 2012). The common methodology to obtain the pose of the moving platform is as follows: the coordinates of the S joints are formulated in terms of active and passive joint variables and then the fixed distance in between the S joints is used as constraint to formulate the constraint equations. The obtained equations are non-linear in terms of active and passive joint variables. Making use of tangent of the half angle substitution, some mathematical manipulations are applied to the non-linear constraint equations and at the end a 16th degree polynomial is determined in terms of one of the passive joint variables. Tsai (1999); Tsai et al. (2003); Li and Xu (2007); Gallardo et al. (2008); Rao and Rao (2013) make use of Sylvester dialytic elimination method to obtain the final 16th degree polynomial in terms of one of the passive joint variables. Tsai et al. (2003) also propose an optimization technique. Srivatsan and Bandyopadhyay (2013) on the other hand, make use of mathematical manipulation techniques to obtain the resulting polynomial. Vallés et al. (2012) follow a numerical procedure: once the 3 non-linear equations are obtained in terms of passive joint variables, Newton-Raphson numerical method is applied to obtain the values of the passive joints variables.

For the velocity and acceleration analysis of 1T2R PMs, it is observed that some prefers to differentiate the loop-closure equations to obtain the required velocities as given in (Li and Xu, 2007; Chen et al., 2013) while some prefers to make use of screw algebra as in (Gallardo et al., 2008).

Besides with several kinematic chain structures which have 1T2R motion characteristics, there are also several studies on the kinematics of 3-RRS PMs. Li et al. (2001) present the methodology to solve the position level inverse kinematics problem. Then by taking the time derivatives of position equations, the velocities and accelerations are obtained. Itul and Pisla (2009) also present a study on the forward and inverse position, velocity and acceleration level kinematics.

2.2. Singularity Analysis

A study on the singularity analysis of closed loop mechanisms is performed by Gosselin and Angeles (1990). In the study, the velocity loop equation for a general closed loop mechanism is defined as:

$$\mathbf{A}\dot{x} + \mathbf{B}\dot{\theta} = 0 \quad (2.1)$$

where \dot{x} is task space velocity column matrix, $\dot{\theta}$ is the active joint velocity column matrix and \mathbf{A} and \mathbf{B} are square matrices, elements of which are in terms position variables. A general closed-loop mechanism with such a velocity loop equation can have 3 types of singularities. The first type occurs when $\det(\mathbf{B}) = 0$, which means that the configuration of the mechanism is at the inner or outer boundaries of its workspace. This type of singularities are related to the inverse kinematics problem of the investigated mechanism. The second type of singularity occurs when $\det(\mathbf{A}) = 0$ and this singularity refers to the situations where the end-effector is movable even though all of the active joints are locked. This type of singularities are due to the forward kinematics problem of the mechanism. The third type of singularities are observed when $\det(\mathbf{A}) = \det(\mathbf{B}) = 0$. In this type of singularities, either the mechanism can have some finite motions when the actuators are locked or actuators can have some finite motion with no motion output.

It is very important to perform a singularity analysis for PMs in order to be able to avoid the singularities when planning the motion for the moving platform and selecting the link dimensions on the design stage (Li and Xu, 2007; Zhang et al., 2012). Zlatanov et al. (2002); Li and Xu (2007); Rezaei et al. (2013); Chen et al. (2013) perform singularity analyses on 1T2R PMs with different kinematic structures. Rezaei et al. (2013) also investigate all types of singularities for a 3-PSP PM. Itul and Pisla (2009) categorize the singularities of a 3-RRS as given above and states that the singularities can be obtained during the design phase of the mechanism.

2.3. Workspace Analysis

Merlet (2001) states that there are several possible methodologies to calculate the workspace boundaries of PMs. One of them is the geometrical approach. In this method, firstly the constraints on the legs are defined. Then, subjected to these constraints, a geometrical volume that describes all the possible locations of the generalized coordinates is obtained. At the end, the intersection of all these volumes for each leg is identified as the workspace of the PM. Another method defined by Merlet (2001) is called the discretization method. In this method, the workspace of the PM is covered by grids of nodes. Then every node is tested if it obeys the constraints derived from the geometry of the PM or not. At the end, the workspace boundary is constituted with the nodes whose at least one close neighbor does not satisfy the constraint equations. Merlet (2001) also mentions several numerical approaches that are used to obtain the workspace boundaries of PMs in the literature.

On the reachable workspace analysis of 1T2R PMs, Li et al. (2007) perform the analysis as follows: Firstly the constraint equations which include the motion limits of the joints and geometrical constraints of the PMs are determined. Then at every elevation level of the moving platform, the possible rotations around horizontal axes are checked whether they satisfy the constraints or not. The rotation values that satisfy the constraint conditions form the workspace of the PM. Rezaei et al. (2013) investigate a novel 3-dof PM which has two operation modes: the first mode is 1T2R and the second mode is fully translational. For the workspace of the PM in the 1T2R mode, the same methodology given above is used. For checking whether a node satisfies the constraint equations or not, it is stated that inverse kinematics solution of the PM can be used. Other than the inverse kinematic solution, it is also possible to use the forward kinematics solution. However it is pointed out that if the forward kinematics is going to be used for the workspace analysis, it is unnecessary to make a constraint check since the forward kinematics automatically obeys the constraint conditions of the PM. Itul and Pisla (2009) also propose that it is possible to use inverse and forward kinematics solutions as given by Rezaei et al. (2013) in order to obtain the workspace of a 3-RRS PM. There are also several studies that investigate the dexterous workspace of 1T2R PMs. Srivatsan and Bandyopadhyay (2014) define another workspace, safe working zone, from which the link interference conditions, physical limits of the joints as well as the singular configurations are excluded from the reachable workspace.

2.4. Dynamic Analysis

The dynamic analysis of spatial PMs have been a difficult task due to their spatial kinematic structure with a large number of passive variables. Three main methods are applied to perform the dynamic analysis of PMs: Newton-Euler classical procedure, application of Lagrange's equations and multipliers, and finally virtual work principle (Staicu, 2012).

The literature on the dynamic analysis problem of 1T2R PMs include each of the approaches listed above. The dynamic analysis of a 3-PRS PM is presented by Li and Xu (2005) by using Lagrange's equations and multipliers. The authors propose to use active and passive joint variables at each limb as generalized coordinates and they obtain a solution for the inverse dynamics problem.

Tsai and Yuan (2010) present the dynamic analysis of a 3-PRS PM, where dynamic equations for the moving platform is formulated using the task space coordinates

whereas the dynamic equations for the limbs are formulated in joint space coordinates. It is claimed that this decomposition simplifies the solution to complex velocity equations defined in different coordinate systems. In order to avoid dealing with complex algebra in the calculation of the reaction forces occurring at the S joints, it is suggested to use a special decomposition method. Basically, the reaction forces are decomposed as constraint and driving forces. Then the constraint forces are eliminated from the equation of motion of the PM.

For a 3-RPS PM, the dynamic analysis is performed by using Lagrange's equations by Pendar et al. (2004). The authors use all of the task and joint space variables as generalized coordinates and obtain 9 Lagrange multipliers. Then, a methodology to eliminate the Lagrange multipliers is presented and finally the equation of motion of the PM is obtained.

Another study proposes to use the virtual work principle to obtain the inverse and forward dynamics equations for a 3-RPS PM (Sokolov and Xirouchakis, 2007). The authors also provide the methodology to obtain the reaction forces on the joints.

Staicu (2012) presents the inverse dynamic analysis of 3-RPS PM in two configurations: at the first configuration the R joints are actuated and at the second configuration P joints are actuated. The author presented the analysis by two different methods: virtual work principle and Lagrange's equations. In the analysis by Lagrange's equations, author makes use of 12 generalized coordinates: 3 active and 3 passive joint variables at joint space and 6 pose parameters at the task space. After eliminating 9 Lagrange multipliers, equations for the inverse dynamics problem is obtained as it is done by the principle of virtual work method.

For the dynamic analysis of 3-RRS PMs, a study using Newton-Euler approach is given by Li et al. (2001). The dynamic force and moment equilibrium equations are presented and the required actuation torques for the desired task are obtained. Itul and Pisla (2009) make use of both Newton-Euler approach and principle of virtual power method. The equation of motion is obtained by Newton-Euler approach with the assumption of no friction at joints. After that, joint frictions are modelled and the required input torques are computed to overcome the frictions. Finally, the obtained torques are summed up and an equation for the required torque for each motor is obtained.

The dynamic analysis of the Tricept Robot is performed for exact and approximate models by Caccavale et al. (2003). The structure of this robot consists of 3 outer limbs having UPS kinematic chain structures and an inner limb allowing 3-dof (1T2R) motion (kinematic structure of the inner limb is not explicitly given). The solution of the exact

model is based on virtual work principle while the solution of the approximate model is based on Lagrangian formulation using some simplifying assumptions. A simulation for both of the methods is run and a comparison is given. It is claimed in the study that the impact of the simplification assumptions on the dynamic model decreases as the motion of the moving platform gets slower.

CHAPTER 3

MODELLING OF THE 3-RRS PARALLEL MANIPULATOR

This chapter consists of the direct and inverse kinematic analysis (position level kinematics are published in (Tetik et al., 2016)), workspace analysis and singularity analysis (workspace and singularity analyses studies will be published in the proceedings of 6th European Conference on Mechanism Science, 2016) and finally dynamic analysis of the 3-RRS manipulator. In order to carry out these analyses, first the geometry of the PM is examined. Then the mobility analysis of the manipulator is performed. Then, the formulations for position, velocity and acceleration level inverse and forward kinematics are presented. Following that, workspace and singularity analyses for the 3-RRS PM is presented. Finally formulation for the inverse dynamic analysis is given.

3.1. Manipulator Geometry

3-RRS PM consists of a fixed base, a moving platform and 3 identical limbs connecting the base and the platform. The limbs lie on separate planes. Each limb plane is normal to the parallel R joint axes and passes through the S joint centers associated with the limb. Each limb is composed of three joints:

- an active R joint connected to the base represented by points O_{0i} on the limb plane,
- a passive R joint between upper and lower limbs represented by points O_{ij} on the limb plane,
- a S joint between upper limb and platform represented by points for $i = 1, 2, 3$ and $j = i + 3$.

In Figure 3.1, a fixed coordinate frame $O_0 - xyz$ is attached on the base, where the origin O_0 is chosen as the center of the circle which is tangent to the three fixed revolute joints. The radius of the base circle is b . The circle coincides with O_{0i} for $i = 1, 2, 3$. The vectors from O_0 to O_{0i} are \vec{b}_i and the x -axis is chosen to be along \vec{b}_1 . The angle between \vec{b}_1 and \vec{b}_2 is $\alpha_{12} = 120^\circ$. The angle between \vec{b}_1 and \vec{b}_3 is $\alpha_{13} = 240^\circ$. A coordinate frame

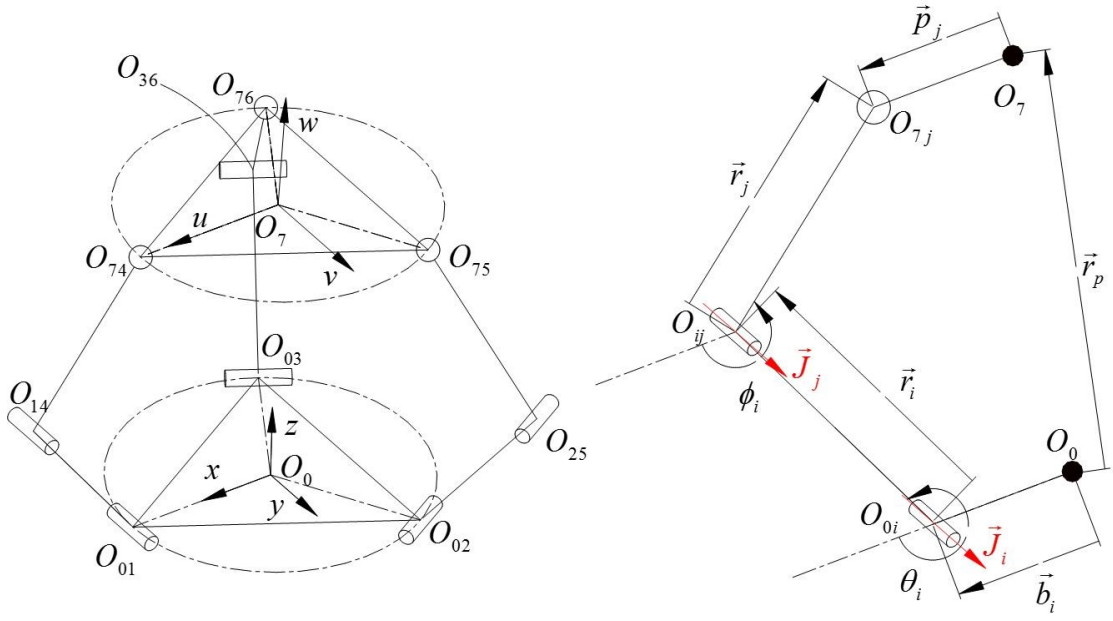


Figure 3.1. Kinematic Diagram of the 3-RRS PM

$O_7 - uvw$ is attached on the moving platform, where the origin O_7 is the center of the circle which passes through the three S joint centers O_{7j} for $j = 4, 5, 6$. The radius of the platform circle is p . The vectors from O_7 to O_{7j} are \vec{p}_j . The u -axis is chosen to be along \vec{p}_4 . The angle between \vec{p}_4 and \vec{p}_5 is $\alpha_{45} = 120^\circ$. The angle between \vec{p}_4 and \vec{p}_6 is $\alpha_{46} = 240^\circ$.

The position vector that defines the location of the moving platform with respect to the fixed coordinate frame is $\vec{r}_P = \overrightarrow{O_0O_7}$. $\vec{r}_i = \overrightarrow{O_{0i}O_{ij}}$ are the lower limb vectors and $\vec{r}_j = \overrightarrow{O_{ij}O_{7j}}$ are the upper limb vectors. The axes of the active R joints are along \vec{J}_i unit vectors and passive R joints are along \vec{J}_j unit vectors. \vec{J}_1 and \vec{J}_4 are along the y -axes of the fixed coordinate frame.

3.2. Mobility Analysis

The mobility of a PM can be calculated by using Grübler's formula:

$$F = \lambda(m - n - 1) + \sum_{i=1}^n f_i \quad (3.1)$$

where

- λ : dof of the motion space,
- m : total number of rigid bodies,
- n : total number of joints,
- f_i : dof of joint i .

The 3-RRS PM works in a $\lambda = 6$ space. $m = 8$, $n = 9$ and $\sum_{i=1}^n f_i = 15$ Then the dof of the manipulator is $F = 6(8 - 9 - 1) + 15 = 3$. The motion type of the 3-dof of the platform will be apparent when the kinematic analysis is performed.

3.3. Constraint Analysis

Let the position vector of the origin of moving coordinate frame represented in the fixed frame be:

$$\bar{r}_P = \begin{bmatrix} O_{7,x} & O_{7,y} & O_{7,z} \end{bmatrix}^T \quad (3.2)$$

and rotation matrix defining the orientation of the moving coordinate frame $O_7 - uvw$ with respect to the fixed frame $O_0 - xyz$ be:

$$\mathbf{R} = \begin{bmatrix} u_x & v_x & w_x \\ u_y & v_y & w_y \\ u_z & v_z & w_z \end{bmatrix} \quad (3.3)$$

which is composed of 3 unit vectors \vec{u} , \vec{v} and \vec{w} (components are the column vectors of \mathbf{R}), which are mutually perpendicular to each other.

Since the manipulator has 3-dof, 3 parameters among the 12 parameters of the components of \bar{r}_P and elements of \mathbf{R} are independent. The remaining dependent 9 parameters should be determined by making use of the constraint equations. By manipulator constraints, 3 dependent parameters will be solved for. The rest of the dependent parameters can be found by making use of the equations due to the orthogonality of the rotation matrix or due to an Euler rotation sequence. In this thesis study, $x - y - z$ Euler rotation sequence is used to form the rotation matrix. Other Euler rotation sequences can be used as well. Due to the motion characteristics of the moving platform, the independent pose parameters are chosen as $O_{7,z}$ the z coordinate of the moving platform center, and ψ_x and ψ_y rotation about horizontal x and y axes.

3.3.1. Manipulator Constraints

Since O_{74} is constrained on xz plane:

$$\overrightarrow{O_0 O_{74}} = \vec{r}_P + \vec{p}_1 \Rightarrow \begin{bmatrix} O_{74,x} \\ O_{74,y} \\ O_{74,z} \end{bmatrix} = \begin{bmatrix} O_{74,x} \\ 0 \\ O_{74,z} \end{bmatrix} = \begin{bmatrix} O_{7,x} \\ O_{7,y} \\ O_{7,z} \end{bmatrix} + \mathbf{R} \begin{bmatrix} p \\ 0 \\ 0 \end{bmatrix} = \begin{bmatrix} O_{7,x} + pu_x \\ O_{7,y} + pu_y \\ O_{7,z} + pu_z \end{bmatrix} \quad (3.4)$$

Since O_{75} is constrained on the $y = \tan(120^\circ)x$ plane:

$$\overrightarrow{O_0 O_{75}} = \vec{r}_P + \vec{p}_2 \Rightarrow \begin{bmatrix} O_{75,x} \\ O_{75,y} \\ O_{75,z} \end{bmatrix} = \begin{bmatrix} O_{75,x} \\ -\sqrt{3}O_{75,x} \\ O_{75,z} \end{bmatrix} = \begin{bmatrix} O_{7,x} \\ O_{7,y} \\ O_{7,z} \end{bmatrix} + \mathbf{R} \cdot \mathbf{Z}(\alpha_{45}) \cdot \begin{bmatrix} p \\ 0 \\ 0 \end{bmatrix} = \begin{bmatrix} O_{7,x} - \frac{pu_x}{2} + \frac{\sqrt{3}pv_x}{2} \\ O_{7,y} - \frac{pu_y}{2} + \frac{\sqrt{3}pv_y}{2} \\ O_{7,z} - \frac{pu_z}{2} + \frac{\sqrt{3}pv_z}{2} \end{bmatrix} \quad (3.5)$$

where $\mathbf{Z}(\cdot)$ represents the rotation matrix around the z -axis. Since O_{76} is constrained on the $y = \tan(240^\circ)x$ plane:

$$\overrightarrow{O_0 O_{76}} = \vec{r}_P + \vec{p}_3 \Rightarrow \begin{bmatrix} O_{76,x} \\ O_{76,y} \\ O_{76,z} \end{bmatrix} = \begin{bmatrix} O_{76,x} \\ \sqrt{3}O_{76,x} \\ O_{76,z} \end{bmatrix} = \begin{bmatrix} O_{7,x} \\ O_{7,y} \\ O_{7,z} \end{bmatrix} + \mathbf{R} \cdot \mathbf{Z}(\alpha_{46}) \cdot \begin{bmatrix} p \\ 0 \\ 0 \end{bmatrix} = \begin{bmatrix} O_{7,x} - \frac{pu_x}{2} - \frac{\sqrt{3}pv_x}{2} \\ O_{7,y} - \frac{pu_y}{2} - \frac{\sqrt{3}pv_y}{2} \\ O_{7,z} - \frac{pu_z}{2} - \frac{\sqrt{3}pv_z}{2} \end{bmatrix} \quad (3.6)$$

From equations 3.4, 3.5 and 3.6:

$$O_{7,y} = -u_y p \quad (3.7)$$

$$O_{7,y} = \frac{pu_y}{2} - \frac{\sqrt{3}pv_y}{2} - \sqrt{3} \left(O_{7,x} - \frac{pu_x}{2} + \frac{\sqrt{3}pv_x}{2} \right) \quad (3.8)$$

$$O_{7,y} = \frac{pu_y}{2} + \frac{\sqrt{3}pv_y}{2} + \sqrt{3} \left(O_{7,x} - \frac{pu_x}{2} - \frac{\sqrt{3}pv_x}{2} \right) \quad (3.9)$$

Adding up Equations 3.8 and 3.9 and subtracting from 2 times of Equation 3.7:

$$\left(\frac{pu_y}{2} - \frac{\sqrt{3}pv_y}{2} - \sqrt{3} \left(O_{7,x} - \frac{pu_x}{2} + \frac{\sqrt{3}pv_x}{2} \right) + \frac{pu_y}{2} + \frac{\sqrt{3}pv_y}{2} + \sqrt{3} \left(O_{7,x} - \frac{pu_x}{2} - \frac{\sqrt{3}pv_x}{2} \right) \right) = -2u_y p \rightarrow v_x = u_y \quad (3.10)$$

Equating Equations. 3.8 and 3.9:

$$O_{7^x} = \frac{p(u_x - v_y)}{2} \quad (3.11)$$

Equations 3.7 and 3.11 constitute the constraint equations for the position of the moving platform and Equation 3.10 is the constraint equation for the orientation of the moving platform due to the geometry of the manipulator. The rotation matrix elements in Equations 3.7 and 3.11 are found using ψ_x and ψ_y as explained in the following subsection.

3.3.2. Rotation Matrix Constraints

\mathbf{R} is defined by using $x - y - z$ -Euler rotation sequence:

$$\mathbf{R} = \begin{bmatrix} u_x & v_x & w_x \\ u_y & v_y & w_y \\ u_z & v_z & w_z \end{bmatrix} = \begin{bmatrix} c\psi_y c\psi_z & -c\psi_y s\psi_z & s\psi_y \\ c\psi_z s\psi_x s\psi_y + c\psi_x s\psi_z & c\psi_x c\psi_z - s\psi_x s\psi_y s\psi_z & -s\psi_x c\psi_y \\ s\psi_x s\psi_z - c\psi_x c\psi_z s\psi_y & s\psi_x c\psi_z + c\psi_x s\psi_y s\psi_z & c\psi_x c\psi_y \end{bmatrix} \quad (3.12)$$

where s and c stand for sin and cos respectively. Since ψ_x and ψ_y are selected as independent orientation parameters, the only unknown parameter of the rotation matrix is ψ_z . By making use of Equations 3.10 and 3.12:

$$\psi_z = \tan^{-1} \left(\frac{-s\psi_x s\psi_y}{c\psi_x + c\psi_y} \right) \quad (3.13)$$

for $c_x + c_y \neq 0$. All the unknown parameters in the rotation matrix can be represented in terms of ψ_x , ψ_y and ψ_z by using Equations 3.12 and 3.13.

3.4. Inverse Kinematics

Inverse kinematics problem is to find the input angles θ_i for given independent pose parameters of moving platform: $\bar{x}_i = \left[O_{7,z} \quad \psi_x \quad \psi_y \right]^T$. For each limb (see Figure 3.1:

$$\vec{r}_P + \vec{p}_j = \vec{b}_i + \vec{r}_i + \vec{r}_j \quad (3.14)$$

First, the positions of O_{7j} points in terms of given pose parameters are determined by using the left-hand side of Equation 3.14. Then using the right-hand side of the Equation 3.14 and resolving into x , y and z components:

$$x : l_2 c\phi_i c\alpha_{1i} = O_{7j,x} - c\alpha_{1i} (b + l_1 c\theta_i) \quad (3.15)$$

$$y : l_2 c\phi_i s\alpha_{1i} = O_{7j,y} - s\alpha_{1i} (b + l_1 c\theta_i) \quad (3.16)$$

$$z : l_2 s\phi_i = -O_{7j,z} - l_1 s\theta_i \quad (3.17)$$

Multiplying Equation 3.17 with $c\alpha_{1i}$ and adding up the square of Equation 3.17 with the square of Equation 3.15:

$$\begin{aligned} & \{l_2 c\alpha_{1i} c\phi_i = O_{7j,x} - c\alpha_{1i} (b + l_1 c\theta_i)\}^2 \\ + & \frac{\{l_2 c\alpha_{1i} s\phi_i = c\alpha_{1i} (-O_{7j,z} - l_1 s\theta_i)\}^2}{A_i c\theta_i + B_i s\theta_i + C_i} = 0 \end{aligned} \quad (3.18)$$

where

$$A_i = 2l_1 c\alpha_{1i} (bc\alpha_{1i} - O_{7j,x})$$

$$B_i = 2l_1 O_{7j,z} c^2\alpha_{1i}$$

$$C_i = O_{7j,x}^2 - 2bO_{7j,x}c\alpha_{1i} + c^2\alpha_{1i} (b^2 + l_1^2 - l_2^2 + O_{7j,z}^2)$$

for $C_i - A_i \neq 0$, $i = 1, 2, 3$ and $j = i + 3$. Applying tangent of the half angle substitution to Equation 3.18 and solving for θ_i :

$$\theta_i = 2 \tan^{-1} \left(\frac{-B_i \pm \sqrt{A_i^2 + B_i^2 - C_i^2}}{C_i - A_i} \right) \quad (3.19)$$

Once the input angles θ_i are found, corresponding passive joint angles can be solved uniquely by using Equations 3.15 and 3.17:

$$\begin{aligned} c\phi_i &= \frac{O_{7j,x} - c\alpha_{1i}(b+l_1c\theta_i)}{l_2c\alpha_{1i}} & s\phi_i &= -\frac{O_{7j,z} + l_1s\theta_i}{l_2} \\ \phi_i &= \text{atan2}(c\phi_i, s\phi_i) \end{aligned} \quad (3.20)$$

As a case study, a set of independent pose parameters are chosen as $\bar{x}_i = [O_{7,z} \ \psi_x \ \psi_y]^T = [900 \ -10^\circ \ 15^\circ]^T$ for $b = 500$ mm, $p = 250$ mm, $l_1 = 750$ mm and $l_2 = 850$ mm. The formulation presented above is implemented into Mathematica[®] software and inverse kinematics solution is sought. Firstly the task space parameters are found as $\bar{t} = [O_{7,x} \ O_{7,y} \ O_{7,z} \ \psi_x \ \psi_y \ \psi_z]^T =$

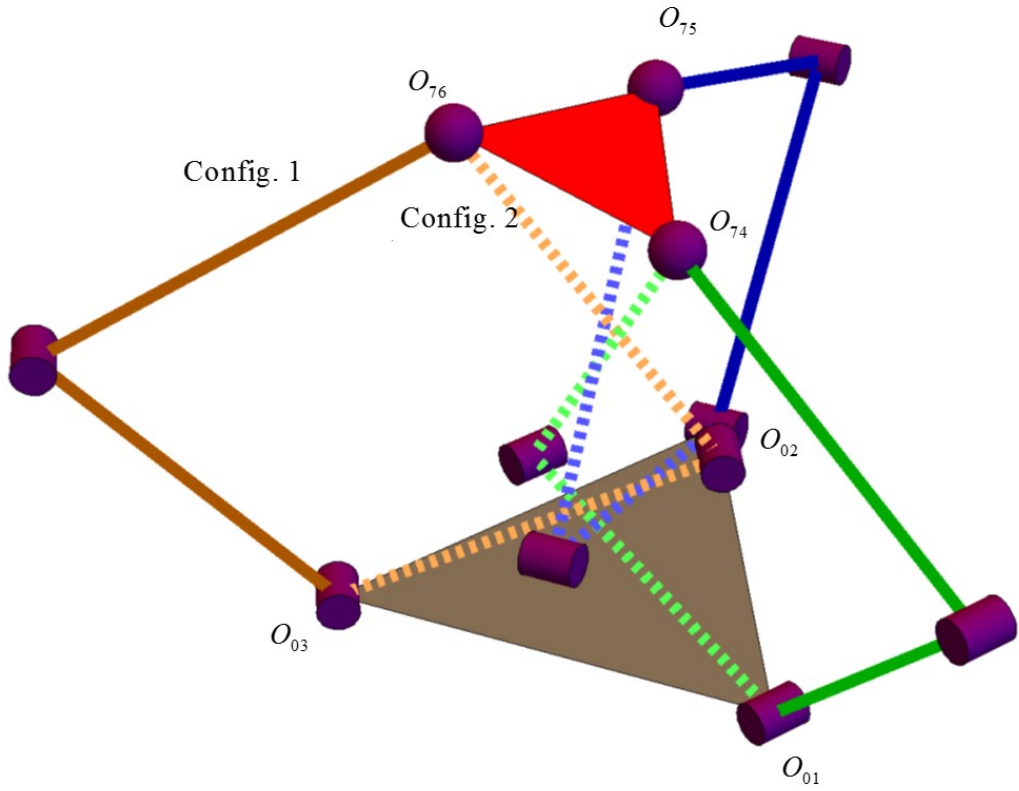


Figure 3.2. Inverse Kinematics Results

$\begin{bmatrix} 0.002 \text{ mm} & 0.005 \text{ mm} & 900 \text{ mm} & -10^\circ & 15^\circ & 1.32^\circ \end{bmatrix}^T$. Then active joint angles are obtained as $\theta_1 = (-44.84^\circ, -169.87^\circ)$, $\theta_2 = (-45.51^\circ, -164.95^\circ)$ and $\theta_3 = (-49.46^\circ, -160.94^\circ)$. The corresponding values of the passive joint angles are $\phi_1 = (-158.87^\circ, -55.84^\circ)$, $\phi_2 = (-154.86^\circ, -55.59^\circ)$ and $\phi_3 = (-152.02^\circ, -58.37^\circ)$. All possible configurations of the limbs for given set of independent pose parameters are presented in Figure 3.2. For each limb, one solution is where the limb faces outwards (Config. 1 in Figure 3.2) and the other solution is where the limb faces inwards (Config. 2). For different configurations of the limbs, there are total 8 inverse kinematics solutions. This number of solutions is generic for any pose of the platform in its workspace.

As it can be seen from Figure 3.2, when 2nd configurations for the input angles are used, there is a risk of link interference. Therefore, for the safety of the operations, 1st configurations of the inverse kinematics are used as the solution for inverse kinematics.

3.5. Forward Kinematics

Forward kinematics problem is to find the task space parameters ψ_x, ψ_y and $O_{7,z}$ for given input angles θ_i . To achieve this, the coordinates of O_{74}, O_{75} and O_{76} will be calculated in terms of joint variables by using the right-hand side of Equation refeqn3.14:

$$\overrightarrow{O_0O_{74}} = \vec{b}_1 + \vec{r}_1 + \vec{r}_4 = \begin{bmatrix} b + l_1c\theta_1 + l_2c\phi_1 \\ 0 \\ -l_1s\theta_1 - l_2s\phi_1 \end{bmatrix} \quad (3.21)$$

$$\overrightarrow{O_0O_{75}} = \vec{b}_2 + \vec{r}_2 + \vec{r}_5 = \begin{bmatrix} -\frac{1}{2}(b + l_1c\theta_2 + l_2c\phi_2) \\ \frac{\sqrt{3}}{2}(b + l_1c\theta_2 + l_2c\phi_2) \\ -l_1s\theta_2 - l_2s\phi_2 \end{bmatrix} \quad (3.22)$$

$$\overrightarrow{O_0O_{76}} = \vec{b}_3 + \vec{r}_3 + \vec{r}_6 = \begin{bmatrix} -\frac{1}{2}(b + l_1c\theta_3 + l_2c\phi_3) \\ -\frac{\sqrt{3}}{2}(b + l_1c\theta_3 + l_2c\phi_3) \\ -l_1s\theta_3 - l_2s\phi_3 \end{bmatrix} \quad (3.23)$$

Since the moving platform has an equilateral triangle shape with a side length of $|O_{74}O_{75}| = |O_{75}O_{76}| = |O_{76}O_{74}| = p\sqrt{3}$:

$$\left\{ \begin{array}{l} \frac{3}{4}(b + l_1c\theta_2 + l_2c\phi_2)^2 + (l_1s\theta_1 + l_2s\phi_1 - l_1s\theta_2 - l_2s\phi_2)^2 \\ + \frac{1}{4}(3b + 2l_1c\theta_1 + 2l_2c\phi_1 + l_1c\theta_2 + l_2c\phi_2)^2 \end{array} \right\} = 3p^2 \quad (3.24)$$

$$\left\{ \begin{array}{l} \frac{1}{4}(l_1c\theta_2 + l_2c\phi_2 - l_1c\theta_3 - l_2c\phi_3)^2 + (l_1s\theta_2 + l_2s\phi_2 - l_1s\theta_3 - l_2s\phi_3)^2 \\ + \frac{3}{4}(2b + l_1(c\theta_2 + c\theta_3) + l_2(c\phi_2 + c\phi_3))^2 \end{array} \right\} = 3p^2 \quad (3.25)$$

$$\left\{ \begin{array}{l} \frac{3}{4}(b + l_1c\theta_3 + l_2c\phi_3)^2 + (l_1s\theta_1 + l_2s\phi_1 - l_1s\theta_3 - l_2s\phi_3)^2 \\ + \frac{1}{4}(3b + 2l_1c\theta_1 + 2l_2c\phi_1 + l_1c\theta_3 + l_2c\phi_3)^2 \end{array} \right\} = 3p^2 \quad (3.26)$$

By making use of Equations 3.24, 3.25 and 3.26, 3 equations can be written in terms of passive joint variables ϕ_i :

$$h_{10} + h_{11}c\phi_1 + h_{12}c\phi_2 + h_{13}c\phi_1c\phi_2 + h_{14}s\phi_1 + h_{15}s\phi_2 + h_{16}s\phi_1s\phi_2 = 0 \quad (3.27)$$

$$h_{20} + h_{21}c\phi_2 + h_{22}c\phi_3 + h_{23}c\phi_2c\phi_3 + h_{24}s\phi_2 + h_{25}s\phi_3 + h_{26}s\phi_2s\phi_3 = 0 \quad (3.28)$$

$$h_{30} + h_{31}c\phi_3 + h_{32}c\phi_1 + h_{33}c\phi_3c\phi_1 + h_{34}s\phi_3 + h_{35}s\phi_1 + h_{36}s\phi_3s\phi_1 = 0 \quad (3.29)$$

where

$$h_{i0} = 3b^2 + 2l_1^2 + 2l_2^2 - 3p^2 + l_1 c\theta_i (3b + l_1 c\theta_{i+1}) + 3bl_1 c\theta_{i+1} - 2l_1^2 s\theta_i s\theta_{i+1}$$

$$h_{i1} = l_2 (3b + 2l_1 c\theta_i + l_1 c\theta_{i+1})$$

$$h_{i2} = l_2 (3b + l_1 c\theta_i + 2l_1 c\theta_{i+1})$$

$$h_{i3} = l_2^2$$

$$h_{i4} = 2l_1 l_2 (s\theta_i - s\theta_{i+1})$$

$$h_{i5} = -2l_1 l_2 (s\theta_i - s\theta_{i+1})$$

$$h_{i6} = -2l_2^2$$

for $i = 1, 2, 3$ and $i + 1 = 1$ for $i = 3$. Applying tangent of the half angle substitutions $t_1 = \tan(\phi_1/2)$, $t_3 = \tan(\phi_3/2)$ to Equations 3.27 and 3.28 and rearranging in terms of ϕ_2 :

$$f_{10} + f_{11}s\phi_2 + f_{12}c\phi_2 = 0 \quad (3.30)$$

$$f_{20} + f_{21}s\phi_2 + f_{22}c\phi_2 = 0 \quad (3.31)$$

where

$$f_{10} = h_{10} + h_{11} + 2h_{14}t_1 + (h_{10} - h_{11})t_1^2 \quad f_{20} = h_{20} + h_{22} + 2h_{25}t_3 + (h_{20} - h_{22})t_3^2$$

$$f_{11} = h_{15} + 2h_{16}t_1 + h_{15}t_1^2 \quad f_{21} = h_{24} + 2h_{26}t_3 + h_{24}t_3^2$$

$$f_{12} = h_{12} + h_{13} + (h_{12} - h_{13})t_1^2 \quad f_{22} = h_{21} + h_{23} + (h_{21} - h_{23})t_3^2$$

Using Equations 3.30 and 3.31, $c\phi_2$ and $s\phi_2$ can be solved:

$$s\phi_2 = \frac{f_{12}f_{20} - f_{10}f_{22}}{f_{11}f_{22} - f_{12}f_{21}}, \quad c\phi_2 = \frac{f_{10}f_{21} - f_{11}f_{20}}{f_{11}f_{22} - f_{12}f_{21}} \quad (3.32)$$

Since $c^2\phi_2 + s^2\phi_2 = 1$, from Equation 3.32:

$$(f_{12}f_{20} - f_{10}f_{22})^2 + (f_{10}f_{21} - f_{11}f_{20})^2 - (f_{11}f_{22} - f_{12}f_{21})^2 = 0 \quad (3.33)$$

Equation 3.33 involves t_1 and t_3 only. Rearranging Equation 3.33, a 4th degree polynomial in terms of t_1 can be obtained:

$$a_0 + a_1 t_1 + a_2 t_1^2 + a_3 t_1^3 + a_4 t_1^4 = 0 \quad (3.34)$$

Coefficients a_i in Equation 3.34 are 4th degree polynomials in terms of t_3 . Also applying tangent of half angle substitution $t_1 = \tan(\phi_1/2)$, $t_3 = \tan(\phi_3/2)$ and rearranging Equation 3.29:

$$b_0 + b_1 t_1 + b_2 t_1^2 = 0 \quad (3.35)$$

The coefficients b_i in Equation 3.35 are 2nd degree polynomials in terms of t_3 . Solving for t_1^2 from Equation 3.35:

$$t_1^2 = -\frac{b_0 + b_1 t_1}{b_2} \quad (3.36)$$

for $b_2 \neq 0$. Substituting Equation 3.36 into Equation 3.34, and solving for t_1 :

$$t_1 = \frac{a_4 b_0 b_1^2 - b_0 (a_4 b_0 + a_3 b_1) b_2 + a_2 b_0 b_2^2 - a_0 b_2^3}{(-a_4 b_1^3 + b_1 (2a_4 b_0 + a_3 b_1) b_2 - (a_3 b_0 + a_2 b_1) b_2^2 + a_1 b_2^3)} \quad (3.37)$$

t_1 given in Equation 3.37 is only a function of t_3 . When Equation 3.37 is substituted into Equation 3.35:

$$\frac{b_2^3 H}{[a_4 b_1^3 - b_1 (2a_4 b_0 + a_3 b_1) b_2 + (a_3 b_0 + a_2 b_1) b_2^2 - a_1 b_2^3]^2} = 0 \quad (3.38)$$

Since $b_2 \neq 0$, $H = 0$ in Equation 3.38:

$$H = \left\{ \begin{array}{l} a_4 \{a_4 b_0^4 + b_1 [-a_3 b_0^3 + b_1 (a_2 b_0^2 - a_1 b_0 b_1 + a_0 b_1^2)]\} + \\ b_2 \left[(a_3^2 - 2a_2 a_4) b_0^3 + (-a_2 a_3 + 3a_1 a_4) b_0^2 b_1 \right] + \\ \quad + (a_1 a_3 - 4a_0 a_4) b_0 b_1^2 - a_0 a_3 b_1^3 \\ b_2^2 [(a_2^2 - 2a_1 a_3 + 2a_0 a_4) b_0^2 + (-a_1 a_2 + 3a_0 a_3) b_0 b_1 + a_0 a_2 b_1^2] + \\ b_2^3 [(a_1^2 - 2a_0 a_2) b_0 - a_0 a_1 b_1] + a_0^2 b_2^4 \end{array} \right\} = 0 \quad (3.39)$$

Equation 3.39 is a 16th degree polynomial in terms of t_3 . Once a numerical solution for t_3 is obtained, then t_1 can be found uniquely by Equation 3.37. Corresponding ϕ_1 and ϕ_3 values can be evaluated as $\phi_i = 2 \tan^{-1}(t_i)$. Finally corresponding ϕ_2 can be found from Equation 3.32 as $\phi_2 = \text{atan2}(c\phi_2, s\phi_2)$. For $b_2 = 0$, t_1 can be uniquely solved from Equation 3.35. Then the value can be substituted in Equation 3.34 and a 4th order polynomial in terms of t_3 is obtained. Equation 3.34 can be solved for t_3 analytically. The corresponding passive joint variables can be found by following the same procedure explained above. When all the passive joint variables are solved for, the position and orientation of the moving platform for given active joint variables can be obtained from Equation 3.14.

The procedure for the forward kinematic analysis given above is implemented in Mathematica[®] and the results of examples are obtained. To be able to compare the results of both inverse and forward kinematics, one set of the solutions of inverse kinematics ($\theta_1 = -65.21^\circ$, $\theta_2 = -68.71^\circ$, $\theta_3 = -60.72^\circ$) is used as input for the forward kinematic analysis. As stated before, there exists maximum 16 solutions of the polynomial given in Equation 3.39. In the numerical example, it is observed that 8 of the solutions are imaginary, hence there are 8 real solutions obtained. The obtained numerical values of

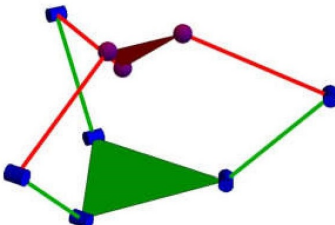
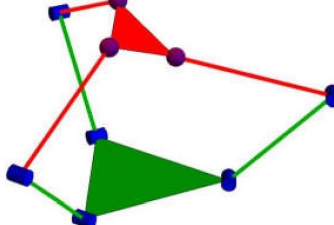
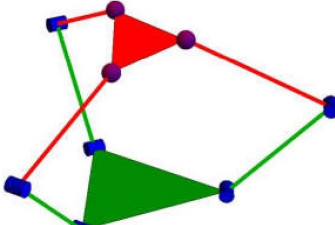
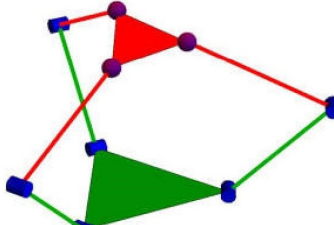
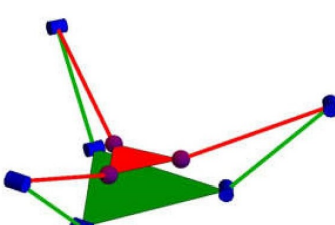
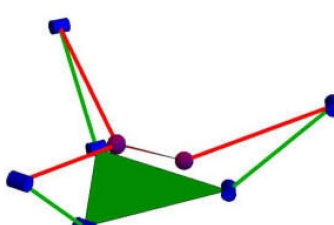
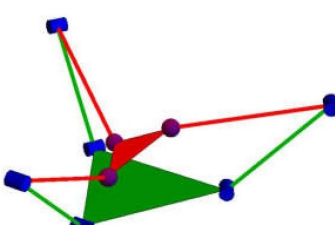
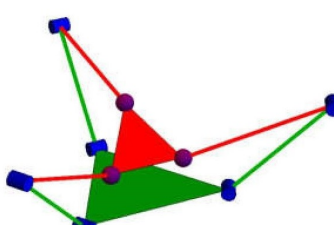
1		2	
$t_3 = 47.70$		$t_3 = 4.16$	
$\phi_1 = -156.39^\circ$		$\phi_1 = -154.56^\circ$	
$\phi_2 = -156.33^\circ$		$\phi_2 = -166.37^\circ$	
$\phi_3 = -177.60^\circ$		$\phi_3 = -152.98^\circ$	
$O_{7,z} = 0.78 \text{ m}$		$O_{7,z} = 0.86 \text{ m}$	
$\psi_x = 41.68^\circ$		$\psi_x = -30.94^\circ$	
$\psi_y = -20.00^\circ$		$\psi_y = -7.40^\circ$	
3		4	
$t_3 = 4.04$		$t_3 = 4.01$	
$\phi_1 = -161.61^\circ$		$\phi_1 = -158.87^\circ$	
$\phi_2 = -154.36^\circ$		$\phi_2 = -154.87^\circ$	
$\phi_3 = -152.24^\circ$		$\phi_3 = -152.02^\circ$	
$O_{7,z} = 0.88 \text{ m}$		$O_{7,z} = 0.9 \text{ m}$	
$\psi_x = -8.98^\circ$		$\psi_x = -10^\circ$	
$\psi_y = 21.48^\circ$		$\psi_y = 15^\circ$	
5		6	
$t_3 = 3.79$		$t_3 = 3.85$	
$\phi_1 = 157^\circ$		$\phi_1 = 168.13^\circ$	
$\phi_2 = 155.76^\circ$		$\phi_2 = 155.04^\circ$	
$\phi_3 = 150.47^\circ$		$\phi_3 = 150.93^\circ$	
$O_{7,z} = 0.17 \text{ m}$		$O_{7,z} = 0.22 \text{ m}$	
$\psi_x = 4.65^\circ$		$\psi_x = 2.96^\circ$	
$\psi_y = 4.30^\circ$		$\psi_y = -29.97^\circ$	
7		8	
$t_3 = 3.88$		$t_3 = 14.15$	
$\phi_1 = 155.86^\circ$		$\phi_1 = 156.69^\circ$	
$\phi_2 = 168.93^\circ$		$\phi_2 = 156.03^\circ$	
$\phi_3 = 151.11^\circ$		$\phi_3 = 171.91^\circ$	
$O_{7,z} = 0.23 \text{ m}$		$O_{7,z} = 0.27 \text{ m}$	
$\psi_x = 30.24^\circ$		$\psi_x = -39.81^\circ$	
$\psi_y = 12.98^\circ$		$\psi_y = 19.88^\circ$	

Figure 3.3. Forward Kinematics Results for 8 Real Solutions

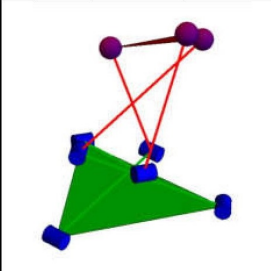
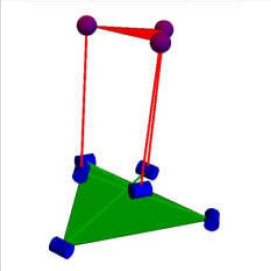
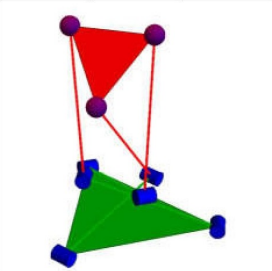
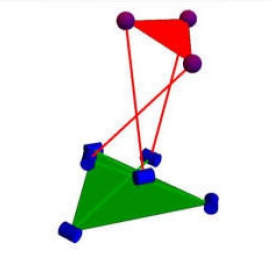
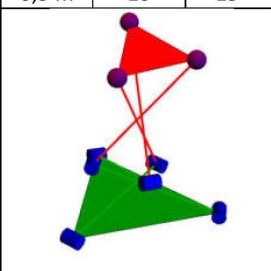
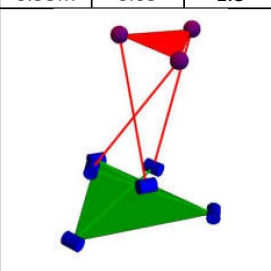
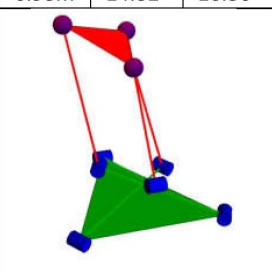
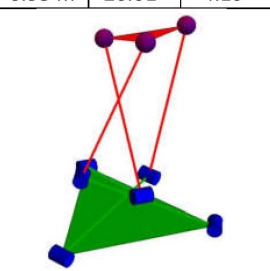
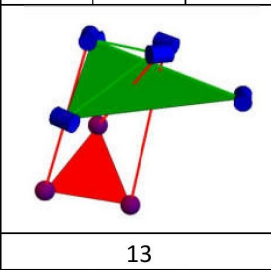
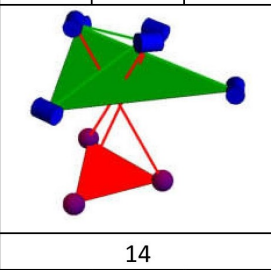
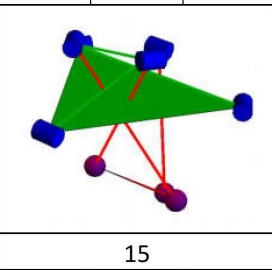
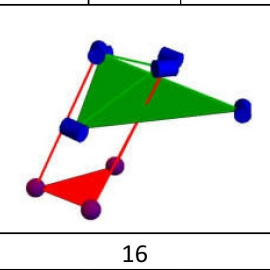
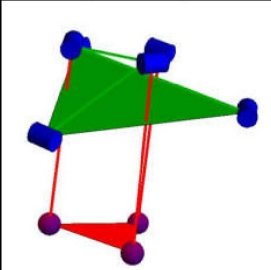
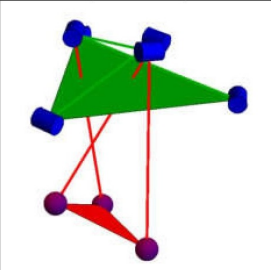
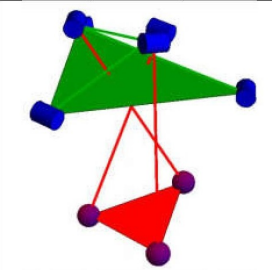
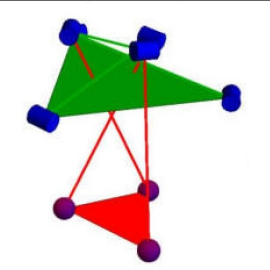
1			2			3			4		
$O_{7,z} =$ 0.92m	$\Psi_x =$ -27.79°	$\Psi_y =$ 16.93°	$O_{7,z} =$ 1.04m	$\Psi_x =$ 6.81°	$\Psi_y =$ -13.46°	$O_{7,z} =$ 0.96 m	$\Psi_x =$ 12.19°	$\Psi_y =$ -52.48°	$O_{7,z} =$ 0.93 m	$\Psi_x =$ 18.46°	$\Psi_y =$ 1.32°
											
5			6			7			8		
$O_{7,z} =$ 0,9 m	$\Psi_x =$ -10°	$\Psi_y =$ 15°	$O_{7,z} =$ 0.93m	$\Psi_x =$ -0.09°	$\Psi_y =$ -1.8°	$O_{7,z} =$ 0.93m	$\Psi_x =$ 14.82°	$\Psi_y =$ 10.56°	$O_{7,z} =$ 0.93 m	$\Psi_x =$ -	$\Psi_y =$ 20.01°
											
9			10			11			12		
$O_{7,z} =$ -0.58m	$\Psi_x =$ 39.68°	$\Psi_y =$ -29.40°	$O_{7,z} =$ -0.51 m	$\Psi_x =$ -4.76°	$\Psi_y =$ 12.02°	$O_{7,z} =$ -0.55m	$\Psi_x =$ -1.16°	$\Psi_y =$ 33.00°	$O_{7,z} =$ -	$\Psi_x =$ -	$\Psi_y =$ 14.43°
											
13			14			15			16		
$O_{7,z} =$ -0.65m	$\Psi_x =$ 6.85°	$\Psi_y =$ -	$O_{7,z} =$ -0.54m	$\Psi_x =$ 7.67°	$\Psi_y =$ 26.88°	$O_{7,z} =$ -0.55m	$\Psi_x =$ -	$\Psi_y =$ 17.44°	$O_{7,z} =$ -0.54m	$\Psi_x =$ 2.55°	$\Psi_y =$ -
											

Figure 3.4. Forward Kinematics Results for 16 Real Solutions

t_3 , corresponding passive joint angles ϕ_i , independent pose parameters and kinematic schemes of the PM are provided in Figure 3.3 Notice that 4th set of the solution matches with the independent task space parameters used for the inverse kinematics.

After performing some trials with different input values of θ_i , it is observed that mathematically 16 real solutions for the pose of the end effector is possible in some configurations. For example when another set of the results from inverse kinematics example, $\theta_1 = -135.7^\circ$, $\theta_2 = -132.75^\circ$, $\theta_3 = -144.47^\circ$ is used and there are 16 real solutions for Equation 3.39. Each possible pose of the moving platform obtained is presented in Figure 3.4. Notice that the 5th solution matches with the independent task space parameters used in the inverse kinematics example. It should be noted that, even though it is possible to have all these 16 real solutions mathematically, some of those solutions are physically impossible due to link interferences and joint limitations.

3.6. Velocity and Acceleration Analysis

The velocity loop equation can be written by differentiating Equation 3.18 respect to time:

$$\dot{A}_i c \theta_i + \dot{B}_i s \theta_i + \dot{C}_i + (B_i c \theta_i - A_i s \theta_i) \dot{\theta}_i = \bar{D}_i \dot{O}_{7j} + E_i \dot{\theta}_i = 0 \quad (3.40)$$

where

$$\begin{aligned} \bar{D}_i &= \begin{bmatrix} -2c\alpha_{1i}(b + l_1 c \theta_i) + 2O_{7j,x} & 0 & 2c\alpha_{1i}^2(O_{7j,z} + l_1 s \theta_i) \end{bmatrix} \\ E_i &= 2l_1 c \alpha_{1i} (c \alpha_{1i} c \theta_i O_{7j,z} + (-b c \alpha_{1i} + O_{7j,x}) s \theta_i) \end{aligned}$$

Equation 3.40 is a function of i^{th} active joint ($\dot{\theta}_i$, $i = 1, 2, 3$) and corresponding spherical joint velocity ($\dot{O}_{7j} = [O_{7j,x} \ O_{7j,y} \ O_{7j,z}]^T$, $j = i + 3$). Equation 3.40 can be written in general form to include all of the active revolute ($\dot{\theta} = [\dot{\theta}_1 \ \dot{\theta}_2 \ \dot{\theta}_3]^T$) and passive spherical ($\dot{S} = [\dot{O}_{74} \ \dot{O}_{75} \ \dot{O}_{76}]^T$) joint velocities:

$$\begin{pmatrix} \bar{D}_1 & 0_{1 \times 3} & 0_{1 \times 3} \\ 0_{1 \times 3} & \bar{D}_2 & 0_{1 \times 3} \\ 0_{1 \times 3} & 0_{1 \times 3} & \bar{D}_3 \end{pmatrix} \dot{S} + \begin{pmatrix} E_1 & 0 & 0 \\ 0 & E_2 & 0 \\ 0 & 0 & E_3 \end{pmatrix} \dot{\theta} = \mathbf{J}_S \dot{S} + \mathbf{J}_\theta \dot{\theta} = \bar{0} \quad (3.41)$$

The spherical joint velocities can be expressed in terms of task space velocities ($\dot{t} = [\dot{O}_{7,x} \ \dot{O}_{7,y} \ \dot{O}_{7,z} \ \dot{\psi}_x \ \dot{\psi}_y \ \dot{\psi}_z]^T$) by taking the time derivative of Equations 3.4, 3.5 and 3.6:

$$\dot{O}_{7j} = \mathbf{J}_{t,O_{7j}} \dot{t} \Rightarrow \dot{S} = \mathbf{J}_{t,S} \dot{t} \quad (3.42)$$

where $\mathbf{J}_{t,S} = \begin{bmatrix} \mathbf{J}_{t,O_{74}} \\ \mathbf{J}_{t,O_{75}} \\ \mathbf{J}_{t,O_{76}} \end{bmatrix}$ and

$$\mathbf{J}_{t,O_{7j}} = \begin{bmatrix} 1 & 0 & 0 & 0 & \begin{pmatrix} -ps\psi_y \\ c(\alpha_{4j} + \psi_z) \end{pmatrix} & -pc\psi_y s(\alpha_{4j} + \psi_z) \\ 0 & 1 & 0 & p \begin{pmatrix} c\psi_x s\psi_y \\ c(\alpha_{4j} + \psi_z) \\ -s\psi_x s(\alpha_{4j} + \psi_z) \end{pmatrix} & \begin{pmatrix} ps\psi_x c\psi_y \\ c(\alpha_{4j} + \psi_z) \end{pmatrix} & p \begin{pmatrix} \psi_x c(\alpha_{4j} + \psi_z) \\ -s\psi_x s\psi_y \\ s(\alpha_{4j} + \psi_z) \end{pmatrix} \\ 0 & 0 & 1 & p \begin{pmatrix} s\psi_x s\psi_y \\ c(\alpha_{4j} + \psi_z) \\ +c\psi_x s(\alpha_{4j} + \psi_z) \end{pmatrix} & \begin{pmatrix} -pc\psi_x c\psi_y \\ c(\alpha_{4j} + \psi_z) \end{pmatrix} & p \begin{pmatrix} s\psi_x c(\alpha_{4j} + \psi_z) \\ c\psi_x s\psi_y \\ s(\alpha_{4j} + \psi_z) \end{pmatrix} \end{bmatrix}$$

Task space velocities can be expressed in terms of independent task space velocities ($\dot{\tilde{x}}_i = [\dot{O}_{7,z} \ \dot{\psi}_x \ \dot{\psi}_y]^T$) by taking the time derivative of Equations 3.7, 3.11 and 3.13:

$$\left. \begin{aligned} \dot{O}_{7,x} &= \mathbf{J}_{O_{7,x}} \dot{\tilde{x}}_i \\ \dot{O}_{7,y} &= \mathbf{J}_{O_{7,y}} \dot{\tilde{x}}_i \\ \dot{\psi}_z &= \mathbf{J}_{\psi_z} \dot{\tilde{x}}_i \end{aligned} \right\} \rightarrow \dot{t} = \mathbf{J}_{x_i,t} \dot{\tilde{x}}_i \quad (3.43)$$

where

$$\mathbf{J}_{x_i,t} = \begin{bmatrix} \mathbf{J}_{O_{7,x}} & \mathbf{J}_{O_{7,y}} & \mathbf{I}_{3 \times 3} & \mathbf{J}_z \end{bmatrix}^T$$

$$\mathbf{J}_{O_{7,x}} = \begin{bmatrix} 0 & -\frac{pc\psi_y s\psi_y(c\psi_x + c\psi_y s\psi_x s\psi_y)}{2(1+c\psi_x c\psi_y)^2} & -\frac{pc\psi_y s\psi_x(c\psi_x + c\psi_y + s\psi_x s\psi_y)}{2(1+c\psi_x c\psi_y)^2} \end{bmatrix}$$

$$\mathbf{J}_{O_{7y}} = \begin{bmatrix} 0 & -\frac{pc\psi_y s\psi_y(c\psi_x + c\psi_y)}{(1+c\psi_x c\psi_y)^2} & \frac{ps\psi_x \left(s^2\psi_x s^4\psi_y - c^4\psi_y - c^2\psi_x c2\psi_y - \frac{1}{4}c\psi_x(5c\psi_y + 3c3\psi_y) \right)}{(1+c\psi_x c\psi_y)^3} \end{bmatrix}$$

$$\mathbf{J}_{\psi_z} = \begin{bmatrix} 0 & \frac{-s\psi_y}{1+c\psi_x c\psi_y} & \frac{-s\psi_x}{1+c\psi_x c\psi_y} \end{bmatrix}$$

When Equations 3.42 and 3.43 are substituted into Equation 3.41:

$$\mathbf{J}_S \mathbf{J}_{t,S} \mathbf{J}_{x_i,t} \dot{\tilde{x}}_i + \mathbf{J}_\theta \dot{\theta} = \mathbf{J}_{x_i} \dot{\tilde{x}}_i + \mathbf{J}_\theta \dot{\theta} = \bar{0} \quad (3.44)$$

Both Jacobian matrices \mathbf{J}_{x_i} and \mathbf{J}_θ are 3 x 3 square matrices. In order to obtain the active joint velocities in terms of independent task space velocities, Equation 3.44 can be rearranged as:

$$\dot{\theta} = -\mathbf{J}_\theta^{-1} \mathbf{J}_S \mathbf{J}_{t,S} \mathbf{J}_{x_i,t} \dot{\tilde{x}}_i = \mathbf{J}_{x_i,\theta} \dot{\tilde{x}}_i \quad (3.45)$$

Then i^{th} passive joint velocity ($\dot{\phi}_i$) can be found in terms of the associated active joint and spherical joint velocity by taking the time derivative of Equation 3.17:

$$\dot{\phi}_i = \mathbf{J}_{S_i, \phi_i} \dot{O}_{7j} + J_{\theta_i, \phi_i} \dot{\theta}_i \quad (3.46)$$

where:

$$\mathbf{J}_{S_i, \phi_i} = \begin{bmatrix} 0 & 0 & \frac{-1}{l_2 c \phi_i} \end{bmatrix}$$

and

$$J_{\theta_i, \phi_i} = -\frac{l_1 c \theta_i}{c \phi_i l_2}$$

Equation 3.46 can be written in general form in order it to contain all of the passive joint ($\dot{\phi} = [\dot{\phi}_1 \quad \dot{\phi}_2 \quad \dot{\phi}_3]^T$) and S joint velocities:

$$\dot{\phi} = \begin{bmatrix} \mathbf{J}_{S_1, \phi_1} & 0_{3 \times 1} & 0_{3 \times 1} \\ 0_{3 \times 1} & \mathbf{J}_{S_2, \phi_2} & 0_{3 \times 1} \\ 0_{3 \times 1} & 0_{3 \times 1} & \mathbf{J}_{S_3, \phi_3} \end{bmatrix} \dot{S} + \begin{bmatrix} J_{\theta_1, \phi_1} & 0 & 0 \\ 0 & J_{\theta_2, \phi_2} & 0 \\ 0 & 0 & J_{\theta_3, \phi_3} \end{bmatrix} \dot{\theta} = \mathbf{J}_{S, \phi} \dot{S} + \mathbf{J}_{\theta, \phi} \dot{\theta} \quad (3.47)$$

Substituting Equations 3.42, 3.43 and 3.45 in Equation 3.47, the passive joint space velocities and independent task space velocities can be interrelated as:

$$\dot{\phi} = (\mathbf{J}_{S, \phi} \mathbf{J}_{x_i, S} + \mathbf{J}_{\theta, \phi} \mathbf{J}_{x_i, \theta}) \dot{x}_i = \mathbf{J}_{x_i, \phi} \dot{x}_i \quad (3.48)$$

where $\mathbf{J}_{x_i, S} = \mathbf{J}_{t, S} \mathbf{J}_{x_i, t}$. To formulate the joint space accelerations ($\ddot{\theta} = [\ddot{\theta}_1 \quad \ddot{\theta}_2 \quad \ddot{\theta}_3]^T$, $\ddot{\phi} = [\ddot{\phi}_1 \quad \ddot{\phi}_2 \quad \ddot{\phi}_3]^T$) in terms of independent pose parameter accelerations ($\ddot{x}_i = [\ddot{O}_{7,z} \quad \ddot{\psi}_x \quad \ddot{\psi}_y]^T$), time derivative of Equations 3.45 and 3.48 are used:

$$\ddot{\theta} = \dot{\mathbf{J}}_{x_i, \theta} \dot{x}_i + \mathbf{J}_{x_i, \theta} \ddot{x}_i \quad (3.49)$$

$$\ddot{\phi} = \dot{\mathbf{J}}_{x_i, \phi} \dot{x}_i + \mathbf{J}_{x_i, \phi} \ddot{x}_i \quad (3.50)$$

The time derivatives of each Jacobian matrix used in Equations 3.49 and 3.50 are provided in Appendix A.

3.7. Singularity Analysis

As stated in Section 2.2, there are 3 types of singularities for PMs. In order to investigate the singular configurations of the 3-RRS PM, the Jacobian matrices given in Equation 3.44 are used. The 1st type singularities singularities, also known as inverse

kinematics singularities, occur when $\text{Det}[\mathbf{J}_\theta] = 0$. \mathbf{J}_θ is a function of the inputs θ_1 , θ_2 and θ_3 . So, $\text{Det}[\mathbf{J}_\theta] = 0$ defines an equation in θ_1 , θ_2 and θ_3 . This is a surface in the joint space, called as the singularity surface. Formulating the singularity surface equation from $\text{Det}[\mathbf{J}_\theta] = 0$ is computationally challenging. Instead, notice that inverse kinematic singularities occur when either of the limbs are in extended or folded configurations, where the two links of the limbs become collinear. So to speak, the singularity conditions can be analysed separately for each limb. Since the limbs of the PM are identical and the base and the platform are symmetrical, the conditions for each limb is equivalent to each other. Without loss of generality, limb 1 can be analysed. Limb 1 is in extended or folded configuration the $A_1^2 + B_1^2 - C_1^2$ term in Equation 3.18 is equal to zero. The 1st type singularities are obtained:

$$A_1^2 + B_1^2 - C_1^2 = \left(\begin{array}{c} -4b^2 + 4l_1^2 - 8l_1l_2 + 4l_2^2 - \\ 4O_{7,z}^2 - 4b^2c_x^2 - b^2c_x^4 \\ + 8l_1^2c_xc_y - 16l_1l_2c_xc_y + \\ 8l_2^2c_xc_y - 8O_{7,z}^2c_xc_y + \\ 6b^2c_x^2c_y^2 + 4l_1^2c_x^2c_y^2 - \\ 8l_1l_2c_x^2c_y^2 + 4l_2^2c_x^2c_y^2 - \\ 4O_{7,z}^2c_x^2c_y^2 - 9b^2c_y^4 + \\ 8bO_{7,z}s_y + 16bO_{7,z}c_xc_ys_y + \\ 8bO_{7,z}c_x^2c_y^2s_y - \\ 4b^2s_y^2 - 8b^2c_xc_ys_y^2 - \\ 4b^2c_x^2c_y^2s_y^2 - 4b^2s_x^2s_y^2 - \\ b^2s_x^4s_y^4 - 2b^2c_x^2s_x^2s_y^2 + \\ 6b^2c_y^2s_x^2s_y^2 + 12b^2c_y^2 \end{array} \right) - \left(\begin{array}{c} -4b^2 + 4l_1^2 + 8l_1l_2 + 4l_2^2 - \\ 4O_{7,z}^2 - 4b^2c_x^2 - b^2c_x^4 + \\ 8l_1^2c_xc_y + 16l_1l_2c_xc_y + \\ 8l_2^2c_xc_y - 8O_{7,z}^2c_xc_y + \\ 12b^2c_y^2 - b^2s_x^4s_y^4 + \\ 6b^2c_x^2c_y^2 + 4l_1^2c_x^2c_y^2 + \\ 8l_1l_2c_x^2c_y^2 + 4l_2^2c_x^2c_y^2 - \\ 4O_{7,z}^2c_x^2c_y^2 - 9b^2c_y^4 + \\ 8bO_{7,z}s_y + 16bO_{7,z}c_xc_ys_y + \\ 8bO_{7,z}c_x^2c_y^2s_y - \\ 4b^2s_y^2 - 8b^2c_xc_ys_y^2 - \\ 4b^2c_x^2c_y^2s_y^2 - 4b^2s_x^2s_y^2 - \\ 2b^2c_x^2s_x^2s_y^2 + 6b^2c_y^2s_x^2s_y^2 \end{array} \right) = 0 \quad (3.51)$$

where subscripts x and y refers to ψ_x and ψ_y . When the condition given in Equation 3.51 is satisfied, the upper and lower links at any of the limbs are collinear. As stated in Section 2.2, 1st type type singularities represent the configurations where the mechanism is at the inner or outer boundaries of its workspace. Therefore, it is more convenient to represent the singularity surface in the task space, rather than the the joint space. Figure 3.5 represents the singularity surface of the 1st limb and Figure 3.6 represents several inverse kinematic singular configurations of the PM. The singularity surface is obtained in spherical coordinates. The heave of the moving platform, $O_{7,z}$, is considered as the

radius of a sphere and rotations of the moving platform, ψ_x and ψ_y , are considered as azimuth and polar angles of the sphere.

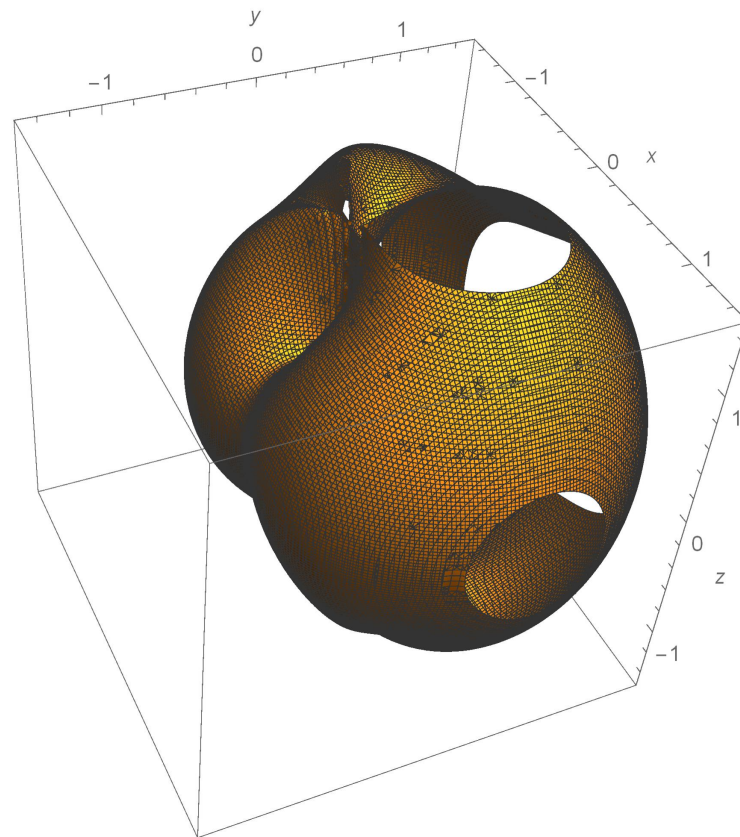


Figure 3.5. The 1st Type Singularity Surface of the 1st Limb

The 2nd type singularities, also known as forward kinematic singularities occur when:

$$\text{Det} [\mathbf{J}_{x_i}] = 0 \quad (3.52)$$

The 2nd type singularities refer to the configurations of the PM when any of the upper links lie on the plane of the moving platform. Unlike the 1st type of singularities, the 2nd type of singularities cannot be evaluated per limb. As a result, the singularity condition given in Equation 3.52 is a very long and highly non-linear equation in terms of the independent task space parameters. For this reason a singularity surface for this type is not plotted. Figure 3.7 represents several configurations that has this type of singularities.

The 3rd type of the singularities are obtained when:

$$\text{Det} [\mathbf{J}_{x_i}] = \text{Det} [\mathbf{J}_\theta] = 0 \quad (3.53)$$

This type of singularities occur when either the platform possess finite motions although the inputs are locked, or the platform is stationary although the inputs are varied. The 3rd type of singularities are not observed for the 3-RRS PM investigated in this thesis study because $\text{Det} [\mathbf{J}_\theta]$ and $\text{Det} [\mathbf{J}_{x_i}]$ are not simultaneously equal to zero.

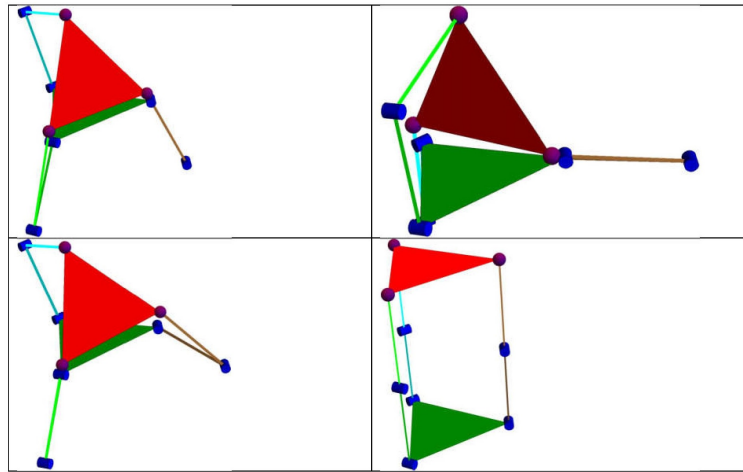


Figure 3.6. 1st Type Singular Configurations of the 3-RRS PM

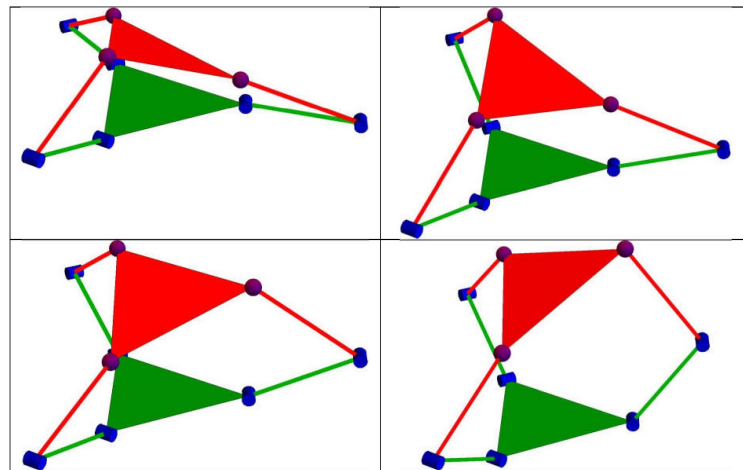


Figure 3.7. 2nd Type Singular Configurations of the 3-RRS PM

3.8. Workspace Analysis

The workspace of the 3-RRS PM investigated in this study is evaluated by using position level kinematic constraint equations. To evaluate the reachable workspace, the position level kinematic equations are implemented into MATLAB[®] and a computation for the reachable workspace of the 3-RRS PM is created. The algorithm makes a research in the ranges of $0.33 \text{ m} \leq O_{7,z} \leq 1.475 \text{ m}$, $-\pi/2 \leq \psi_x \leq \pi/2$ and $-\pi/2 \leq \psi_y \leq \pi/2$ with the step sizes of $\Delta O_{7,z} = 10 \text{ mm}$ and $\Delta\psi_x = \Delta\psi_y = 2^\circ$. Using these independent task space parameters, it evaluates the active and passive joint variables. If the given task space parameters are achievable by the manipulator, the given parameters are saved as the reachable workspace of the PM. To represent the workspace of the manipulator, spherical coordinate system is preferred. The heave of the moving platform, $O_{7,z}$, is considered as the radius of a sphere and rotations of the moving platform, ψ_x and ψ_y , are considered as azimuth and polar angles of the sphere and required conversion is performed.

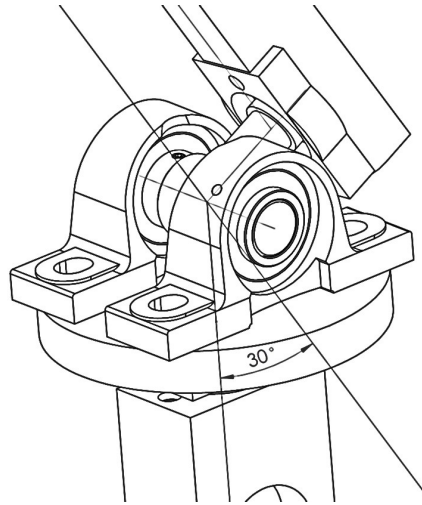


Figure 3.8. Link Interference Condition for Spherical Joints

After obtaining the reachable workspace of the PM, singularity and link interference conditions are introduced to the workspace computation. The resulting workspace is defined as the Safe Working Zone of the PM by Srivatsan and Bandyopadhyay (2014) and a study to obtain the safe working zone of the 3-RRS PM investigated in this thesis study is presented in the 6th European Conference on Mechanism Science (EUCOMES 2016). As joint limits, 3-RRS PM has two types of joint limitations. First one is at active

joints whose value must be in the range of $-\pi/2 \leq \theta_i \leq 0$. The other joint limitation is with the spherical joints. The angle in between an upper limb and the corresponding $\overrightarrow{O_7 O_{7j}}$ vector cannot exceed 30° due to the joint construction as presented in Figure 3.8. The safe working zone of the PM is also represented using spherical coordinates.

To visualise the workspace of the PM better, sections of the workspaces at certain heave values are presented in Figure 3.10. Figure 3.10 (a)-(b) represents the reachable workspace and safe working zone at $O_{7,z} = 0.75$ m and Figure 3.10 (b)-(c) at $O_{7,z} = 1$ m.

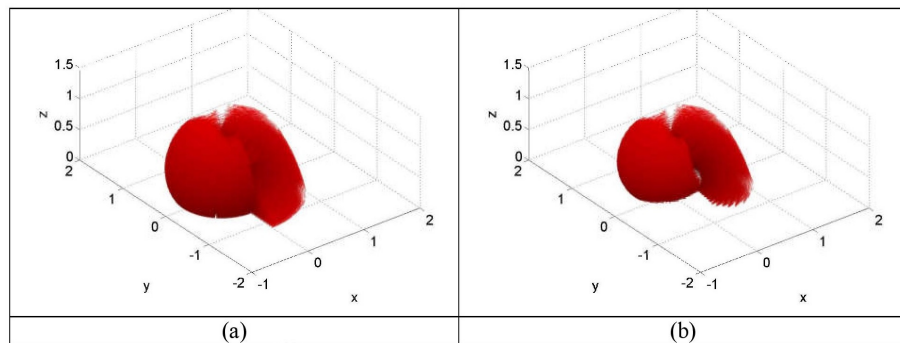


Figure 3.9. a) Reachable Workspace and b) Safe Working Zone

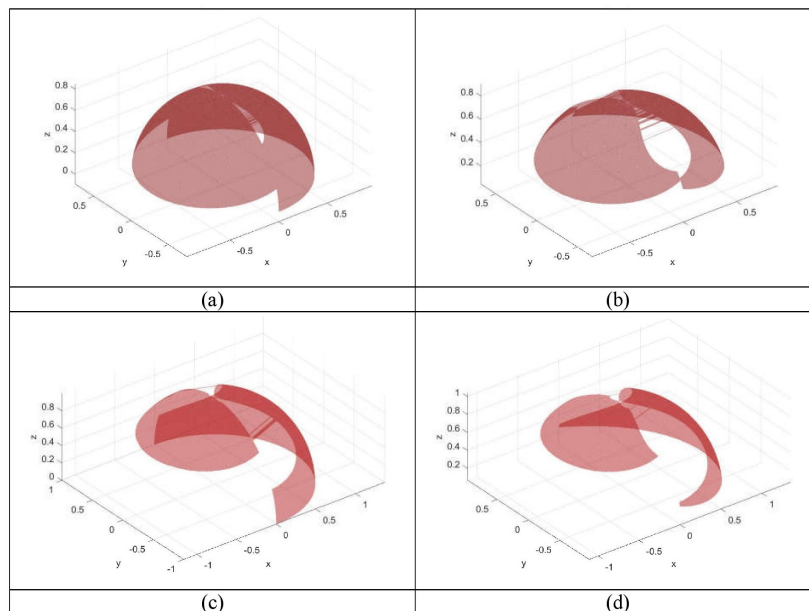


Figure 3.10. Reachable Workspace and Safe Working Zone for: a-b) $O_{7,z} = 750$ mm, c-d) $O_{7,z} = 1000$ mm

3.9. Dynamic Analysis

Dynamic analysis consists of obtaining the required input torques in order to track a desired trajectory (inverse dynamics) or obtaining the trajectory of the moving platform with given input torques (forward dynamics). In this thesis study, only inverse dynamics of the 3-RRS PM is formulated. In order to formulate the inverse dynamics of the 3-RRS PM, firstly velocities and accelerations of mass centers are determined. Then the forces on the system are defined. At the end, the analytical dynamic models of the system which is obtained by using virtual work method and Lagranges's approach are presented.

3.9.1. Mass Center Positions, Velocities and Accelerations

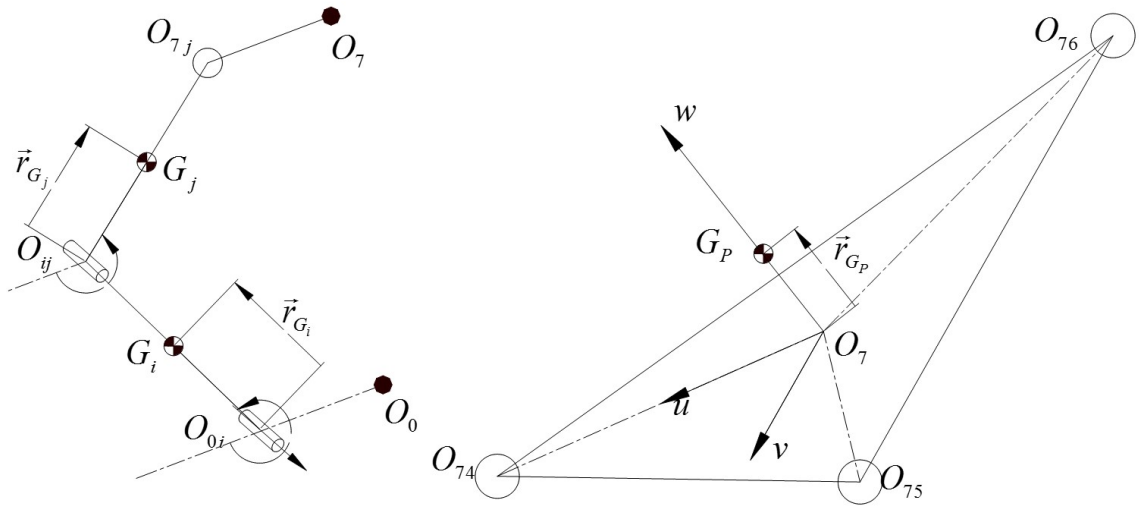


Figure 3.11. Mass Centers

Starting from the lower link at i^{th} limb, the distance of the mass center G_i from point O_{1i} is shown with d_1 and its mass is m_1 . The distance of the mass center G_j of the upper link at i^{th} limb from point O_{ij} is denoted by d_2 and mass is shown with m_2 . Due to symmetric construction of the limbs, G_i and G_j are assumed to lie on $O_{0i}O_{ij}$ and $O_{ij}O_{7j}$, respectively. Since the cross section of the moving platform is an equilateral triangle, the

center of mass lies on the w -axis. The distance of the mass center of the platform from point O_7 along w -axis is shown with d_p and its mass is called m_p as presented in Figure 3.11. The position, velocity and acceleration of G_i can be formulated as:

$$\bar{p}_{G_i} = \overline{O_0 G_i} = \begin{bmatrix} c \alpha_{1i} (b + d_1 c \theta_i) \\ s \alpha_{1i} (b + d_1 c \theta_i) \\ -d_1 s \theta_i \end{bmatrix} \quad (3.54)$$

$$\bar{v}_{G_i} = \dot{\bar{p}}_{G_i} = \mathbf{J}_{\theta_i, G_i} \dot{\theta}_i \quad (3.55)$$

where

$$\mathbf{J}_{\theta_i, G_i} = - \begin{bmatrix} d_1 c \alpha_{1i} s \theta_i \\ d_1 s \alpha_{1i} s \theta_i \\ d_1 c \theta_i \end{bmatrix}$$

$$\bar{a}_{G_i} = \ddot{\bar{p}}_{G_i} = \dot{\mathbf{J}}_{\theta_i, G_i} \dot{\theta}_i + \mathbf{J}_{\theta_i, G_i} \ddot{\theta}_i \quad (3.56)$$

where

$$\dot{\mathbf{J}}_{\theta_i, G_i} = \begin{bmatrix} -d_1 c \alpha_{1i} c \theta_i \\ -d_1 s \alpha_{1i} c \theta_i \\ d_1 s \theta_i \end{bmatrix} \dot{\theta}_i$$

The position, velocity and acceleration of G_j are formulated as:

$$\bar{p}_{G_j} = \overline{O_0 G_j} = \begin{bmatrix} c \alpha_{1i} (b + l_1 c \theta_i + d_2 c \phi_i) \\ s \alpha_{1i} (b + l_1 c \theta_i + d_2 c \phi_i) \\ -l_1 s \theta_i - d_2 s \phi_i \end{bmatrix} \quad (3.57)$$

$$\bar{v}_{G_j} = \dot{\bar{p}}_{G_j} = \mathbf{J}_{\theta_i, G_j} \dot{\theta}_i + \mathbf{J}_{\phi_i, G_j} \dot{\phi}_i \quad (3.58)$$

where

$$\mathbf{J}_{\theta_i, G_j} = - \begin{bmatrix} l_1 c \alpha_{1i} s \theta_i \\ l_1 s \alpha_{1i} s \theta_i \\ l_1 c \theta_i \end{bmatrix}$$

and

$$\mathbf{J}_{\phi_i, G_j} = - \begin{bmatrix} d_2 c \alpha_{1i} s \phi_i \\ d_2 s \alpha_{1i} s \phi_i \\ d_2 c \phi_i \end{bmatrix}$$

$$\bar{a}_{G_j} = \ddot{\bar{p}}_{G_j} = \mathbf{J}_{\theta_i, G_j} \ddot{\theta}_i + \mathbf{J}_{\theta_i, G_j} \dot{\theta}_i + \mathbf{J}_{\phi_i, G_j} \dot{\phi}_i + \mathbf{J}_{\phi_i, G_j} \ddot{\phi}_i \quad (3.59)$$

where

$$\mathbf{J}_{\theta_i, G_j} = \begin{bmatrix} -l_1 c \alpha_{1i} c \theta_i \\ -l_1 s \alpha_{1i} c \theta_i \\ l_1 s \theta_i \end{bmatrix} \dot{\theta}_i$$

and

$$\mathbf{J}_{\phi_i, G_j} = \begin{bmatrix} l_1 c \alpha_{1i} s \theta_i \\ l_1 s \alpha_{1i} s \theta_i \\ l_1 c \theta_i \end{bmatrix} \dot{\phi}_i$$

The mass center of the platform:

$$\bar{p}_{G_P} = \overline{O_0 G_P} = \vec{r}_P + \begin{bmatrix} d_p s \psi_y \\ -d_p s \psi_x c \psi_y \\ d_p c \psi_x c \psi_y \end{bmatrix} \quad (3.60)$$

$$\bar{v}_{G_P} = \dot{\bar{p}}_{G_P} = \dot{\vec{r}}_P + \mathbf{J}_{\psi, G_P} \dot{\psi} \quad (3.61)$$

where

$$\mathbf{J}_{\psi, G_P} = \begin{bmatrix} 0 & d_p c \psi_y & 0 \\ -d_p c \psi_x c \psi_y & d_p s \psi_x s \psi_y & 0 \\ -d_p c \psi_y s \psi_x & -d_p c \psi_x s \psi_y & 0 \end{bmatrix}$$

$$\bar{a}_{G_P} = \ddot{\bar{p}}_{G_P} = \ddot{\vec{r}}_P + \mathbf{J}_{\psi, G_P} \dot{\psi} + \mathbf{J}_{\psi, G_P} \ddot{\psi} \quad (3.62)$$

where

$$\mathbf{J}_{\psi, G_P} = d_p \begin{bmatrix} 0 & -s \psi_y \dot{\psi}_y & 0 \\ \left(s \psi_x c \psi_y \dot{\psi}_x + c \psi_x s \psi_y \dot{\psi}_y \right) & \left(c \psi_x s \psi_y \dot{\psi}_x + s \psi_x c \psi_y \dot{\psi}_y \right) & 0 \\ \left(s \psi_x s \psi_y \dot{\psi}_y - c \psi_x c \psi_y \dot{\psi}_x \right) & \left(s \psi_x s \psi_y \dot{\psi}_x - c \psi_x c \psi_y \dot{\psi}_y \right) & 0 \end{bmatrix}$$

3.9.2. Inertial, Gravitational and External Forces and Moments

The internal forces (composed of gravitational and inertial forces) acting on the lower limbs, upper limbs and the moving platform can be formulated as:

$$\bar{F}_i^{\text{int}} = m_1 (\bar{g} + \bar{a}_{G_i}) \quad (3.63)$$

$$\bar{F}_j^{\text{int}} = m_2 (\bar{g} + \bar{a}_{G_j}) \quad (3.64)$$

$$\bar{F}_P^{\text{int}} = m_P (\bar{g} + \bar{a}_{G_P}) \quad (3.65)$$

where $\bar{g} = [0 \ 0 \ -9.81]^T$. The inertial moments occurring on the links and platform can be expressed as:

$$\bar{M}_1^{\text{in}} = I_{1,yy} [\ddot{\theta}_1 \ \ddot{\theta}_2 \ \ddot{\theta}_3]^T \quad (3.66)$$

$$\bar{M}_2^{\text{in}} = I_{2,yy} [\ddot{\phi}_1 \ \ddot{\phi}_2 \ \ddot{\phi}_3]^T \quad (3.67)$$

$$\bar{M}_P^{\text{in}} = \mathbf{I}_P \bar{\alpha}_P \quad (3.68)$$

where $I_{1,yy}$ and $I_{2,yy}$ are the yy - component of the moments of inertia of the lower and upper limbs about their centers of masses, \mathbf{I}_P is the moment of inertia matrix of the mobile platform and $\bar{\alpha}_P$ is the angular acceleration array of the moving platform with respect to the fixed frame. $\bar{\alpha}_P$ is calculated as:

$$\begin{aligned} \tilde{\omega}_P = \dot{\mathbf{R}}\mathbf{R}^T &= \begin{bmatrix} 0 & -\omega_z & \omega_y \\ \omega_z & 0 & -\omega_x \\ -\omega_y & \omega_x & 0 \end{bmatrix} \Rightarrow \bar{\omega}_P = \begin{bmatrix} \omega_x \\ \omega_y \\ \omega_z \end{bmatrix} = \mathbf{J}_{t,\omega} \dot{t} \\ &\Rightarrow \bar{\alpha}_P = \dot{\mathbf{J}}_{t,\omega} \dot{t} + \mathbf{J}_{t,\omega} \ddot{t} \end{aligned} \quad (3.69)$$

where

$$\mathbf{J}_{t,\omega} = \begin{bmatrix} 0 & 0 & 0 & 1 & 0 & s\psi_y \\ 0 & 0 & 0 & 0 & c\psi_x & -s\psi_x c\psi_y \\ 0 & 0 & 0 & 0 & s\psi_x & c\psi_x c\psi_y \end{bmatrix}$$

and

$$\dot{\mathbf{J}}_{t,\omega} = \begin{bmatrix} 0 & 0 & 0 & 0 & 0 & c\psi_y \dot{\psi}_y \\ 0 & 0 & 0 & 0 & -s\psi_x \dot{\psi}_x & s\psi_x s\psi_y \dot{\psi}_y - c\psi_x c\psi_y \dot{\psi}_x \\ 0 & 0 & 0 & 0 & c\psi_x \dot{\psi}_x & -s\psi_x c\psi_y \dot{\psi}_x - c\psi_x s\psi_y \dot{\psi}_y \end{bmatrix}$$

The equivalent external force acting on the center of the mobile platform are formulated as:

$$\bar{F}_P^{ext} = \begin{bmatrix} F_x^{ext} & F_y^{ext} & F_z^{ext} \end{bmatrix}^T \quad (3.70)$$

The input torques applied on the active revolute joints are formulated as:

$$\bar{\tau}^a = \begin{bmatrix} \tau_1 & \tau_2 & \tau_3 \end{bmatrix}^T \quad (3.71)$$

3.9.3. Virtual Work Method

For the dynamic analysis of the 3-RRS PM, virtual work method can be applied as follows:

$$\left\{ \begin{array}{l} \dot{\theta}^T \bar{\tau}^a + \bar{v}_P^T \bar{F}_P^{ext} + \bar{v}_{G_P}^T \bar{F}_P^{int} + \bar{\omega}_P^T \bar{M}_P^{in} + \\ \sum_{i=1}^3 \bar{v}_{G_i}^T \bar{F}_i^{int} + \sum_{j=1}^3 \bar{v}_{G_j}^T \bar{F}_j^{int} + \dot{\theta}^T \bar{M}_{G_1}^{in} + \dot{\phi}^T \bar{M}_{G_2}^{in} \end{array} \right\} = 0 \quad (3.72)$$

When the virtual displacements are written in terms of $\dot{\bar{x}}_i$:

$$\dot{\bar{x}}_i^T \left\{ \begin{array}{l} \mathbf{J}_{x_i, \theta}^T \bar{\tau}^a + \mathbf{J}_{x_i, P}^T \bar{F}_P^{ext} + \mathbf{J}_{x_i, G_P}^T \bar{F}_P^{int} + \mathbf{J}_{x_i, \omega}^T \bar{M}_P^{in} + \\ \sum_{i=1}^3 \mathbf{J}_{x_i, P_{G_i}}^T \bar{F}_i^{int} + \sum_{j=1}^3 \mathbf{J}_{x_i, P_{G_j}}^T \bar{F}_j^{int} + \mathbf{J}_{x_i, \theta}^T \bar{M}_{G_1}^{in} + \mathbf{J}_{x_i, \phi}^T \bar{M}_{G_2}^{in} \end{array} \right\} = 0 \quad (3.73)$$

For known external forces and torques acting on the moving platform, the required input torques can be determined as:

$$\bar{\tau}^a = -(\mathbf{J}_{x_i, \theta}^T)^{-1} \left\{ \begin{array}{l} \mathbf{J}_{x_i, P}^T \bar{F}_P^{ext} + \mathbf{J}_{x_i, G_P}^T \bar{F}_P^{int} + \mathbf{J}_{x_i, \omega}^T \bar{M}_P^{in} + \\ \sum_{i=1}^3 \mathbf{J}_{x_i, P_{G_i}}^T \bar{F}_i^{int} + \sum_{j=1}^3 \mathbf{J}_{x_i, P_{G_j}}^T \bar{F}_j^{int} + \mathbf{J}_{x_i, \theta}^T \bar{M}_{G_1}^{in} + \mathbf{J}_{x_i, \phi}^T \bar{M}_{G_2}^{in} \end{array} \right\} \quad (3.74)$$

3.9.4. Lagrange's Approach

n^{th} Lagrange's equation for the dynamics of the 3-RRS PM is written as:

$$\sum_{k=1}^9 \lambda_k \frac{\partial \Gamma_k}{\partial q_n} = L_n - Q_n^* \quad (3.75)$$

where λ_k s are Lagrange's multipliers, Γ_k s are constraint equations, q_n is n^{th} generalized coordinate, L is the Lagrangian function, $L_n = \frac{d}{dt} \left(\frac{\partial L}{\partial \dot{q}_n} \right) - \frac{\partial L}{\partial q_n}$ and Q_n^* is the corresponding generalized force.

In the inverse dynamic analysis, generalized coordinates (\bar{q}) include all of the joint and task space parameters:

$$\bar{q} = \left[\bar{\theta}^T \quad \bar{\phi}^T \quad \bar{O}_7^T \quad \bar{\psi}^T \right]^T \quad (3.76)$$

In order to formulate the Lagrangian function, the kinetic and potential energies of the moving platform and links should be formulated. The kinetic energies of the i^{th} lower and upper limbs and the moving platform can be formulated as:

$$\begin{aligned} KE_i &= \frac{1}{2} (I_{1,yy} + m_1 d_1^2) \dot{\theta}_i^2 \\ KE_j &= \frac{1}{2} \left[m_2 l_1^2 \dot{\theta}_i^2 + (I_{2,yy} + m_2 d_2^2) \dot{\phi}_i^2 + 2m_2 l_1 d_2 c(\theta_i - \phi_i) \dot{\phi}_i \dot{\theta}_i \right] \\ KE_P &= \frac{1}{2} \left[m_p V_{G_P}^2 + \bar{\omega}_P^T \mathbf{I}_P \bar{\omega}_P \right] \end{aligned} \quad (3.77)$$

The potential energy expressions of i^{th} the lower and upper limbs and the moving platform can be formulated as:

$$\begin{aligned} PE_i &= -g d_1 s \theta_i \\ PE_j &= -g (l_1 s \theta_i + d_2 s \phi_i) \\ PE_P &= g (O_{7,z} + d_p c \psi_x c \psi_y) \end{aligned} \quad (3.78)$$

Then the Lagrangian function $L = \sum KE - \sum PE$ can be formulated as:

$$L = \left\{ \begin{aligned} &-g m_P (d_P c \psi_x c \psi_y + O_{7,z}) + d_1 g m_1 s \theta_1 + d_1 g m_1 s \theta_2 + d_1 g m_1 s \theta_3 \\ &\quad -g m_2 (-l_1 s \theta_1 - d_2 s \phi_1) - g m_2 (-l_1 s \theta_2 - d_2 s \phi_2) \\ &\quad -g m_2 (-l_1 s \theta_3 - d_2 s \phi_3) + 0.5 m_P \dot{O}_{7,x}^2 + 0.5 m_P \dot{O}_{7,y}^2 + 0.5 m_P \dot{O}_{7,z}^2 \\ &\quad + 0.5 (I_{G_1} + d_1^2 m_1 + l_1^2 m_2) (\dot{\theta}_1^2 + \dot{\theta}_2^2 + \dot{\theta}_3^2) \\ &\quad + d_2 l_1 m_2 c(\theta_1 - \phi_1) \dot{\theta}_1 \dot{\phi}_1 + d_2 l_1 m_2 c(\theta_2 - \phi_2) \dot{\theta}_2 \dot{\phi}_2 \\ &\quad + d_2 l_1 m_2 c(\theta_3 - \phi_3) \dot{\theta}_3 \dot{\phi}_3 + 0.5 (I_{G_2} + d_2^2 m_2) (\dot{\phi}_1^2 + \dot{\phi}_2^2 + \dot{\phi}_3^2) \\ &\quad + d_P m_P c \psi_y \left(-c \psi_x \dot{O}_{7,y} - s \psi_x \dot{O}_{7,z} \right) \dot{\psi}_x \\ &\quad + (0.5 I_{P,x} + 0.25 d_P^2 m_P + 0.25 d_P^2 m_P c 2 \psi_y) \dot{\psi}_x^2 \\ &+ (0.25 I_{P,y} + 0.25 I_{P,z} + 0.5 d_P^2 m_P + (0.25 I_{P,y} - 0.25 I_{P,z}) c 2 \psi_x) \dot{\psi}_y^2 \\ &\quad + d_P m_P \left(c \psi_y \dot{O}_{7,x} + s \psi_y (s \psi_x \dot{O}_{7,y} - s \psi_x \dot{O}_{7,z}) \right) \dot{\psi}_y \\ &\quad + \left(I_{P,x} s \psi_y \dot{\psi}_x + (-I_{P,y} + I_{P,z}) c \psi_x s \psi_x c \psi_y \dot{\psi}_y \right) \dot{\psi}_z \\ &\quad + 0.5 (I_{P,x} s^2 \psi_y + c^2 \psi_y (I_{P,z} c^2 \psi_x + I_{P,y} s^2 \psi_x)) \dot{\psi}_z^2 \end{aligned} \right\} \quad (3.79)$$

Then L_n term in Equation 3.75 is formulated for $n = 1, 2, \dots, 12$ as:

$$L_1 = \left\{ \begin{array}{l} g(-d_1 m_1 - l_2 m_2) c \theta_1 + d_2 l_2 m_2 s(\theta_1 - \phi_1) \dot{\phi}_1^2 \\ + (I_{1,yy} + d_1^2 m_1 + l_2^2 m_2) \ddot{\theta}_1 + d_2 l_2 m_2 c(\theta_1 - \phi_1) \ddot{\phi}_1 \end{array} \right\} \quad (3.80)$$

$$L_2 = \left\{ \begin{array}{l} g(-d_1 m_1 - l_2 m_2) c \theta_2 + d_2 l_2 m_2 s(\theta_2 - \phi_2) \dot{\phi}_2^2 \\ + (I_{1,yy} + d_1^2 m_1 + l_2^2 m_2) \ddot{\theta}_2 + d_2 l_2 m_2 c(\theta_2 - \phi_2) \ddot{\phi}_2 \end{array} \right\} \quad (3.81)$$

$$L_3 = \left\{ \begin{array}{l} g(-d_1 m_1 - l_2 m_2) c \theta_3 + d_2 l_2 m_2 s(\theta_3 - \phi_3) \dot{\phi}_3^2 \\ + (I_{1,yy} + d_1^2 m_1 + l_2^2 m_2) \ddot{\theta}_3 + d_2 l_2 m_2 c(\theta_3 - \phi_3) \ddot{\phi}_3 \end{array} \right\} \quad (3.82)$$

$$L_4 = -d_2 g m_2 c \phi_1 + I_{2,yy} \ddot{\phi}_1 + d_2 m_2 \left(\begin{array}{l} -l_2 s(\theta_1 - \phi_1) \dot{\theta}_1^2 + \\ l_2 c(\theta_1 - \phi_1) \ddot{\theta}_1 + d_2 \ddot{\phi}_1 \end{array} \right) \quad (3.83)$$

$$L_5 = -d_2 g m_2 c \phi_2 + I_{2,yy} \ddot{\phi}_2 + d_2 m_2 \left(\begin{array}{l} -l_2 s(\theta_2 - \phi_2) \dot{\theta}_2^2 + \\ l_2 c(\theta_2 - \phi_2) \ddot{\theta}_2 + d_2 \ddot{\phi}_2 \end{array} \right) \quad (3.84)$$

$$L_6 = -d_2 g m_2 c \phi_3 + I_{2,yy} \ddot{\phi}_3 + d_2 m_2 \left(\begin{array}{l} -l_2 s(\theta_3 - \phi_3) \dot{\theta}_3^2 + \\ l_2 c(\theta_3 - \phi_3) \ddot{\theta}_3 + d_2 \ddot{\phi}_3 \end{array} \right) \quad (3.85)$$

$$L_7 = m_P \left(-d_P s \psi_y \dot{\psi}_y^2 + \ddot{O}_{7,x} + d_P c \psi_y \ddot{\psi}_y \right) \quad (3.86)$$

$$L_8 = m_P \left(\ddot{O}_{7,y} + d_P \left(\begin{array}{l} s \psi_x c \psi_y \dot{\psi}_x^2 + 2 c \psi_x s \psi_y \dot{\psi}_x \dot{\psi}_y + \\ s \psi_x c \psi_y \dot{\psi}_y^2 - c \psi_x c \psi_y \ddot{\psi}_x + s \psi_x s \psi_y \ddot{\psi}_y \end{array} \right) \right) \quad (3.87)$$

$$L_9 = m_P \left(g + \ddot{O}_{7,z} + d_P \left(\begin{array}{l} -c \psi_x c \psi_y \dot{\psi}_x^2 + 2 s \psi_x s \psi_y \dot{\psi}_x \dot{\psi}_y - \\ c \psi_x c \psi_y \dot{\psi}_y^2 - s \psi_x c \psi_y \ddot{\psi}_x - c \psi_x s \psi_y \ddot{\psi}_y \end{array} \right) \right) \quad (3.88)$$

$$L_{10} = \left\{ \begin{array}{l} -d_P g m_P s \psi_x c \psi_y - d_P^2 m_P s 2 \psi_y \dot{\psi}_x \dot{\psi}_y + 0.5 (I_{P,y} - I_{P,z}) s 2 \psi_x \dot{\psi}_y^2 - \\ d_P m_P c \psi_x c \psi_y \ddot{O}_{7,y} + (I_{P,x} + (I_{P,y} - I_{P,z}) c 2 \psi_x) c \psi_y \dot{\psi}_y \dot{\psi}_z - \\ I_{P,y} c \psi_x s \psi_x c^2 \psi_y \dot{\psi}_z^2 + 0.5 I_{P,z} s 2 \psi_x c^2 \psi_y \dot{\psi}_z^2 - d_P m_P s \psi_x c \psi_y \ddot{O}_{7,z} + \\ I_{P,x} \ddot{\psi}_x + 0.5 d_P^2 m_P \ddot{\psi}_x + 0.5 d_P^2 m_P c 2 \psi_y \ddot{\psi}_x + I_{P,x} s \psi_y \ddot{\psi}_z \end{array} \right\} \quad (3.89)$$

$$L_{11} = \left\{ \begin{array}{l} -d_P g m_P c \psi_x s \psi_y + 0.5 d_P^2 m_P s 2\psi_y \dot{\psi}_x^2 \\ + 0.5 (I_{P,z} c^2 \psi_x s 2\psi_y + (-I_{P,x} + I_{P,y} s^2 \psi_x) s 2\psi_y) \dot{\psi}_z^2 \\ + \dot{\psi}_x \left(-I_{P,x} c \psi_y \dot{\psi}_z + (-I_{P,y} + I_{P,z}) (s 2\psi_x \dot{\psi}_y + c 2\psi_x c \psi_y \dot{\psi}_z) \right) \\ + d_P m_P c \psi_y \ddot{\Gamma}_{7,x} + d_P m_P s \psi_x s \psi_y \ddot{\Gamma}_{7,y} \\ - d_P m_P c \psi_x s \psi_y \ddot{\Gamma}_{7,z} + 0.5 (I_{P,y} + I_{P,z}) \ddot{\psi}_y \\ + d_P^2 m_P \ddot{\psi}_y + 0.5 c 2\psi_x (I_{P,y} - I_{P,z}) \ddot{\psi}_y \\ - 0.5 s 2\psi_x c \psi_y (I_{P,y} - I_{P,z}) \ddot{\psi}_z \end{array} \right\} \quad (3.90)$$

$$L_{12} = \left\{ \begin{array}{l} 0.5 (I_{P,y} - I_{P,z}) s 2\psi_x s \psi_y \dot{\psi}_y^2 + \\ (-I_{P,z} c^2 \psi_x + (I_{P,x} - I_{P,y} s^2 \psi_x)) s 2\psi_y \dot{\psi}_y \dot{\psi}_z \\ + (I_{P,x} + (-I_{P,y} + I_{P,z}) c 2\psi_x) c \psi_y \dot{\psi}_x \dot{\psi}_y \\ + (I_{P,y} - I_{P,z}) s 2\psi_x c^2 \psi_y \dot{\psi}_x \dot{\psi}_z \\ + \left(0.5 (-I_{P,y} + I_{P,z}) s 2\psi_x c \psi_y \ddot{\psi}_y \right) \\ + (I_{P,z} c^2 \psi_x + I_{P,y} s^2 \psi_x) c^2 \psi_y \ddot{\psi}_z \\ + I_{P,x} s \psi_y (\ddot{\psi}_x + s \psi_y \ddot{\psi}_z) \end{array} \right\} \quad (3.91)$$

The generalized forces are defined as input torques (τ_1^a , τ_2^a and τ_3^a) for $n = 1, 2, 3$ and external force components acting on point $O_{7,z}$ (F_x^{ext} , F_y^{ext} and F_z^{ext}) for $n = 7, 8, 9$. With the formulation of L_n , all terms at the right-hand side of Equation 3.75 are formulated. For the left-hand side of the equation, constraint equations Γ_k correspond to the scalar components of the Equations 3.4 , 3.5 and 3.6. With the formulations presented above, first the numerical values of the Lagrange multipliers are found as:

$$\begin{pmatrix} \lambda_1 \\ \lambda_2 \\ \lambda_3 \\ \lambda_4 \\ \lambda_5 \\ \lambda_6 \\ \lambda_7 \\ \lambda_8 \\ \lambda_9 \end{pmatrix} = \begin{pmatrix} \partial\Gamma_1/\partial\phi_1 & \partial\Gamma_2/\partial\phi_1 & \dots & \partial\Gamma_9/\partial\phi_1 \\ \partial\Gamma_1/\partial\phi_2 & \partial\Gamma_2/\partial\phi_2 & \dots & \partial\Gamma_9/\partial\phi_2 \\ \vdots & \vdots & \vdots & \vdots \\ \partial\Gamma_1/\partial\psi_z & \partial\Gamma_2/\partial\psi_z & \dots & \partial\Gamma_9/\partial\psi_z \end{pmatrix}_{9 \times 9}^{-1} \begin{pmatrix} L_4 \\ L_5 \\ L_6 \\ L_7 - F_x^{ext} \\ L_8 - F_y^{ext} \\ L_9 - F_z^{ext} \\ L_{10} \\ L_{11} \\ L_{12} \end{pmatrix} \quad (3.92)$$

Once the Lagrange multipliers are obtained using Equation 3.92, the input torques can be found as:

$$\begin{pmatrix} L_1 \\ L_2 \\ L_3 \end{pmatrix} + \begin{pmatrix} \partial\Gamma_1/\partial\theta_1 & \partial\Gamma_2/\partial\theta_1 & \dots & \partial\Gamma_9/\partial\theta_1 \\ \partial\Gamma_1/\partial\theta_2 & \partial\Gamma_2/\partial\theta_2 & \dots & \partial\Gamma_9/\partial\theta_2 \\ \partial\Gamma_1/\partial\theta_3 & \partial\Gamma_2/\partial\theta_3 & \dots & \partial\Gamma_9/\partial\theta_3 \end{pmatrix} \begin{pmatrix} \lambda_1 \\ \lambda_2 \\ \lambda_3 \\ \lambda_4 \\ \lambda_5 \\ \lambda_6 \\ \lambda_7 \\ \lambda_8 \\ \lambda_9 \end{pmatrix} = \begin{pmatrix} \tau_1^a \\ \tau_2^a \\ \tau_3^a \end{pmatrix} \quad (3.93)$$

CHAPTER 4

DYNAMIC SIMULATIONS

In order to confirm the mathematical model developed in Chapter 3, several simulations are run using MATLAB/Simulink[®] software. In this chapter, firstly the mechanical structure of the PM is explained, and then the performed simulations are presented.

4.1. Mechanical Structure of the PM

The mathematical models formed in the Chapter 3 are used to model the 3-RRS manipulator in IzTech Rasim Alizade Mechatronics Laboratory. Starting with the mechanical components from bottom to top, the base part of the manipulator is fixed on a concrete block as presented in Figure 4.1. The radius of the base circle is $b = 544$ mm.

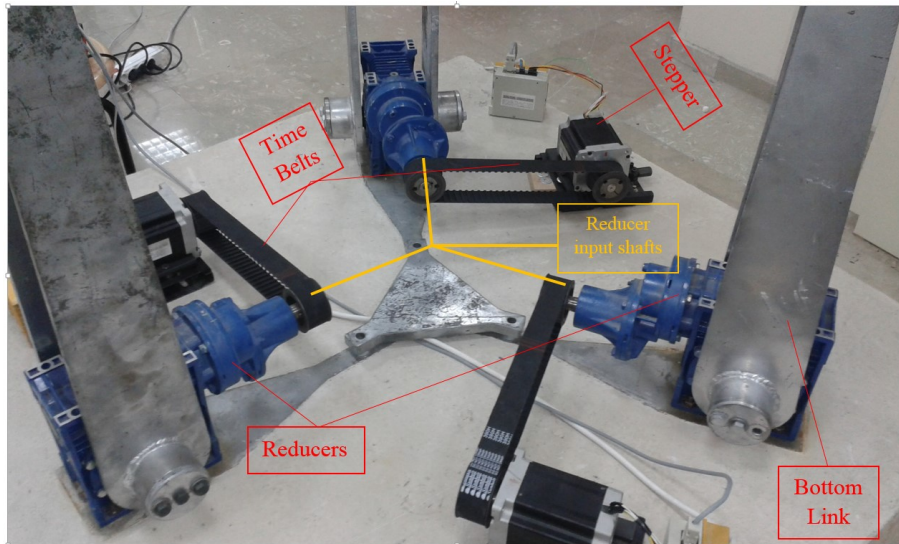


Figure 4.1. Manipulator's Base and Its Components

3 reducers fixed on the base are attached to the lower limbs. The axes of input shafts of the reducers meet at the base center of the circle and have 120° between each

other. The output shaft of the reducers are tangent to the base circle. Reducers have 1/149 reduction ratio and their brand and model is Yılmaz Redüktör oil filled EN080-00+NT101.

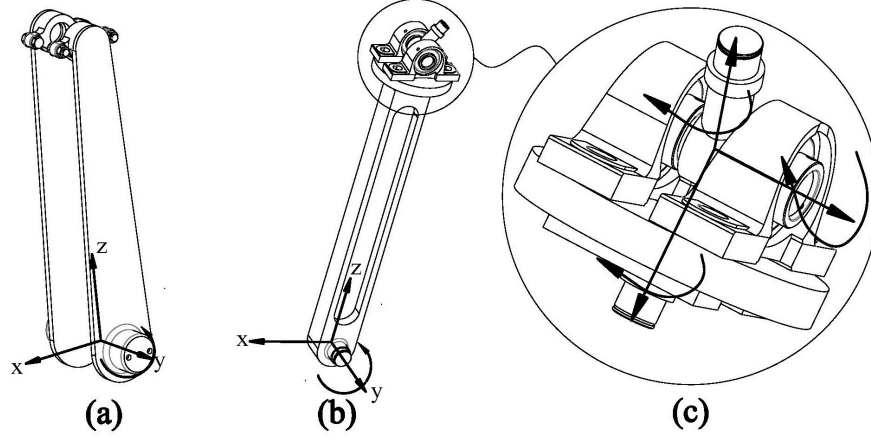


Figure 4.2. a) Lower Limb, b) Upper Limb and c) Spherical Joint

Lower limbs are attached to the reducer from their local coordinate frames as presented in Figure 4.2. Each lower limb is symmetrical with respect to its local xz -plane. The effective lengths of the lower limbs are $l_1 = 700$ mm and upper limbs are $l_2 = 775$ mm. Center of mass of each link lies on local z -axis and their distances from local coordinate frames are found as $d_1 = 200$ mm and $d_2 = 420$ mm using Solidworks[®] CAD models of the parts. The mass of the lower limb including all the fasteners and flanges is measured as $m_1 = 28.55$ kg and the inertia tensor is found as $I_1 = [2.18, 0, 0; 0, 2.02, 0; 0, 0, 0.21]$ kg.m². The mass of the upper limb is measured as $m_2 = 25.32$ kg and inertia tensor is $I_2 = [2.08, 0, 0; 0, 2.09, 0; 0, 0, 0.05]$ kg.m² including the spherical joint parts attached (See Figure 4.2c).

Figure 4.3 presents the 3D view of the moving platform. The radius of the platform circle is $p = 544$ mm. By using the CAD model of the part, the distance of the center of mass from the plane passing through points O_{74} , O_{75} and O_{76} is found as $d_P = 150$ mm along the w -axis. The mass of the moving platform including all fasteners and bearings is measured as 35.87 kg and the inertia tensor is found as $I_P = [0.27, 0, 0; 0, 0.27, 0; 0, 0, 0.54]$ kg.m².

Other than masses of the links, an external force applied on point $O_{7,z}$ and a payload attached to the moving platform with a distance of $d_P = 250$ mm along w -axis are

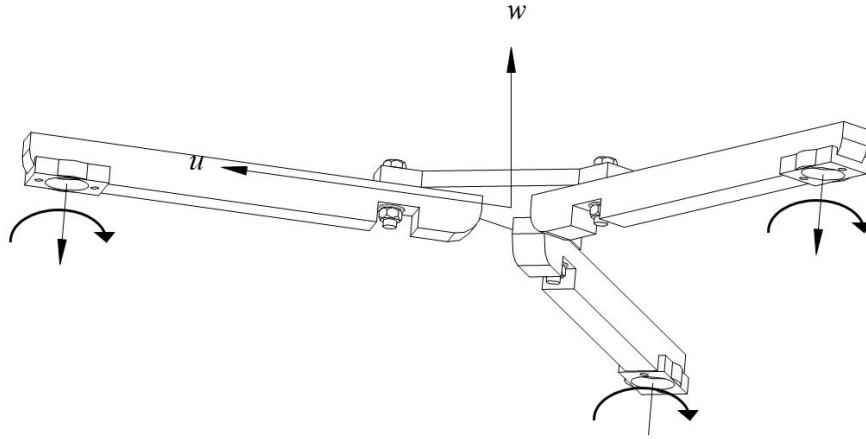


Figure 4.3. Moving Platform

considered. For illustration the force vector is taken as $F^{ext} = [100 \ 200 \ 150]^T$ N and the mass of the payload is taken as $m_L = 50$ kg. The inertia tensor of the payload is taken as $I_L = [1, 0, 0; 0, 0.7, 0; 0, 0, 1.3]$ kg.m². The effects of the external force and payload are added to the inverse dynamic formulation given in Chapter 3.

4.2. Inverse Dynamic Model

A dynamic motion simulation is prepared to simulate the behavior of the joints and moving platform in MATLAB/Simulink[®] environment. In this simulation, the equations for inverse kinematics and dynamics derived in Chapter 3 are used to simulate the motion of the PM in task and joint spaces. The step size used in the simulation is 0.0001 s and solver type is assigned as ODE4 (Runge-Kutta order 4 integrator).

To start the simulation, a path for the moving platform is generated. In order to avoid infinite jerks, the non-stationary motion parts of the moving platform is modelled as trapezoidal jerk motion by using Repeating Sequence blocks. The displacement values of the independent task space parameters are presented in Figure 4.4. The z - displacement is from 332 mm, where all of active joints (θ_i) are equal to zero, to 1000 mm and the amount of rotations (ψ_x and ψ_y) are $\pm 15^\circ$.

For the given trajectory of the moving platform, the displacement, velocity and acceleration of each active and passive R joints are obtained by implementing inverse

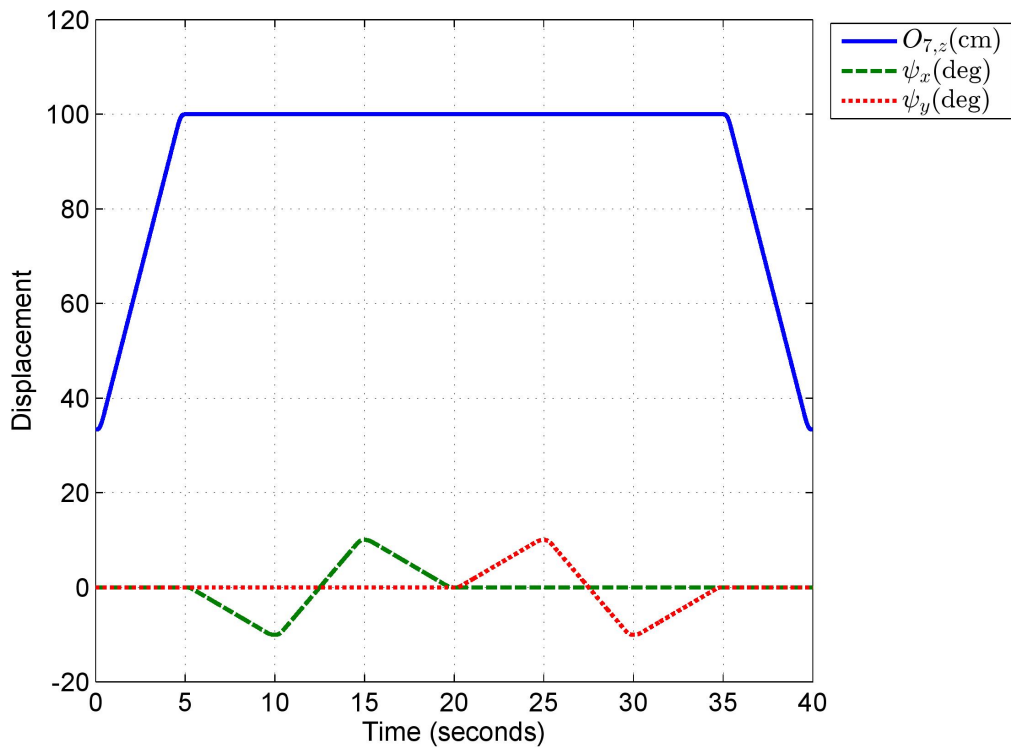


Figure 4.4. Trajectory of the Task Space

kinematic analysis formulation given in the Chapter 3 into MATLAB Function blocks and the displacement, velocity and acceleration variations for the active and passive joint variables are obtained as in Figures 4.5-4.10.

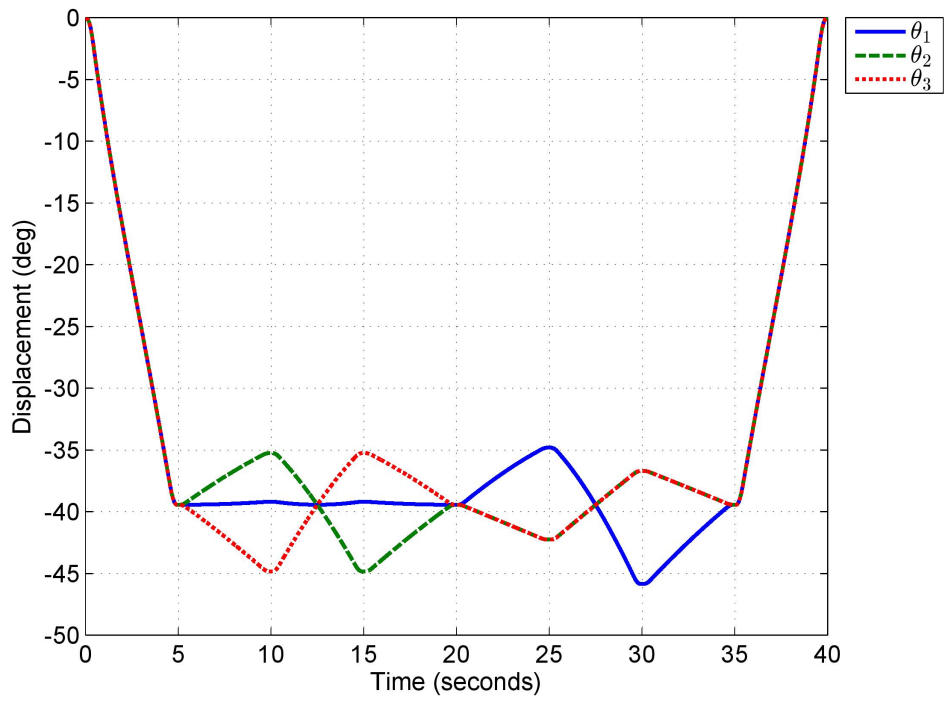


Figure 4.5. Active R Joint Displacements

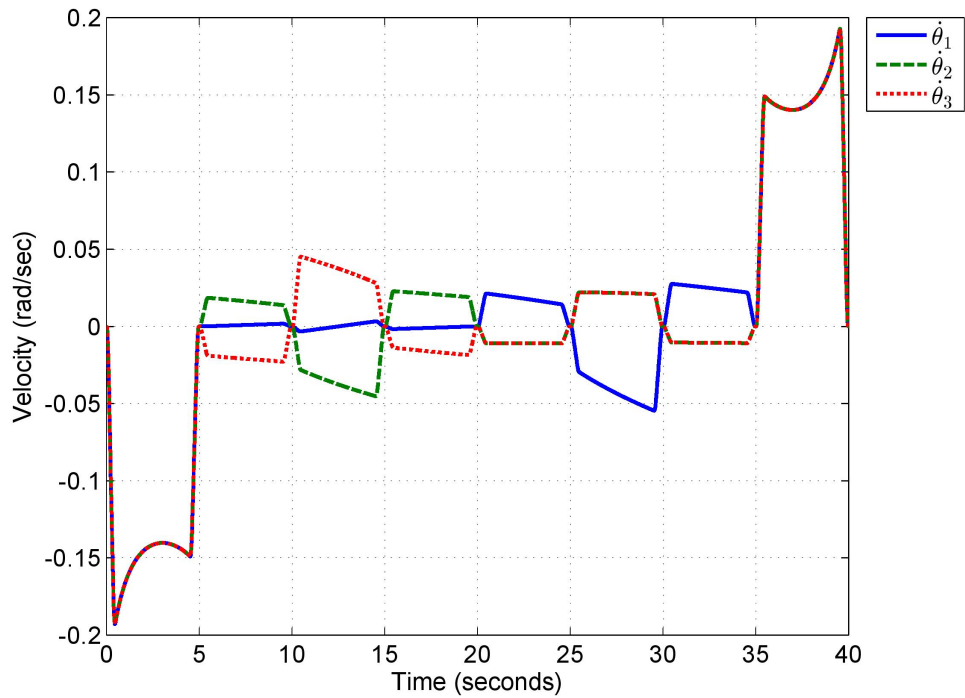


Figure 4.6. Active R Joint Velocity

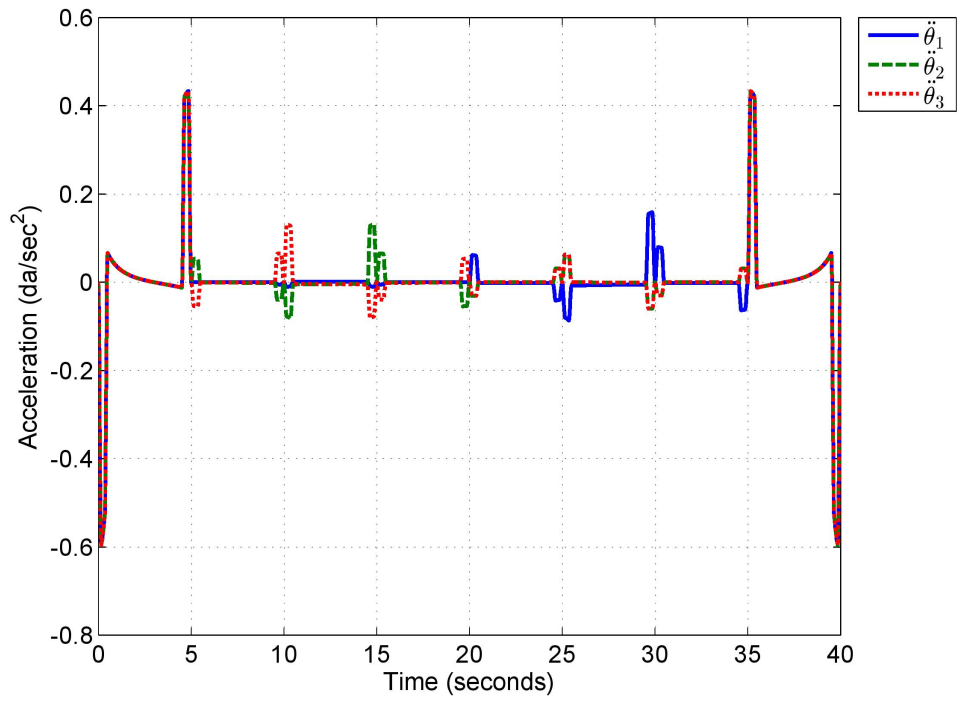


Figure 4.7. Active R Joint Acceleration

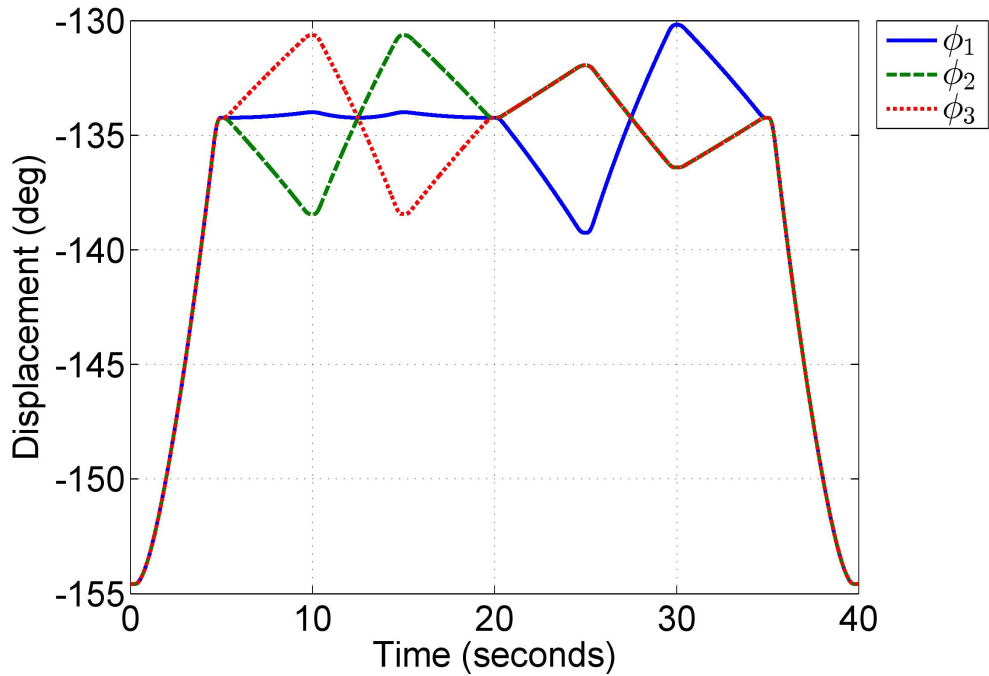


Figure 4.8. Passive R Joint Displacement

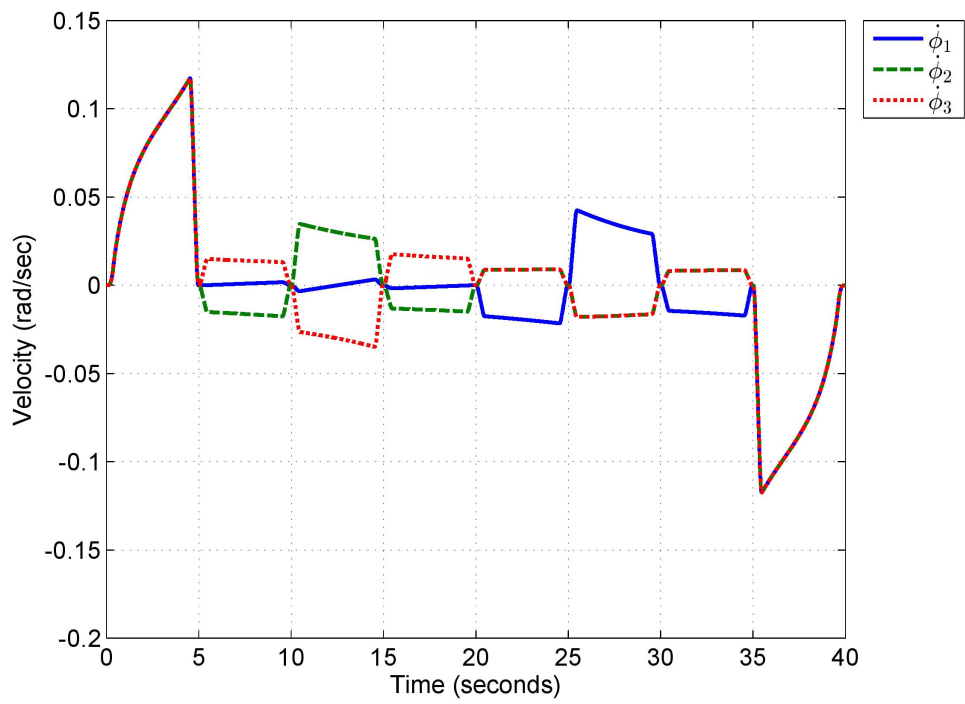


Figure 4.9. Passive R Joint Velocity

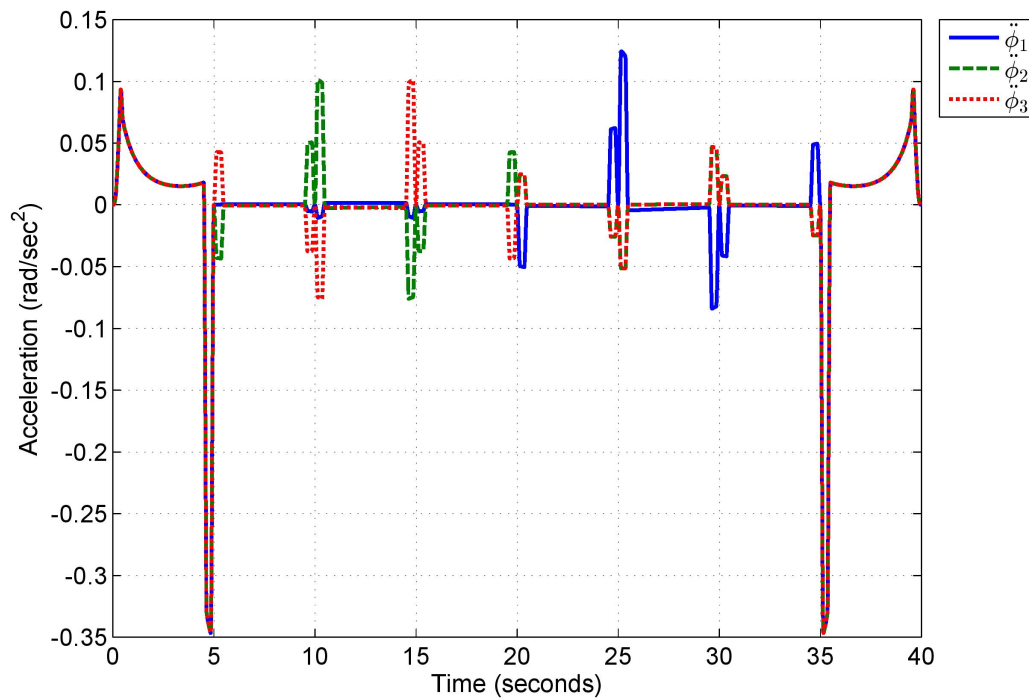


Figure 4.10. Passive R Joint Acceleration

After obtaining all of the task and joint space parameters, the required input torques are found by implementing the formulations given in Chapter 3 into a MATLAB Function block. Inverse dynamic analysis is performed for both virtual work and Lagrange's dynamics methods for verification purposes. The variations of the input torques required to track the desired trajectory are presented in Figure 4.11.

As expected, the input torques obtained for both methods are the same. To obtain the required motor displacements, velocities and accelerations, input link values are divided by the reduction ratio of $1/149$. The torque requirements from the motors are obtained by multiplying input torque values with the reduction ratio again.

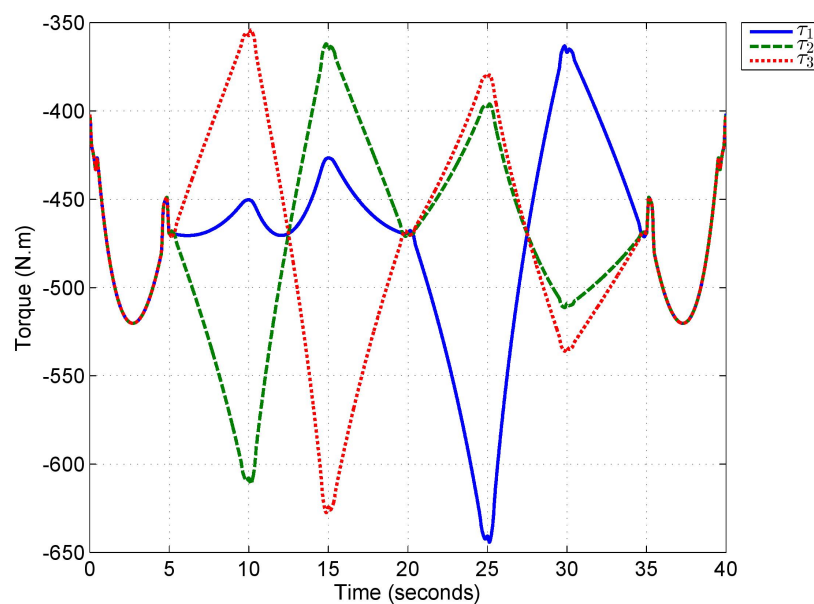


Figure 4.11. Required Input Torques

4.3. SimMechanics Model

Besides the analytical model, a virtual model of the 3-RRS PM is created in MATLAB/Simulink[®] environment using SimMechanics[®] blocks. As the first step, the structural parameters like link lengths, masses, initial conditions of bodies and joints etc. are defined as "InitFcn" under the "Callbacks" tab of "Model Explorer" window. Then, the manipulator is modelled by using SimMechanics[®] blocks. A sample block that rep-

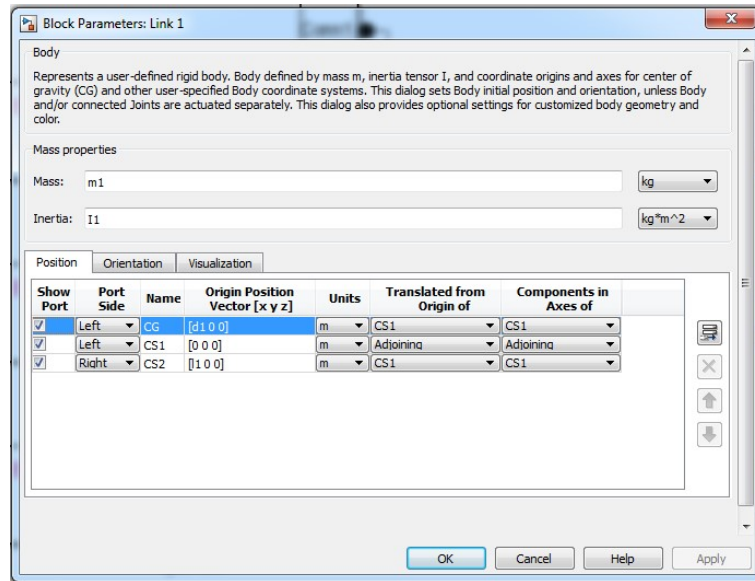


Figure 4.12. Body Block of the Bottom Link at Limb 1

resents the body block of a lower limb is presented in Figure 4.12. With the "Body" and "Joint" blocks, a virtual model of the 3-RRS PM is obtained. The parameters of the body and joint blocks are taken from previously defined "InitFcn" and assigned to the blocks presented in Figure 4.12.

Limbs are connected by the base and the platform blocks. The overall block diagram of the 3-RRS PM is presented in Figure 4.13. The virtual model of the PM is presented in Figure 4.14.

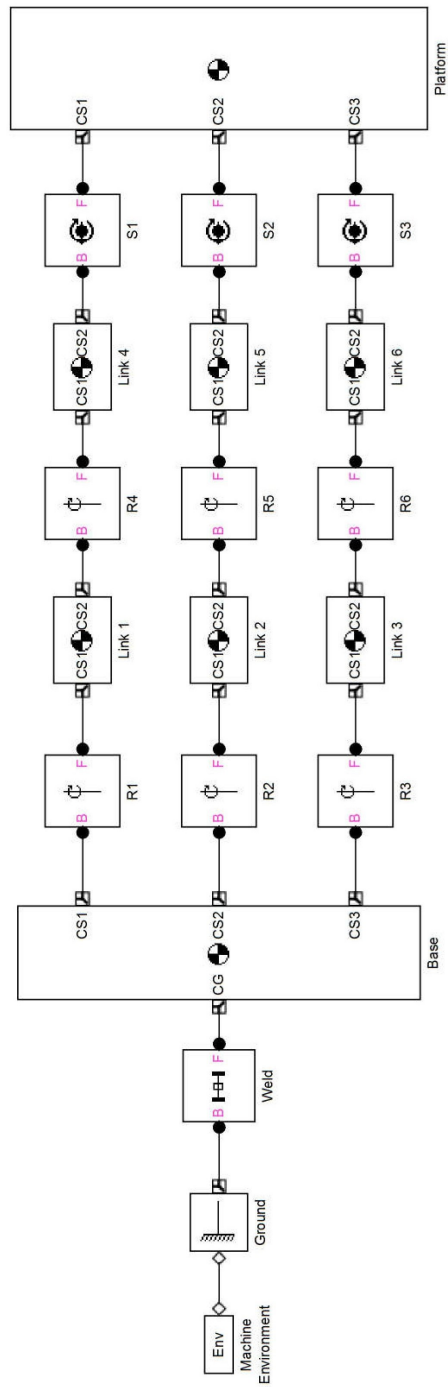


Figure 4.13. SimMechanics Blocks for 3-RRS PM

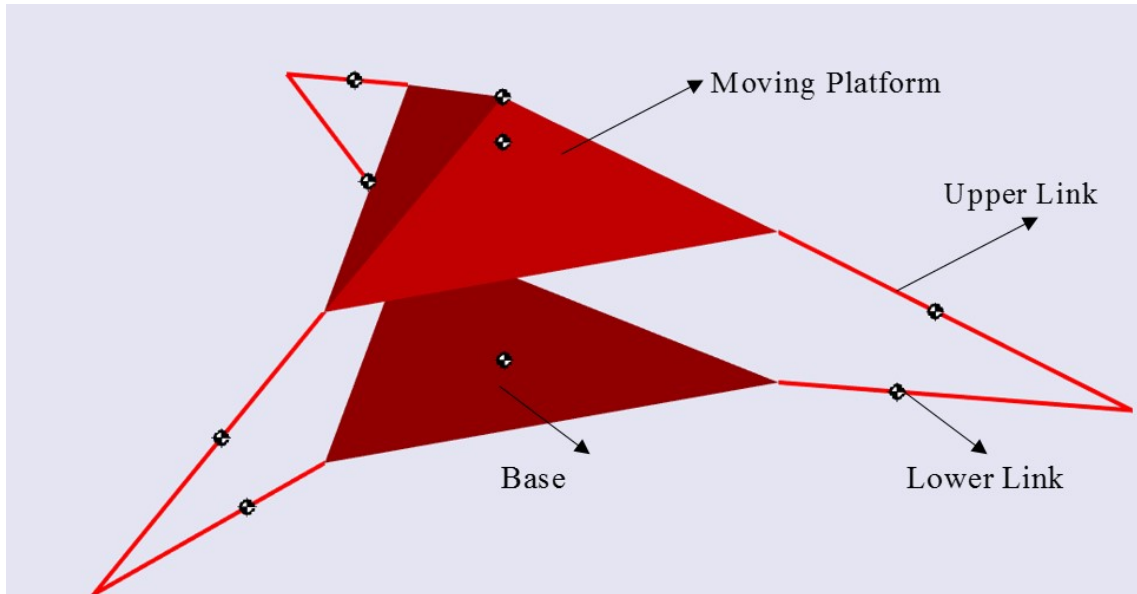


Figure 4.14. Virtual Model of the 3-RRS PM

To test the accuracy of the inverse kinematic formulations and obtained input torque values, a simulation is run using motion inputs with the displacement, velocity and acceleration values of active joints. In this simulation, the values of task and joint space parameters are checked. It is seen that the difference between calculated values of each parameter and their obtained values from the sensor blocks on the SimMechanics[®] model are ignorable. Furthermore, torque sensors are attached to active input joints to measure the computed torque values that the simulation calculates for each actuator. Then the calculated analytical values of the torques are compared with the torques obtained from the torque sensors. As presented in Figure 4.15, the errors in between the torque values are ignorable.

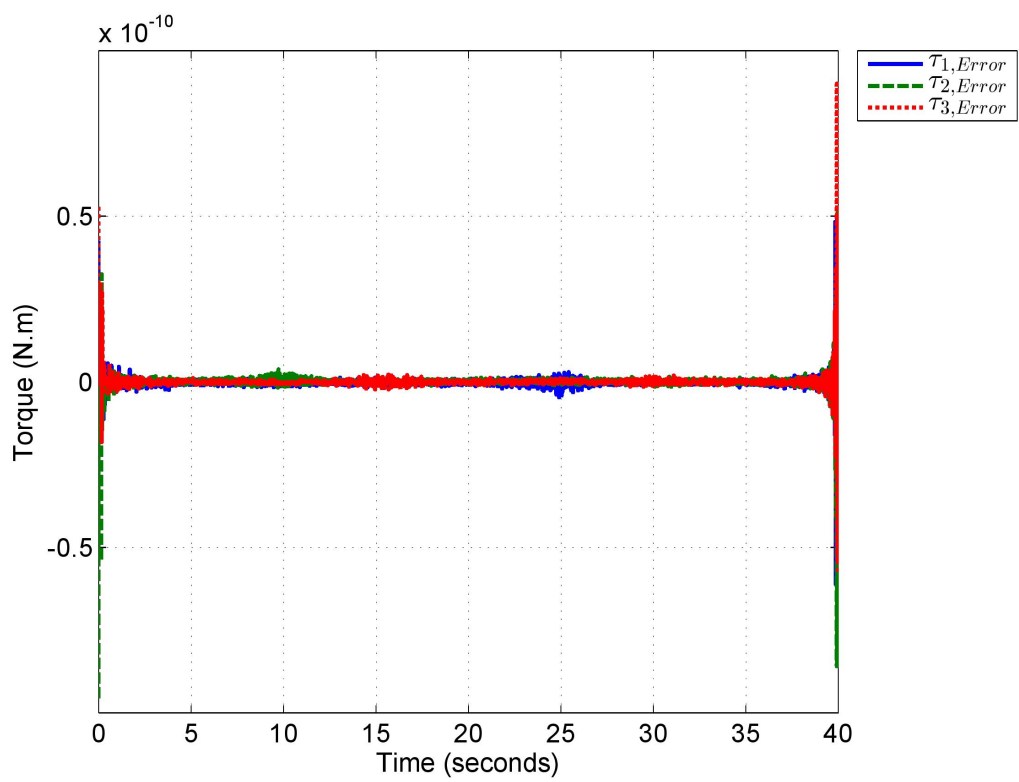


Figure 4.15. Input Torque Errors

CHAPTER 5

CONTROL OF THE PM

This chapter includes the performed control studies of the 3-RRS PM. Firstly the control hardware is presented. Then, performed studies are explained. Finally, the results of the control studies are presented.

5.1. Control Setup

The details of the mechanical components of the 3-RRS PM are given in Chapter 4. In this chapter, firstly the electronics used for the control of the manipulator are presented. Then, the control strategy is explained. Finally, the results are presented. The components of the control system is presented in Figures 5.1 and 5.2.

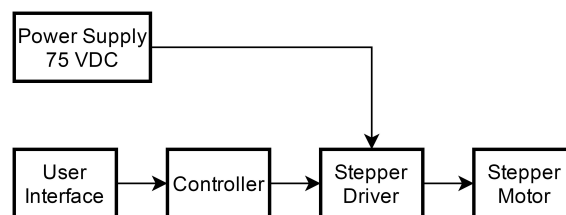


Figure 5.1. Control Setup



Figure 5.2. Control Setup Components

The controller that is used to send the required step, direction and enable signals with a frequency of 100 KHz to the stepper drivers is a GOYA 100[®] CNC controller. The controller has an operator interface including a keyboard and an LCD graphics display. This controller can control 3 separate stepper motors for point to point positioning and linear/circular interpolation. Controller can also communicate with a PC over RS-232 serial port using ASCII communication protocol.

User interface of the controller provided by the supplier is BACH Elite[®] software. Using the software it is possible to write a program using GCodes and implement it to the controller. Once the program is implemented into the controller, it can be run using the controller's interface without having PC connection. Other than that, it is also possible to use the motors in jogging mode and online control modes. Besides creating or running programs, it is possible to make changes on the configuration of the motors such as velocity profiles or motion limits etc.

To convert the step, direction and enable signals into currents, Pacific Scientific[®] MA6410 stepper drivers are used. Driver's supply voltage is between 24 and 75 VDC and it can supply current ranging from 0.625 to 5 A with a frequency of 20 kHz. Stepper motors are from PowerPac series of Pacific Scientific[®] motors with step angle of 1.8°. The model of the motors is N42 HRFM-LNK-NS-01 . The angular velocity and power of the motor is given as 1500 rpm and 425 W, respectively. The holding torque of the motor is 22.2 N.m and the rated current as 4.9 A in its data sheet.

To control the stepper motors with GOYA 100[®] CNC controller and MA640 stepper drivers, there are some important adjustments that must to be done. First of all, to use the motors in microstepping mode, the DIP switch on the drivers are set suitable for microstepping mode as given in the user manual. It should be noted here that in the microstepping mode, 50000 pulses from the driver creates a complete rotation on the motor shaft.

To set the configuration parameters of GOYA 100[®] CNC controller, its user interface, BACH Elite[®] software is used. Firstly, it should be mentioned that the CNC controller is designed for Cartesian tables and control of the motors are done by giving the desired position of the Cartesian table. To adjust the controller to 3-RRS PM, 1 mm displacement of each axis of Cartesian table is set as 1° of shaft rotation at the motors. Then, the motion limits of the motors are defined as $-13410^\circ \leq \theta_i^M \leq 0^\circ$, which is equal to a motion range of $-90^\circ \leq \theta_i \leq 0^\circ$ at the input links. For the velocity of the motors, controller creates a trapezoidal velocity profile for the motors. In order to avoid any accidents during the tests, the maximum velocity of the motors are set as 50 rpm.

5.2. Cabling of the Control Setup

The steppers have 8 wire configuration which allows the user to have bipolar series, bipolar parallel and unipolar wiring configuration. In order to obtain better torque characteristics at lower speeds, series wire configuration is selected. The connection diagram of the motors provided in the data sheet is presented Figure 5.3

CONNECTION	DRIVER CONNECTION	LEAD COLOR	TERMINAL #
4-LEAD BIPOLAR SERIES	A	BLACK (BLK)	1
	\bar{A}	ORANGE (ORG)	3
	B	RED	2
	\bar{B}	YELLOW (YEL)	4
	NONE	WHT/BLK & WHT/ORG	6 & 5
	NONE	WHT/RED & WHT/YEL	8 & 7
4-LEAD BIPOLAR PARALLEL	A	BLK & WHT/ORG	1 & 5
	\bar{A}	ORG & WHT/BLK	3 & 6
	B	RED & WHT/YEL	2 & 7
	\bar{B}	YEL & WHT/RED	4 & 8
6-LEAD UNIPOLAR	A	BLACK (BLK)	1
	B	ORANGE (ORG)	3
	C	RED	2
	D	YELLOW (YEL)	4
	+V	WHT/BLK & WHT/ORG	6 & 5
	+V	WHT/RED & WHT/YEL	8 & 7
GND		GREEN/YELLOW	

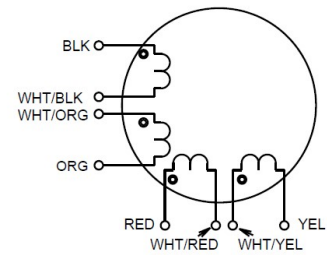


Figure 5.3. Wiring Configurations of the Stepper Motors
(Source: PacificScientific, 2000)

The wires of the motors and power supply are mounted to the driver's J2 and J3 ports respectively as presented in Figure 5.4. To obtain better angular resolution, motors are run at micro step mode. At this mode 1 step signal results in 0.0072° rotation at the shaft and a complete rotation of the shaft requires 50000 pulses. The step configuration is set using DIP switches on MA6410 stepper drivers.

The connection diagram in between the controller and stepper drivers is presented in Figure 5.5. Enable, direction and pulse signal inputs to the drivers are supplied by using 9 pole D connectors. Each pin on this connector is numbered from 1 to 9. The first 3 pins of the drivers require constant 5 VDC signals and they are connected together. This signal is supplied by the 4th pin of the controller. 6th pin of the driver is connected to 3rd pin of

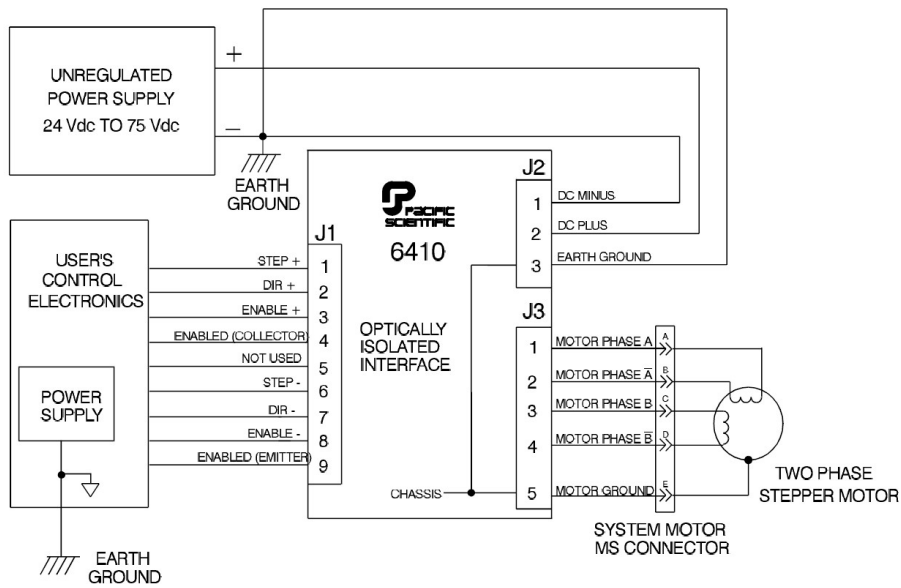


Figure 5.4. Motor Driver's Connection Diagram
(Source: PacificScientific, 1998)

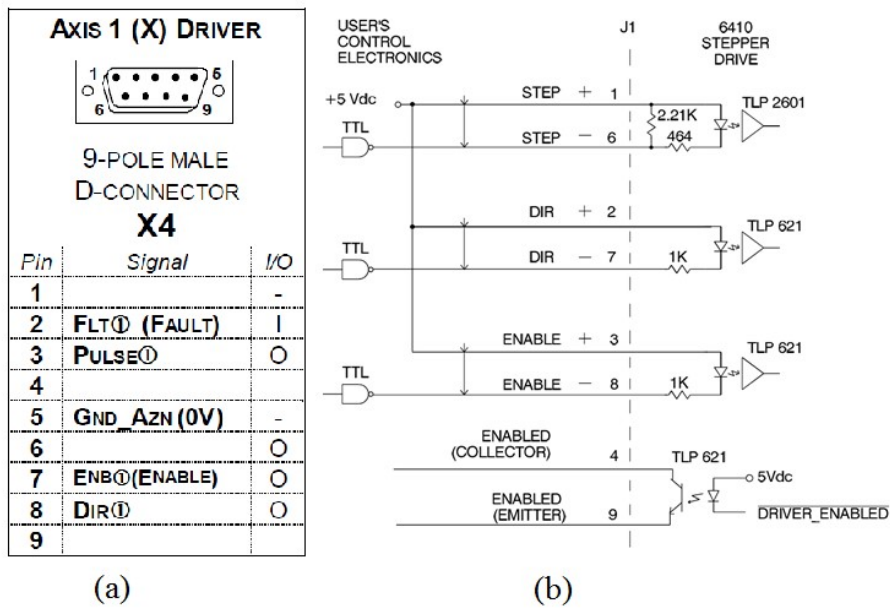


Figure 5.5. a) Driver Connection Port of Controller, b) Signal Inputs of Driver
(Source: S&H, 2000)

the controller and pulse signals are received over this cable. 7th pin of the driver, which is the direction input signal, is connected to 8th pin of the controller. And finally 8th pin of the driver is connected to 7th pin of the controller so that enable signal connection is done. The connection in between controller and PC is done by using standard cross-over type serial cable.

5.3. Control Algorithm

Although no closed-loop feedback control is utilized, in order to test the accuracy of the control, several motion sensors are attached to the vital points (3 magnetic encoders attached on active R joints and a 3 axis gyroscope attached on the moving platform) on the PM and signals received from the sensors are compared with the desired values. The result plots showing the error in between actual and desired values of the motion are presented at the end of this Chapter.

Since the controller is a 3-axis CNC controller, a point-to-point type of motion control is applied. For this type of control, both inverse and forward kinematic models of the 3-RRS PM is used. To apply point-to-point control algorithm, firstly motion planning is done. Desired points for the moving platform are given as input to a MATLAB/Simulink[®] file. This input data is processed and converted into motor trajectories considering the motion characteristics of the stepper motors. Then, using the forward kinematics model of the 3-RRS PM, the trajectory-time curve of the moving platform is obtained. Following that, a check is performed for the singularity and joint limit conditions using the trajectory curves of the input links and moving platform. If the desired trajectory of the PM is achievable, then the control algorithm proceeds to the next step.

When it is confirmed that the desired motion is achievable by the manipulator, position input commands to the controller should be given. For that, the position given in task space are converted into joint space coordinates by using the inverse kinematic model in MATLAB/Simulink[®] environment. Then the joint space coordinates are converted into GCodes and implemented as CNC program into the CNC controller by using its interface, BACH Elite[®].

When the program is run, the controller converts the GCodes into step signals and transmits to the motor drivers. Stepper drivers receive the step signals and convert them into currents and transmits to the stepper motors. At that instant, desired rotary motion from the shafts of the motors is obtained. The time belts transmit the motion to the reducers and then active R joints. Finally the desired motion of the end effector is

obtained. Figure 5.5 represents the control algorithm scheme of the 3-RRS PM.

5.4. Control Test

To test the control system an example set of desired independent task space parameters for the moving platform are selected and then the corresponding active link and motor positions are found. The values of these positions are presented in Table 5.1.

Table 5.1. Desired Task Space Positions and Corresponding Input Values

#	Task Space Positions			Active Joint Positions			Motor Positions		
	$O_{7,z}$ (mm)	ψ_x (deg)	ψ_y (deg)	θ_1 (deg)	θ_2 (deg)	θ_3 (deg)	$\theta_{1,m}$ (deg)	$\theta_{2,m}$ (deg)	$\theta_{3,m}$ (deg)
1	0.332	0	0	0	0	0	0	0	0
2	1000	0	0	-39.44	-39.44	-39.44	-5876.54	-5876.54	-5876.54
3	1000	-10	0	-39.2	-35.25	-44.84	-5841.33	-5252.78	-6681.29
4	1000	10	0	-39.2	-44.84	-35.25	-5841.33	-6681.92	-5252.78
5	1000	0	0	-39.44	-39.44	-39.44	-5876.84	-5876.84	-5876.84
6	1000	0	10	-34.81	-42.26	-42.26	-5187.25	-6297.58	-6297.58
7	1000	0	-10	-45.85	-36.7	-36.7	-6832.06	-5468.17	-5468.17
8	1000	0	0	-39.44	-39.44	-39.44	-5876.54	-5876.54	-5876.54
9	0.332	0	0	0	0	0	0	0	0

The motor positions are converted into GCodes using MATLAB/Simulink[®] easily. Each position set of the motors given in Table 5.1 refers to a single line on the CNC program and motors reach to the position given in a line at the same time. The maximum velocity for each motor at each line of the code is determined considering the motor which travels the maximum distance.

After obtaining the required positions of the motors, the trajectories are generated considering the motion characteristics of the motors and controllers. As stated before, CNC controller generates a trapezoidal velocity curve for each motor. Using the motor positions given in Table 5.1, the velocity profile of each motor is generated. Then, using an Integral block in Simulink[®], motor trajectories are generated and converted to the trajectories of the active joints. The corresponding active joint trajectories for the positions given in Table 5.1 are presented in the Figure 5.7.

The obtained active joint trajectories are given as motion input to the SimMechanics[®] model of the 3-RRS PM and the corresponding path of the moving platform is generated. The desired trajectory of the moving platform is presented in Figure 5.8.

Once the trajectory of the moving platform is obtained, a check for the singular configurations and joint limits is performed. The check algorithm is implemented into

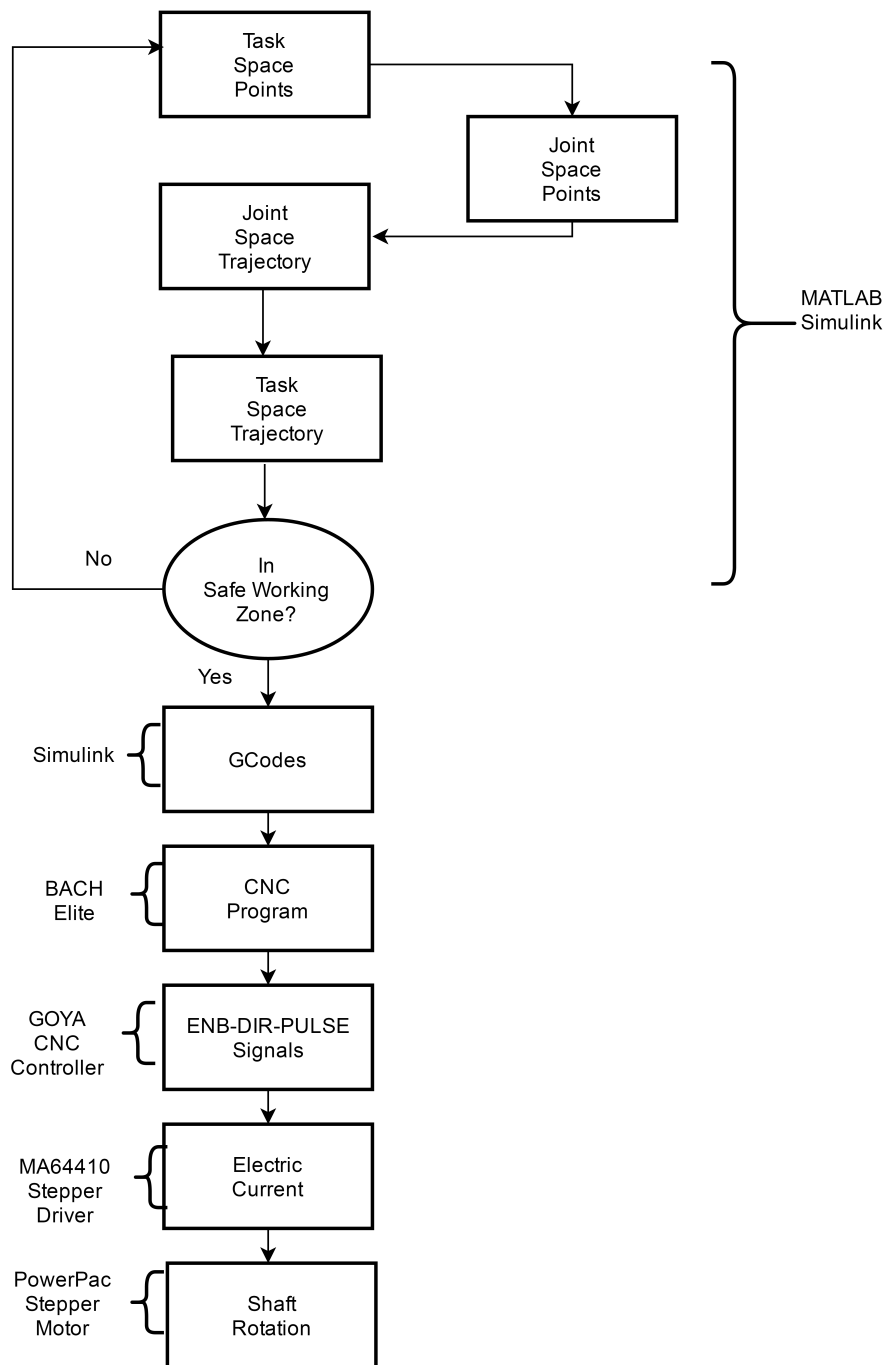


Figure 5.6. Point-to-point Control Algorithm

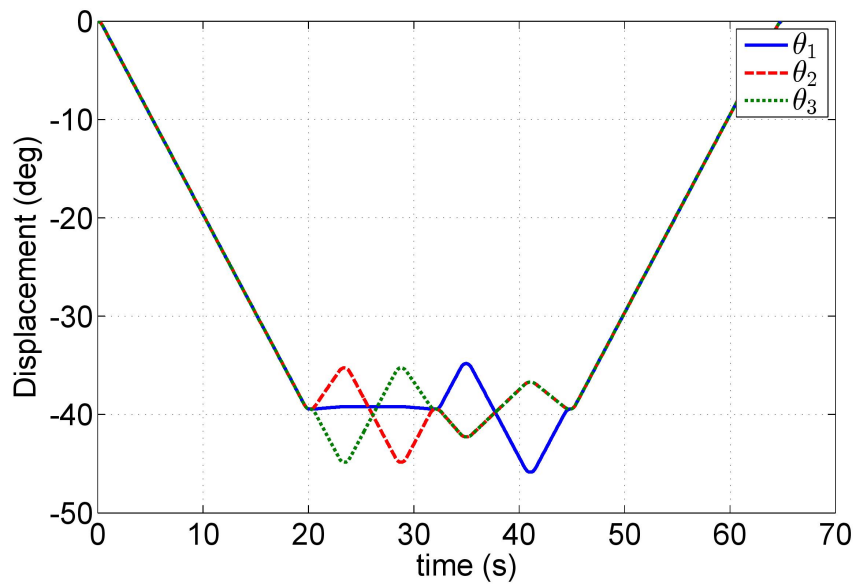


Figure 5.7. Desired Active Joint Trajectories

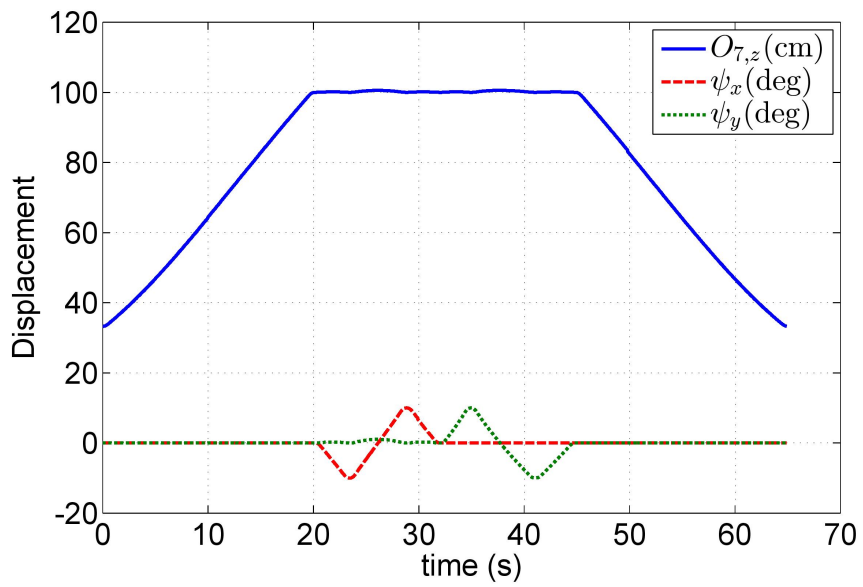


Figure 5.8. Desired Moving Platform Trajectory

the Simulink[®] model. If the motion is safe, the obtained GCodes are given as inputs to the CNC controller and a CNC program is created. This is done using the user interface (BACH Elite[®]) of the CNC controller.

When the CNC program is created and run, the PM starts following its trajectory. To test the accuracy of the motion, 3 magnetic rotary encoders (AS5048B 14 Bit) are attached to the shafts of active links . Furthermore a 3 axis gyroscope (MPU 6050) is attached to the center of the moving platform . With the gyroscope, the angular displacement of the moving platform is measured. To check the motion accuracy of the PM, same motion is performed for 20 times and the means of the sensor data is used. The displacement plots for the active joints and errors are provided in Figure 5.9. The desired and obtained orientation of the moving platform are compared in Figure 5.10.

Since GOYA 100[®] is not an ideal controller for robot manipulators, another control study is done with a Humusoft[®] MF624 - PCI multifunction I/O card. It is used for applying velocity control over stepper motors. In contrast to the CNC controller, it is possible to design the motion profile of the motors with trapezoidal jerk using the Humusoft[®] controller. By that, the accelerations and decelerations of the motors are smoothed.

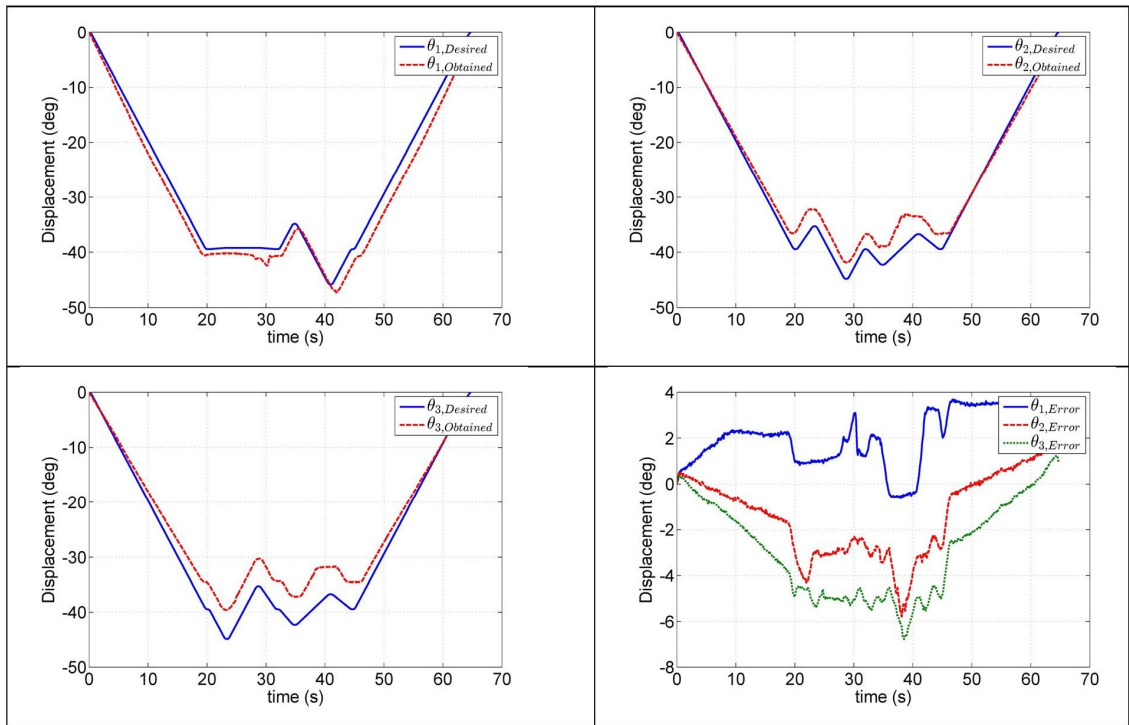


Figure 5.9. Displacement and Errors of Active Joints

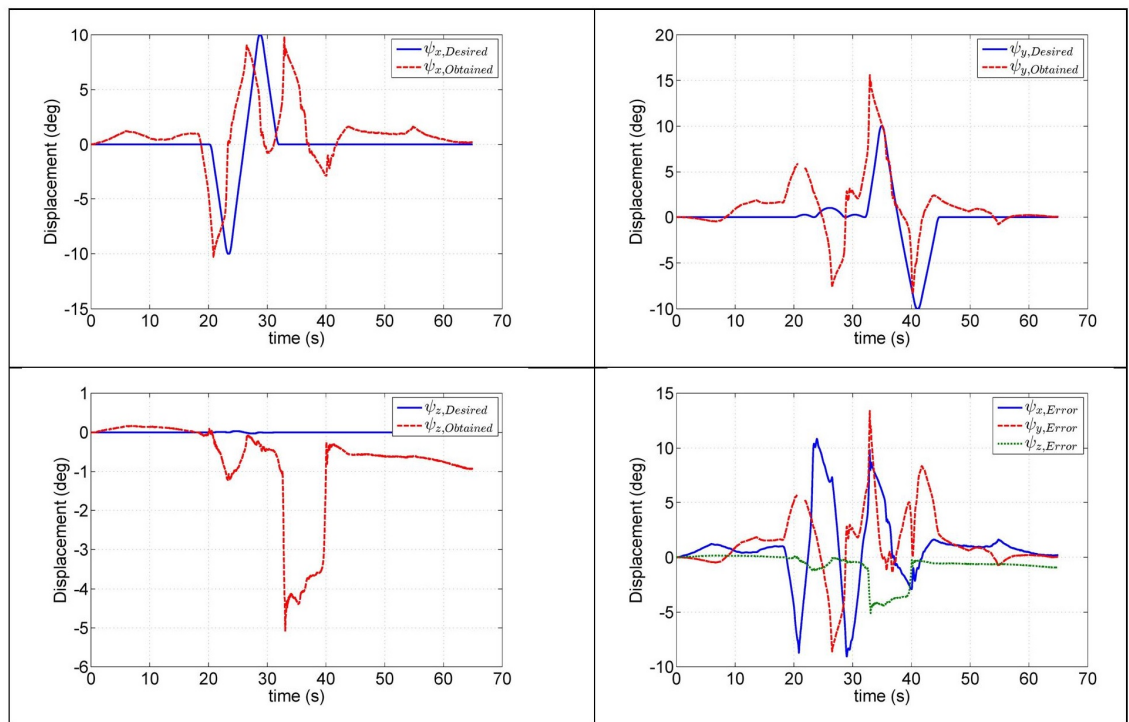


Figure 5.10. Orientation Errors of the Moving Platform

Using a Simulink[®] model, firstly the trajectories of the motors are generated using an algorithm similar to the one used with GOYA 100 CNC controller. While generating the trajectories of the motors, it is preferred to have trapezoidal jerks instead of trapezoidal velocities. The maximum velocity for each motor is set as 50 rpm again due to safety issues. With respect to the velocity profiles of each motor, using a "Frequency Output" block, "Pulse Width Modulation" (PWM) signals are generated in Simulink[®] Real Time Desktop Environment. Generated PWM signals are transmitted to the stepper drivers through the "Timer/Counter Output" of the MF624 - PCI multifunction I/O card. Figure 5.11 represents the Simulink model generated to obtain frequency output over Simulink[®] Desktop Real Time by Humusoft MF624 PCI card.

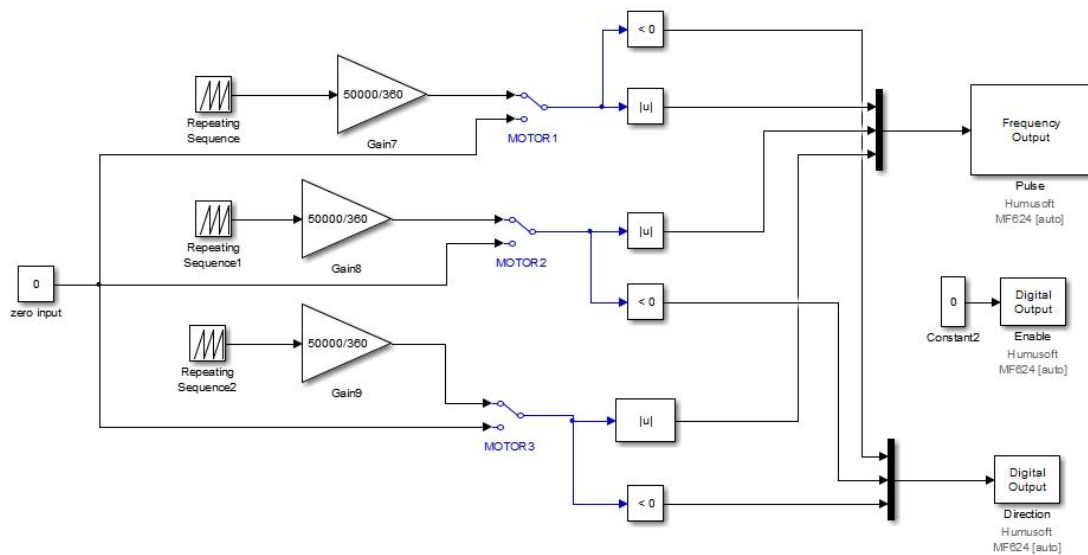


Figure 5.11. Simulink[®] Model for Humusoft[®] MF624 PCI Card

In order to compare both controllers, the same desired points for the pose of the moving platform are selected. With these parameters, the trajectory of each motor is generated with a trapezoidal jerk profile. Figure 5.12 represents the desired and obtained motion for each input link and their errors.

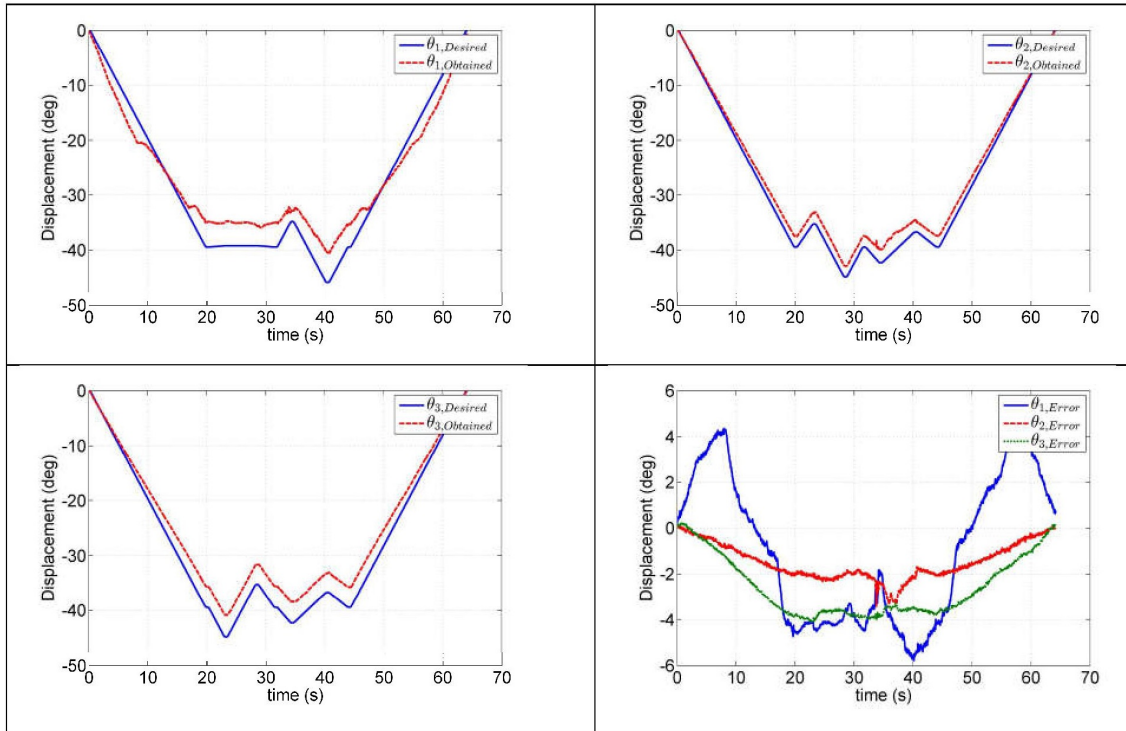


Figure 5.12. Displacement and Errors of Active Joints with Humusoft® MF624 PCI Card

CHAPTER 6

DISCUSSIONS AND CONCLUSION

In this thesis study, formulations in order to obtain a mathematical model of a 3-RRS PM is presented. For inverse kinematic analysis, firstly the constraint equations for moving platform are formulated. Then using the loop equations, from which passive joint variables are eliminated, the active joint parameters are obtained in terms of independent task space parameters. Forward kinematics equations are formulated by eliminating the task space parameters from the loop equations. After applying some mathematical manipulations, a 16th degree univariate polynomial is obtained in terms of one of the passive joint variables. Then, all of the passive joint variables are evaluated and task space parameters are obtained in terms of active and passive joint variables. For the velocity and acceleration level kinematics, derivatives of the loop equations are used and all of the joint and task space velocities and accelerations are obtained.

The singularities of the 3-RRS PM are determined using the Jacobian matrices of the loop equations. 1st and 2nd type of singularities are observed for the PM. The 3rd type singularities are not detected for the 3-RRS PM investigated in this thesis study. For the workspace of the PM, two types of workspaces are defined. Using the search algorithm, the reachable workspace of the manipulator is obtained. Then, by defining the limitations on active R and S joints and singularity conditions, safe working zone of the PM is obtained.

Inverse dynamic analysis for the PM is performed using both virtual work method and Lagrange's approach. The obtained input torques for both methods for a hypothetical trajectory of the moving platform match with each other. Furthermore, a SimMechanics[®] model is prepared to test the kinematic and dynamic formulations. Results of the simulations confirmed that the derived formulations are correct.

An open-loop control algorithm is used for the control of the physical model of the manipulator. Using an industrial CNC controller and a PCI Card, point-to-point control is applied over the manipulator. With the CNC controller, trapezoidal velocity profiles are generated to control the stepper motors where trapezoidal jerk profiles are used with the PCI card. The error plots for both controllers are given in Figures 5.9, 5.10 and 5.11. As can be seen from these plots, the error on the trajectory of the active links and moving platform can not be ignored. While performing the control tests, it is observed that there

is backlash at the reducers and clearance at the joints, especially S joints. This situation of the mechanical structure of the PM is the reason of the errors.

As further studies, the mechanical structure of the PM should be improved so that the trajectory tracking errors will be reduced. After that, a more comprehensive dynamic model, which includes joint frictions and actuator dynamics, can be created. Following that, using the PCI card, a closed-loop control algorithm can be used to apply a control over the PM. When the tracking errors are minimised, then the serial arm to be attached on the moving platform can be designed, produced.

REFERENCES

- Bi, Z. M. and Y. Jin 2011. Kinematic modeling of exechon parallel kinematic machine. *Robotics and Computer-Integrated Manufacturing* 27(1), 186–193.
- Briot, S. and I. Bonev 2007. Are parallel robots more accurate than serial robots? *CSME Transactions* 31(4), 445–456.
- Caccavale, F., B. Siciliano, and L. Villani 2003. The tricept robot: dynamics and impedance control. *Mechatronics, IEEE/ASME Transactions on* 8(2), 263–268.
- Can, F. C. 2008, 12. *Analysis and synthesis of parallel manipulators*. Ph. D. thesis, İzmir Institute of Technology.
- Cappel, K. L. 1967, January 3. Motion simulator. US Patent 3,295,224.
- Carretero, J. A., M. Nahon, and R. P. Podhorodeski 1998. Workspace analysis of a 3-dof parallel mechanism. In *Intelligent Robots and Systems, 1998. Proceedings., 1998 IEEE/RSJ International Conference on*, Volume 2, pp. 1021–1026. IEEE.
- Chen, Q., Z. Chen, X. Chai, and Q. Li 2013. Kinematic analysis of a 3-axis parallel manipulator: The p3. *Advances in Mechanical Engineering* 5, 589156.
- Chen, X., X.-J. Liu, F. Xie, and T. Sun 2014. A comparison study on motion/force transmissibility of two typical 3-dof parallel manipulators: the sprint z3 and a3 tool heads. *International Journal of Advanced Robotic Systems* 11.
- Clavel, R. 1988. Delta, a fast robot with parallel geometry. In *Proc. 18th Int. Symp. on Industrial Robots, Lausanne, 1988*, pp. 91–100.
- Dasgupta, B. and T. Mruthyunjaya 2000. The stewart platform manipulator: a review. *Mechanism and machine theory* 35(1), 15–40.
- Dunlop, G. and T. Jones 1999. Position analysis of a two dof parallel mechanismthe canterbury tracker. *Mechanism and Machine Theory* 34(4), 599–614.

- Elkady, A., G. Elkobrosy, S. Hanna, and T. Sobh 2008. *Cartesian parallel manipulator modeling, control and simulation*. Citeseer.
- Fan, C., H. Liu, and Y. Zhang 2009. Kinematics and singularity analysis of a novel 1t2r fully-decoupled parallel mechanism. In *Intelligent Computing and Intelligent Systems, 2009. ICIS 2009. IEEE International Conference on*, Volume 2, pp. 312–316. IEEE.
- Gallardo, J., H. Orozco, and J. M. Rico 2008. Kinematics of 3-rps parallel manipulators by means of screw theory. *The International Journal of Advanced Manufacturing Technology* 36(5-6), 598–605.
- Gosselin, C. and J. Angeles 1990. Singularity analysis of closed-loop kinematic chains. *Robotics and Automation, IEEE Transactions on* 6(3), 281–290.
- Gosselin, C., E. St Pierre, and M. Gagne 1996. On the development of the agile eye. *Robotics & Automation Magazine, IEEE* 3(4), 29–37.
- Gwinnett, J. E. 1931, January 20. Amusement device. US Patent 1,789,680.
- Harib, K. H., A. S. Ullah, K. A. Moustafa, and S. Zenieh 2012. *Parallel, serial and hybrid machine tools and robotics structures: comparative study on optimum kinematic designs*. INTECH Open Access Publisher.
- Itul, T. and D. Pisla 2009. 446. on the kinematics and dynamics of 3-dof parallel robots with triangle platform. *Journal of Vibroengineering* 11(1).
- Lee, K.-M. and D. K. Shah 1988. Kinematic analysis of a three-degrees-of-freedom in-parallel actuated manipulator. *Robotics and Automation, IEEE Journal of* 4(3), 354–360.
- Li, B., Y. Hu, and H. Wang 2007. Analysis and simulation for a parallel drill point grinder. *The International Journal of Advanced Manufacturing Technology* 31(9-10), 915–925.
- Li, J., J. Wang, W. Chou, Y. Zhang, T. Wang, and Q. Zhang 2001. Inverse kinematics and dynamics of the 3-rrs parallel platform. In *Robotics and Automation, 2001. Pro-*

- ceedings 2001 ICRA. IEEE International Conference on*, Volume 3, pp. 2506–2511. IEEE.
- Li, Q. and J. M. Hervé 2010. 1t2r parallel mechanisms without parasitic motion. *Robotics, IEEE Transactions on* 26(3), 401–410.
- Li, Y. and Q. Xu 2005. Kinematics and inverse dynamics analysis for a general 3-prs spatial parallel mechanism. *Robotica* 23(02), 219–229.
- Li, Y. and Q. Xu 2007. Kinematic analysis of a 3-prs parallel manipulator. *Robotics and Computer-Integrated Manufacturing* 23(4), 395–408.
- Merlet, J.-P. 2001. *Parallel robots. Vol. 74*. Springer New York.
- PacificScientific 1998. *MA6410 Drive Installation and Hardware Reference Manual*.
- PacificScientific 2000. *Step Motors Data Sheet*.
- Patel, Y., P. George, et al. 2012. Parallel manipulators applicationsa survey. *Modern Mechanical Engineering* 2(03), 57.
- Pendar, H., M. Vakil, and H. Zohoor 2004. Efficient dynamic equations of 3-rps parallel mechanism through lagrange method. In *Robotics, Automation and Mechatronics, 2004 IEEE Conference on*, Volume 2, pp. 1152–1157. IEEE.
- Pierrot, F., F. Marquet, O. Company, and T. Gil 2001. H4 parallel robot: modeling, design and preliminary experiments. In *Robotics and Automation, 2001. Proceedings 2001 ICRA. IEEE International Conference on*, Volume 4, pp. 3256–3261. IEEE.
- Pollard, W. L. V. 1942, June 16. Position-controlling apparatus. US Patent 2,286,571.
- Pouliot, N. A., Clé, m. M. Gosselin, and M. A. Nahon 1998. Motion simulation capabilities of three-degree-of-freedom flight simulators. *Journal of Aircraft* 35(1), 9–17.
- Rao, P. S. and N. M. Rao 2013. Position analysis of spatial 3-rps parallel manipulator.
- Rezaei, A., A. Akbarzadeh, P. M. Nia, and M.-R. Akbarzadeh-T 2013. Position, jaco-

bian and workspace analysis of a 3-psp spatial parallel manipulator. *Robotics and Computer-Integrated Manufacturing* 29(4), 158–173.

S&H 2000. *GOYA STD1 User's Manual*.

Siciliano, B. 1999. The tricept robot: Inverse kinematics, manipulability analysis and closed-loop direct kinematics algorithm. *Robotica* 17(04), 437–445.

Sokolov, A. and P. Xirouchakis 2007. Dynamics analysis of a 3-dof parallel manipulator with r-p-s joint structure. *Mechanism and Machine Theory* 42(5), 541–557.

Srivatsan, R. A. and S. Bandyopadhyay 2013. On the position kinematic analysis of mapaman: A reconfigurable three-degrees-of-freedom spatial parallel manipulator. *Mechanism and Machine Theory* 62, 150–165.

Srivatsan, R. A. and S. Bandyopadhyay 2014. Determination of the safe working zone of a parallel manipulator. In *Computational Kinematics*, pp. 201–208. Springer.

Staicu, Ș. 2012. Inverse dynamics of the spatial 3-rps parallel robot. *Proc. of the Romanian Academy* 13(1), 62–70.

Stewart, D. 1965. A platform with six degrees of freedom. *Proceedings of the institution of mechanical engineers* 180(1), 371–386.

Taghirad, H. D. 2013. *Parallel robots: mechanics and control*. CRC press.

Tetik, H., R. Kalla, G. Kiper, and S. Bandyopadhyay 2016. Position kinematics of a 3-rrs parallel manipulator. In *ROMANSY 21-Robot Design, Dynamics and Control*, pp. 65–72. Springer.

Tsai, L.-W. 1999. *Robot analysis: the mechanics of serial and parallel manipulators*. John Wiley & Sons.

Tsai, M.-S., T.-N. Shiau, Y.-J. Tsai, and T.-H. Chang 2003. Direct kinematic analysis of a 3-prs parallel mechanism. *Mechanism and Machine Theory* 38(1), 71–83.

Tsai, M.-S. and W.-H. Yuan 2010. Inverse dynamics analysis for a 3-prs parallel mech-

- anism based on a special decomposition of the reaction forces. *Mechanism and Machine Theory* 45(11), 1491–1508.
- Vallés, M., M. Díaz-Rodríguez, Á. Valera, V. Mata, and Á. Page 2012. Mechatronic development and dynamic control of a 3-dof parallel manipulator. *Mechanics based design of structures and machines* 40(4), 434–452.
- Verdes, D., S.-D. Stan, M. Manic, R. Bălan, and V. Maties 2009. Kinematics analysis, workspace, design and control of 3-rps and triglide medical parallel robots. In *Human System Interactions, 2009. HSI'09. 2nd Conference on*, pp. 103–108. IEEE.
- Wahl, J. 2002, August 13. Articulated tool head. US Patent 6,431,802.
- Zhang, D. 2009. *Parallel robotic machine tools*. Springer Science & Business Media.
- Zhang, D., Z. Gao, X. Su, and J. Li 2012. A comparison study of three degree-of-freedom parallel robotic machine tools with/without actuation redundancy. *International Journal of Computer Integrated Manufacturing* 25(3), 230–247.
- Zhang, D., L. Wang, and E. Esmailzadeh 2006. Pkm capabilities and applications exploration in a collaborative virtual environment. *Robotics and Computer-Integrated Manufacturing* 22(4), 384–395.
- Zhang, Y. and K.-l. Ting 2013. Design and analysis of a spatial 3-dof parallel manipulator with 2t1r-type. *International Journal of Advanced Robotic Systems* 10.
- Zhao, Y. 2013. Dimensional synthesis of a three translational degrees of freedom parallel robot while considering kinematic anisotropic property. *Robotics and Computer-Integrated Manufacturing* 29(1), 169–179.
- Zlatanov, D., I. A. Bonev, and C. M. Gosselin 2002. Constraint singularities of parallel mechanisms. In *Robotics and Automation, 2002. Proceedings. ICRA'02. IEEE International Conference on*, Volume 1, pp. 496–502. IEEE.

APPENDIX A

TIME DERIVATIVES OF JACOBIAN MATRICES

The time derivatives of the Jacobian matrices used in the acceleration analysis

Chapter 3 are presented below:

$$\dot{\mathbf{J}}_{x_i,t} = \left[\dot{\mathbf{J}}_{O_{7x}} \quad \dot{\mathbf{J}}_{O_{7y}} \quad \dot{\mathbf{J}}_{O_{7z}} \quad \dot{\mathbf{J}}_{\psi_x} \quad \dot{\mathbf{J}}_{\psi_y} \quad \dot{\mathbf{J}}_{\psi_z} \right]^T$$

$$\begin{aligned} \dot{\mathbf{J}}_{O_{7,x}} = & [0, (p c \psi_x (2 c \psi_x^2 c \psi_y + c \psi_x^3 c \psi_y^2 + c \psi_y^3 + 3 c \psi_x c \psi_y^4 + c \psi_x^2 c (3 \psi_y) + \\ & c \psi_y (-1 + c \psi_x c \psi_y) s \psi_x^2 s \psi_y^2) \dot{\psi}_x) / (2 (c \psi_x + c \psi_y)^3 ((1 + c \psi_x c \psi_y)^2 / (c \psi_x + c \psi_y)^2)^{3/2}) - \\ & (3 p s \psi_x (2 c \psi_x^2 c \psi_y + c \psi_x^3 c \psi_y^2 + c \psi_y^3 + 3 c \psi_x c \psi_y^4 + c \psi_x^2 c (3 \psi_y) + \\ & c \psi_y (-1 + c \psi_x c \psi_y) s \psi_x^2 s \psi_y^2) ((-s \psi_x) \dot{\psi}_x - s \psi_y \dot{\psi}_y)) / (2 (c \psi_x + c \psi_y)^4 ((1 + c \psi_x c \psi_y)^2 / \\ & (c \psi_x + c \psi_y)^2)^{3/2}) - (3 p s \psi_x (2 c \psi_x^2 c \psi_y + c \psi_x^3 c \psi_y^2 + c \psi_y^3 + 3 c \psi_x c \psi_y^4 + c \psi_x^2 c (3 \psi_y) + \\ & c \psi_y (-1 + c \psi_x c \psi_y) s \psi_x^2 s \psi_y^2) (-((2(1 + c \psi_x c \psi_y)^2 ((-s \psi_x) \dot{\psi}_x - s \psi_y \dot{\psi}_y)) / (c \psi_x + c \psi_y)^3) \\ & + (2(1 + c \psi_x c \psi_y) ((-c \psi_y) s \psi_x \dot{\psi}_x - c \psi_x s \psi_y \dot{\psi}_y)) / (c \psi_x + c \psi_y)^2)) / (4 (c \psi_x + c \psi_y)^3 ((1 + \\ & c \psi_x c \psi_y)^2 / (c \psi_x + c \psi_y)^2)^{5/2}) + (p s \psi_x (-4 c \psi_x c \psi_y s \psi_x \dot{\psi}_x - 3 c \psi_x^2 c \psi_y^2 s \psi_x \dot{\psi}_x - \\ & 3 c \psi_y^4 s \psi_x \dot{\psi}_x - 2 c \psi_x c (3 \psi_y) s \psi_x \dot{\psi}_x + 2 c \psi_x c \psi_y (-1 + c \psi_x c \psi_y) s \psi_x s \psi_y^2 \dot{\psi}_x - \\ & 2 c \psi_x^2 s \psi_y \dot{\psi}_y - 2 c \psi_x^3 c \psi_y s \psi_y \dot{\psi}_y - 3 c \psi_y^2 s \psi_y \dot{\psi}_y - 12 c \psi_x c \psi_y^3 s \psi_y \dot{\psi}_y + \\ & 2 c \psi_y^2 (-1 + c \psi_x c \psi_y) s \psi_x^2 s \psi_y \dot{\psi}_y - (-1 + c \psi_x c \psi_y) s \psi_x^2 s \psi_y^3 \dot{\psi}_y - 3 c \psi_x^2 s (3 \psi_y) \dot{\psi}_y + \\ & c \psi_y s \psi_x^2 s \psi_y^2 ((-c \psi_y) s \psi_x \dot{\psi}_x - c \psi_x s \psi_y \dot{\psi}_y)) / (2 (c \psi_x + c \psi_y)^3 ((1 + c \psi_x c \psi_y)^2 / (c \psi_x + \\ & c \psi_y)^2)^{3/2}), -((3 p (24 c (3 \psi_x) c \psi_y^2 s \psi_y + (-61 + 4 c (2 \psi_x) + c (4 \psi_x)) s (2 \psi_y) - \\ & 2 c \psi_x (31 s \psi_y + 15 s (3 \psi_y)) + 2 c \psi_x^2 (-3 + c (2 \psi_x)) s (4 \psi_y)) ((-s \psi_x) \dot{\psi}_x - s \psi_y \dot{\psi}_y)) / \\ & (64 (c \psi_x + c \psi_y)^4 ((1 + c \psi_x c \psi_y)^2 / (c \psi_x + c \psi_y)^2)^{3/2})) + (p (-72 c \psi_y^2 s (3 \psi_x) s \psi_y \dot{\psi}_x + \\ & 2 s \psi_x (31 s \psi_y + 15 s (3 \psi_y)) \dot{\psi}_x - 4 c \psi_x (-3 + c (2 \psi_x)) s \psi_x s (4 \psi_y) \dot{\psi}_x - \\ & 4 c \psi_x^2 s (2 \psi_x) s (4 \psi_y) \dot{\psi}_x + s (2 \psi_y) (-8 s (2 \psi_x) \dot{\psi}_x - 4 s (4 \psi_x) \dot{\psi}_x) + 24 c (3 \psi_x) c \psi_y^3 \dot{\psi}_y + 2 (-61 + \\ & 4 c (2 \psi_x) + c (4 \psi_x)) c (2 \psi_y) \dot{\psi}_y + 8 c \psi_x^2 (-3 + c (2 \psi_x)) c (4 \psi_y) \dot{\psi}_y - 48 c (3 \psi_x) c \psi_y s \psi_y^2 \dot{\psi}_y - \\ & 2 c \psi_x (31 c \psi_y \dot{\psi}_y + 45 c (3 \psi_y) \dot{\psi}_y)) / (64 (c \psi_x + c \psi_y)^3 ((1 + c \psi_x c \psi_y)^2 / (c \psi_x + c \psi_y)^2)^{3/2}) - \\ & (3 p (24 c (3 \psi_x) c \psi_y^2 s \psi_y + (-61 + 4 c (2 \psi_x) + c (4 \psi_x)) s (2 \psi_y) - 2 c \psi_x (31 s \psi_y + 15 s (3 \psi_y)) + \\ & 2 c \psi_x^2 (-3 + c (2 \psi_x)) s (4 \psi_y)) (-((2(1 + c \psi_x c \psi_y)^2 ((-s \psi_x) \dot{\psi}_x - s \psi_y \dot{\psi}_y)) / (c \psi_x + c \psi_y)^3) + \\ & (2(1 + c \psi_x c \psi_y) ((-c \psi_y) s \psi_x \dot{\psi}_x - c \psi_x s \psi_y \dot{\psi}_y)) / (c \psi_x + c \psi_y)^2)) / (128 (c \psi_x + c \psi_y)^3 ((1 + \\ & c \psi_x c \psi_y)^2 / (c \psi_x + c \psi_y)^2)^{5/2})] \end{aligned}$$

$$\begin{aligned}
\mathbf{J}_{O_{7,y}} = & [0, -((pc\psi_y^2\dot{\psi}_y)/((1+c\psi_x c\psi_y)\text{sqrt}((1+c\psi_x c\psi_y)^2/(c\psi_x+c\psi_y)^2)))+ \\
& (ps\psi_y^2\dot{\psi}_y)/((1+c\psi_x c\psi_y)\text{sqrt}((1+c\psi_x c\psi_y)^2/(c\psi_x+c\psi_y)^2))+ \\
& (pc\psi_y s\psi_y((-c\psi_y) s\psi_x\dot{\psi}_x - c\psi_x s\psi_y\dot{\psi}_y))/((1+c\psi_x c\psi_y)^2\text{sqrt}((1+c\psi_x c\psi_y)^2/(c\psi_x+c\psi_y)^2)) + \\
& (pc\psi_y s\psi_y(-((2(1+c\psi_x c\psi_y)^2((-s\psi_x)\dot{\psi}_x - s\psi_y\dot{\psi}_y))/(c\psi_x+c\psi_y)^3) + \\
& (2(1+c\psi_x c\psi_y)((-c\psi_y) s\psi_x\dot{\psi}_x - c\psi_x s\psi_y\dot{\psi}_y))/(c\psi_x+c\psi_y)^2))/((2(1+c\psi_x c\psi_y)((1+c\psi_x c\psi_y)^2/(c\psi_x+c\psi_y)^2)^{3/2}), (pc\psi_x(-c\psi_y^4 - c\psi_x^2 c(2\psi_y) - \\
& (1/4)c\psi_x(5c\psi_y + 3c(3\psi_y)) + s\psi_x^2 s\psi_y^4)\dot{\psi}_x)/((c\psi_x+c\psi_y)^3((1+c\psi_x c\psi_y)^2/(c\psi_x+c\psi_y)^2)^{3/2}) - (3ps\psi_x(-c\psi_y^4 - c\psi_x^2 c(2\psi_y) - \\
& (1/4)c\psi_x(5c\psi_y + 3c(3\psi_y)) + s\psi_x^2 s\psi_y^4)((-s\psi_x)\dot{\psi}_x - s\psi_y\dot{\psi}_y))/((c\psi_x+c\psi_y)^4((1+c\psi_x c\psi_y)^2/(c\psi_x+c\psi_y)^2)^{3/2}) - (3ps\psi_x(-c\psi_y^4 - c\psi_x^2 c(2\psi_y) - (1/4)c\psi_x(5c\psi_y + \\
& 3c(3\psi_y)) + s\psi_x^2 s\psi_y^4)(-((2(1+c\psi_x c\psi_y)^2((-s\psi_x)\dot{\psi}_x - s\psi_y\dot{\psi}_y))/(c\psi_x+c\psi_y)^3) + \\
& (2(1+c\psi_x c\psi_y)((-c\psi_y) s\psi_x\dot{\psi}_x - c\psi_x s\psi_y\dot{\psi}_y))/(c\psi_x+c\psi_y)^2))/((2(c\psi_x+c\psi_y)^3((1+c\psi_x c\psi_y)^2/(c\psi_x+c\psi_y)^2)^{5/2}) + (ps\psi_x(2c\psi_x c(2\psi_y) s\psi_x\dot{\psi}_x + \\
& (1/4)(5c\psi_y + 3c(3\psi_y)) s\psi_x\dot{\psi}_x + 2c\psi_x s\psi_x s\psi_y^4\dot{\psi}_x + 4c\psi_y^3 s\psi_y\dot{\psi}_y + 4c\psi_y s\psi_x^2 s\psi_y^3\dot{\psi}_y + \\
& 2c\psi_x^2 s(2\psi_y)\dot{\psi}_y - (1/4)c\psi_x(-5s\psi_y\dot{\psi}_y - 9s(3\psi_y)\dot{\psi}_y)))/((c\psi_x+c\psi_y)^3((1+c\psi_x c\psi_y)^2/(c\psi_x+c\psi_y)^2)^{3/2})]
\end{aligned}$$

$$\mathbf{J}_{O_{7,z}} = [0, 0, 0]$$

$$\mathbf{J}_{\psi_x} = [0, 0, 0]$$

$$\mathbf{J}_{\psi_y} = [0, 0, 0]$$

$$\begin{aligned}
\mathbf{J}_{\psi_z} = & [0, -((c\psi_y\dot{\psi}_y)/(1+c\psi_x c\psi_y))+(s\psi_y((-c\psi_y) s\psi_x\dot{\psi}_x - c\psi_x s\psi_y\dot{\psi}_y))/(1+c\psi_x c\psi_y)^2, -((c\psi_x\dot{\psi}_x)/(1+c\psi_x c\psi_y)) + (s\psi_x((-c\psi_y) s\psi_x\dot{\psi}_x - c\psi_x s\psi_y\dot{\psi}_y))/(1+c\psi_x c\psi_y)^2]
\end{aligned}$$

$$\mathbf{J}_{x_i S} = \mathbf{J}_{tS}\mathbf{J}_{x_it} + \mathbf{J}_{tS}\dot{\mathbf{J}}_{x_it}$$

$$\begin{aligned}
\mathbf{J}_{tS} = & [0, 0, 0, 0, (-p)c\psi_y c(\alpha_{44} + \psi_z)\dot{\psi}_y + ps\psi_y s(\alpha_{44} + \psi_z)\dot{\psi}_z, p(s\psi_y s(\alpha_{44} + \psi_z)\dot{\psi}_y - c\psi_y c(\alpha_{44} + \psi_z)\dot{\psi}_z); 0, 0, 0, (-p)((c(\alpha_{44} + \psi_z) s\psi_x s\psi_y + c\psi_x s(\alpha_{44} + \psi_z))\dot{\psi}_x - \\
& c\psi_x c\psi_y c(\alpha_{44} + \psi_z)\dot{\psi}_y + (c(\alpha_{44} + \psi_z) s\psi_x + c\psi_x s\psi_y s(\alpha_{44} + \psi_z))\dot{\psi}_z), p(c\psi_x c\psi_y c(\alpha_{44} + \psi_z)\dot{\psi}_x - s\psi_x(c(\alpha_{44} + \psi_z) s\psi_y\dot{\psi}_y + c\psi_y s(\alpha_{44} + \psi_z)\dot{\psi}_z)), \\
& (-p)((c(\alpha_{44} + \psi_z) s\psi_x + c\psi_x s\psi_y s(\alpha_{44} + \psi_z))\dot{\psi}_x + c\psi_y s\psi_x s(\alpha_{44} + \psi_z)\dot{\psi}_y + (c(\alpha_{44} + \psi_z) s\psi_x s\psi_y + c\psi_x s(\alpha_{44} + \psi_z))\dot{\psi}_z); 0, 0, 0, p((c\psi_x c(\alpha_{44} + \psi_z) s\psi_y - s\psi_x s(\alpha_{44} + \psi_z))\dot{\psi}_x +
\end{aligned}$$

$$\begin{aligned}
& c \psi_y c(\alpha_{44} + \psi_z) s \psi_x \dot{\psi}_y + (c \psi_x c(\alpha_{44} + \psi_z) - s \psi_x s \psi_y s(\alpha_{44} + \psi_z)) \dot{\psi}_z, \\
& p c(\alpha_{44} + \psi_z) (c \psi_y s \psi_x \dot{\psi}_x + c \psi_x s \psi_y \dot{\psi}_y) + p c \psi_x c \psi_y s(\alpha_{44} + \psi_z) \dot{\psi}_z, p((c \psi_x c(\alpha_{44} + \psi_z) - \\
& s \psi_x s \psi_y s(\alpha_{44} + \psi_z)) \dot{\psi}_x + c \psi_x c \psi_y s(\alpha_{44} + \psi_z) \dot{\psi}_y + (c \psi_x c(\alpha_{44} + \psi_z) s \psi_y - s \psi_x s(\alpha_{44} + \\
& \psi_z)) \dot{\psi}_z); 0, 0, 0, 0, (-p) c \psi_y c(\alpha_{45} + \psi_z) \dot{\psi}_y + p s \psi_y s(\alpha_{45} + \psi_z) \dot{\psi}_z, p(s \psi_y s(\alpha_{45} + \psi_z) \dot{\psi}_y - \\
& c \psi_y c(\alpha_{45} + \psi_z) \dot{\psi}_z); 0, 0, 0, \\
& (-p)((c(\alpha_{45} + \psi_z) s \psi_x s \psi_y + c \psi_x s(\alpha_{45} + \psi_z)) \dot{\psi}_x - c \psi_x c \psi_y c(\alpha_{45} + \psi_z) \dot{\psi}_y + (c(\alpha_{45} + \\
& \psi_z) s \psi_x + c \psi_x s \psi_y s(\alpha_{45} + \psi_z)) \dot{\psi}_z), p(c \psi_x c \psi_y c(\alpha_{45} + \psi_z) \dot{\psi}_x - s \psi_x (c(\alpha_{45} + \psi_z) s \psi_y \dot{\psi}_y + \\
& c \psi_y s(\alpha_{45} + \psi_z) \dot{\psi}_z)), (-p)((c(\alpha_{45} + \psi_z) s \psi_x + c \psi_x s \psi_y s(\alpha_{45} + \psi_z)) \dot{\psi}_x + c \psi_y s \psi_x s(\alpha_{45} + \\
& \psi_z) \dot{\psi}_y + (c(\alpha_{45} + \psi_z) s \psi_x s \psi_y + c \psi_x s(\alpha_{45} + \psi_z)) \dot{\psi}_z); 0, 0, 0, p((c \psi_x c(\alpha_{45} + \psi_z) s \psi_y - \\
& s \psi_x s(\alpha_{45} + \psi_z)) \dot{\psi}_x + c \psi_y c(\alpha_{45} + \psi_z) s \psi_x \dot{\psi}_y + (c \psi_x c(\alpha_{45} + \psi_z) - s \psi_x s \psi_y s(\alpha_{45} + \\
& \psi_z)) \dot{\psi}_z), p c(\alpha_{45} + \psi_z) (c \psi_y s \psi_x \dot{\psi}_x + c \psi_x s \psi_y \dot{\psi}_y) + p c \psi_x c \psi_y s(\alpha_{45} + \psi_z) \dot{\psi}_z, \\
& p((c \psi_x c(\alpha_{45} + \psi_z) - s \psi_x s \psi_y s(\alpha_{45} + \psi_z)) \dot{\psi}_x + c \psi_x c \psi_y s(\alpha_{45} + \psi_z) \dot{\psi}_y + (c \psi_x c(\alpha_{45} + \\
& \psi_z) s \psi_y - s \psi_x s(\alpha_{45} + \psi_z)) \dot{\psi}_z); 0, 0, 0, 0, \\
& (-p) c \psi_y c(\alpha_{46} + \psi_z) \dot{\psi}_y + p s \psi_y s(\alpha_{46} + \psi_z) \dot{\psi}_z, p(s \psi_y s(\alpha_{46} + \psi_z) \dot{\psi}_y - c \psi_y c(\alpha_{46} + \\
& \psi_z) \dot{\psi}_z); 0, 0, 0, (-p)((c(\alpha_{46} + \psi_z) s \psi_x s \psi_y + c \psi_x s(\alpha_{46} + \psi_z)) \dot{\psi}_x - c \psi_x c \psi_y c(\alpha_{46} + \\
& \psi_z) \dot{\psi}_y + (c(\alpha_{46} + \psi_z) s \psi_x + c \psi_x s \psi_y s(\alpha_{46} + \psi_z)) \dot{\psi}_z), \\
& p(c \psi_x c \psi_y c(\alpha_{46} + \psi_z) \dot{\psi}_x - s \psi_x (c(\alpha_{46} + \psi_z) s \psi_y \dot{\psi}_y + c \psi_y s(\alpha_{46} + \psi_z) \dot{\psi}_z)), (-p)((c(\alpha_{46} + \\
& \psi_z) s \psi_x + c \psi_x s \psi_y s(\alpha_{46} + \psi_z)) \dot{\psi}_x + c \psi_y s \psi_x s(\alpha_{46} + \psi_z) \dot{\psi}_y + (c(\alpha_{46} + \psi_z) s \psi_x s \psi_y + \\
& c \psi_x s(\alpha_{46} + \psi_z)) \dot{\psi}_z); 0, 0, 0, p((c \psi_x c(\alpha_{46} + \psi_z) s \psi_y - s \psi_x s(\alpha_{46} + \psi_z)) \dot{\psi}_x + c \psi_y c(\alpha_{46} + \\
& \psi_z) s \psi_x \dot{\psi}_y + (c \psi_x c(\alpha_{46} + \psi_z) - s \psi_x s \psi_y s(\alpha_{46} + \psi_z)) \dot{\psi}_z), p c(\alpha_{46} + \psi_z) (c \psi_y s \psi_x \dot{\psi}_x + \\
& c \psi_x s \psi_y \dot{\psi}_y) + p c \psi_x c \psi_y s(\alpha_{46} + \psi_z) \dot{\psi}_z, p((c \psi_x c(\alpha_{46} + \psi_z) - s \psi_x s \psi_y s(\alpha_{46} + \psi_z)) \dot{\psi}_x + \\
& c \psi_x c \psi_y s(\alpha_{46} + \psi_z) \dot{\psi}_y + (c \psi_x c(\alpha_{46} + \psi_z) s \psi_y - s \psi_x s(\alpha_{46} + \psi_z)) \dot{\psi}_z)]
\end{aligned}$$

$$\mathbf{J}_{x_i \theta} = \mathbf{J}_{S \theta} \mathbf{J}_{x_i S} + \mathbf{J}_{S \theta} \dot{\mathbf{J}}_{x_i S}$$

$$\begin{aligned}
\mathbf{J}_{S \theta} &= [(c \theta_1 ((-O_{74,z} + l_1 s \theta_1)) \dot{O}_{74,x} + ((-c \alpha_{11})(b + l_1 c \theta_1) + O_{74,x}) \dot{O}_{74,z}) + \\
& (b c \alpha_{11} - O_{74,x}) \sec \alpha_{11} ((-c \theta_1) O_{74,x} + c \alpha_{11} (l_1 + b c \theta_1 + O_{74,z} s \theta_1)) \dot{\theta}_1) / \\
& (l_1 (c \alpha_{11} c \theta_1 O_{74,z} + ((-b) c \alpha_{11} + O_{74,x}) s \theta_1)^2), 0, (c \alpha_{11} (s \theta_1 ((O_{74,z} + l_1 s \theta_1)) \dot{O}_{74,x} + \\
& (c \alpha_{11} (b + l_1 c \theta_1) - O_{74,x}) \dot{O}_{74,z}) - O_{74,z} ((-c \theta_1) O_{74,x} + c \alpha_{11} (l_1 + b c \theta_1 + O_{74,z} s \theta_1)) \dot{\theta}_1) / \\
& (l_1 (c \alpha_{11} c \theta_1 O_{74,z} + ((-b) c \alpha_{11} + O_{74,x}) s \theta_1)^2), 0, 0, 0, 0, 0, 0, 0, 0, \\
& (c \theta_2 ((-O_{75,z} + l_1 s \theta_2)) \dot{O}_{75,x} + ((-c \alpha_{12})(b + l_1 c \theta_2) + O_{75,x}) \dot{O}_{75,z}) + \\
& (b c \alpha_{12} - O_{75,x}) \sec \alpha_{12} ((-c \theta_2) O_{75,x} + c \alpha_{12} (l_1 + b c \theta_2 + O_{75,z} s \theta_2)) \dot{\theta}_2) / \\
& (l_1 (c \alpha_{12} c \theta_2 O_{75,z} + ((-b) c \alpha_{12} + O_{75,x}) s \theta_2)^2), 0, (c \alpha_{12} (s \theta_2 ((O_{75,z} + l_1 s \theta_2)) \dot{O}_{75,x} + \\
& (c \alpha_{12} (b + l_1 c \theta_2) - O_{75,x}) \dot{O}_{75,z}) - O_{75,z} ((-c \theta_2) O_{75,x} + c \alpha_{12} (l_1 + b c \theta_2 + O_{75,z} s \theta_2)) \dot{\theta}_2) / \\
& (l_1 (c \alpha_{12} c \theta_2 O_{75,z} + ((-b) c \alpha_{12} + O_{75,x}) s \theta_2)^2), 0, 0, 0, 0, 0, 0, 0, 0, 0,
\end{aligned}$$

$$\begin{aligned}
& (c \theta_3((-O_{76,z} + l_1 s \theta_3))\dot{O}_{76,x} + ((-c \alpha_{13})(b + l_1 c \theta_3) + O_{76,x})\dot{O}_{76,z}) + \\
& (b c \alpha_{13} - O_{76,x}) \sec \alpha_{13}((-c \theta_3)O_{76,x} + c \alpha_{13}(l_1 + b c \theta_3 + O_{76,z} s \theta_3))\dot{\theta}_3) / (l_1(c \alpha_{13} c \theta_3 O_{76,z} + \\
& ((-b) c \alpha_{13} + O_{76,x}) s \theta_3)^2), 0, (c \alpha_{13}(s \theta_3((O_{76,z} + l_1 s \theta_3)\dot{O}_{76,x} + (c \alpha_{13}(b + l_1 c \theta_3) - \\
& O_{76,x})\dot{O}_{76,z}) - O_{76,z}((-c \theta_3)O_{76,x} + c \alpha_{13}(l_1 + b c \theta_3 + O_{76,z} s \theta_3))\dot{\theta}_3)) / (l_1(c \alpha_{13} c \theta_3 O_{76,z} + \\
& ((-b) c \alpha_{13} + O_{76,x}) s \theta_3)^2)]
\end{aligned}$$

$$\dot{\mathbf{J}}_{x_i \phi} = \dot{\mathbf{J}}_{S\phi} \mathbf{J}_{x_i S} + \dot{\mathbf{J}}_{\theta\phi} \mathbf{J}_{x_i \theta} + \mathbf{J}_{S\phi} \dot{\mathbf{J}}_{x_i S} + \mathbf{J}_{\theta\phi} \dot{\mathbf{J}}_{x_i \theta}$$

$$\begin{aligned}
\dot{\mathbf{J}}_{\theta\phi} &= [(l_1 \sec \phi_1 (s \theta_1 \dot{\theta}_1 - c \theta_1 \tan \phi_1 \dot{\phi}_1)) / l_2, 0, 0; \\
& 0, (l_1 \sec \phi_2 (s \theta_2 \dot{\theta}_2 - c \theta_2 \tan \phi_2 \dot{\phi}_2)) / l_2, 0; 0, 0, (l_1 \sec \phi_3 (s \theta_3 \dot{\theta}_3 - c \theta_3 \tan \phi_3 \dot{\phi}_3)) / l_2]
\end{aligned}$$

$$\begin{aligned}
\dot{\mathbf{J}}_{S\phi} &= [0, 0, -((\sec \phi_1 \tan \phi_1 \dot{\phi}_1) / l_2), 0, 0, 0, 0, 0, 0; \\
& 0, 0, 0, 0, 0, -((\sec \phi_2 \tan \phi_2 \dot{\phi}_2) / l_2), 0, 0, 0; 0, 0, 0, 0, 0, 0, -((\sec \phi_3 \tan \phi_3 \dot{\phi}_3) / l_2)]
\end{aligned}$$